NOTE TO USERS

MATHEMATICAL INVESTIGATION OF HEAT TRANSFER IN INDUSTRIAL CRUDE OIL TANK DURING A FIRE

by

Khalid Abdulrahman Alnasser, B.Sc. in Chemical Engineering

King Fahad University of Petroleum and Minerals

Dhahran, Saudi Arabia, Jan. 2001

A THESIS SUMITTED IN PARTIAL FULFILLMENT

OF THE REQUIREMENTS FOR THE DEGREE OF

Master of Applied Science

Department of Civil and Environmental Engineering

Ottawa-Carleton Institute for Civil and Environmental Engineering

Carleton University

Ottawa, Canada

January 2006

Your file Votre référence
ISBN: 0-494-13434-8
Our file Notre référence
ISBN: 0-494-13434-8

Abstract

A mathematical study of heat transfer in an industrial crude oil storage tank during a fire leading to boilover has been conducted. Boilover, which might happen during a fire of an open top industrial storage oil tank, is caused by the enormous water vapour generated as the hot front (hot zone) in the crude oil reaches the water located at the bottom of the tank. This water consists of water that settled at the bottom of the tank over time, or water added during the firefighting operations. To solve the governing partial differential equations for heat transfer and fluid flow in crude oil and the water layer, a computational fluid dynamics (CFD) model has been developed. The model solves the governing equations of mass, momentum, and energy using an implicit control-volume formulation method with the SIMPLEC algorithm. The studies conducted using the model focus on calculating the transient, coupled heat and mass transfer taking place in the tank as a result of exposure to external radiation due to the fire. The model predicts the liquid heat transfer profiles. Beside the predictions of the container conditions, the model estimates the effect of various parameters on the heat penetration rate and the time needed to reach the water layer.

Key words: crude oil, boilover, hot zone, thermal radiation, radiant heat flux, CFD, SIMPLEC, Boussinesq approximation, burning rate, heat and mass transfer, pool fire, industrial tank fire, crude oil storage tank.

To my parents, family, KFUPM and Saudi Aramco

for their undying support.

Acknowledgments

My heartfelt gratitude is toward my supervisor, **Prof. George V. Hadjisophocleous** for his valuable comments, guidelines, and suggestions during the coursework. His endless dedication, enthusiasm and patience were the key to this study. I thank him for his consistent and enormous support and encouragement during my master's study.

Special thanks are sent to the following organizations who directly and indirectly contributed to this academic investigation.

Carleton University	Department of Civil and Environmental Engineering Carleton University Library - Interlibrary Loans Carleton University Housing Office
Saudi Aramco	Fire Protection Department Career Development Department
Aramco Services Company	Career Development Group.
Saudi Embassy in Ottawa	Educational & Career Section

Table of Contents

List of Tables

List of Figures

1. INTRODUCTION

Crude oil storage tank fires are less likely to occur today due to the increased safety and maintenance procedures followed by the petroleum industry. In spite of the rarity of tank fires, the importance of fire control measures should not be ignored. Fires in crude oil tanks pose a high threat to life safety, and may result in severe damages including unpredictable capital losses and environmental destruction. Crude oil tank fires, if left to burn, may lead to unpredictable fuel eruptions.

Classification of the possible types of fuel eruptions during the self-sustaining combustion of crude oil in atmospheric storage tanks has been undertaken by the American Petroleum Institute (API). API-2021 has classified fuel eruptions into three forms: slopover, frothover, and boilover [1].

The least serious form of fuel eruption is called slopover [2]. In this type of fuel eruption, limited quantities of fuel leave the tank over one wall. Slopover may be caused by firefighters, who spray foam or water used for firefighting over a layer of oil having a temperature higher than the boiling temperature of water. Detailed safety procedures are usually included in a facility's fire safety plan and precautions and defensive manoeuvres are usually taken by firefighters and facility's operators to prevent slopover.

Frothover is a continuous process characterized by a low intensity fire, accompanied by the ejection of burning fuel. This scenario can also occur during filling operations of crude oil tanks [2]. Water content in this form of eruption is fully mixed with crude oil.

The final form of eruption, which is the most dangerous one, is called boilover. Boilover is distinguished by the sudden eruption of violently burning fuel, coupled with an intense fireball [2]. In this form of fuel eruption, water is found in a separate layer at the bottom of the tank. Understanding the conditions in a crude oil tank during a fire leading to boilover is the topic of this study.

The API Classification methodology is based on the shape and quantity of fuel emitted, which is directly related to the quantitative and qualitative aspects of the tank contents. Qualitative aspects of the crude oil and water layers, including physical composition, play a role in determining what type of fuel eruption may occur [1]. Figure 1.1 illustrates the three types of fuel eruptions possible during storage tank fires.

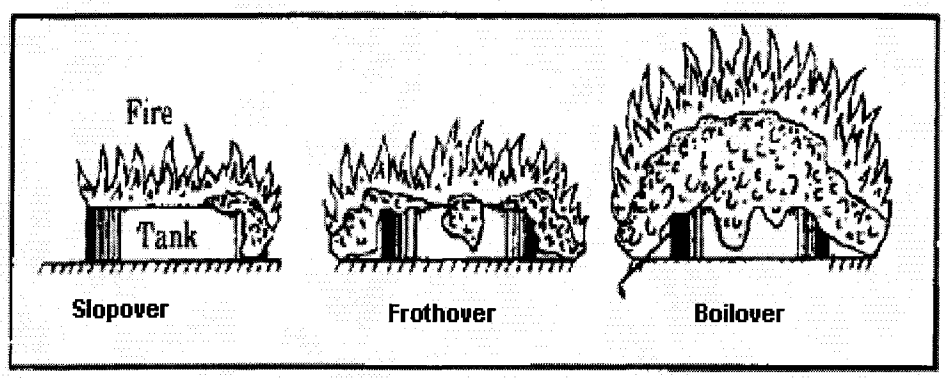

Figure (1.1): The Three Types of Fuel Ejections from Burning Oil Tanks [2].

The National Fire Protection Association (NFPA) in NFPA-30 [3] defined boilover as "*an event in the burning of certain oils in an open-top tank when, after a long period of quiescent burning, there is a sudden increase in fire intensity associated with expulsion of burning oil from the tank. Boilover occurs when the residues from the burning surface become more dense than the unburned oil and sink below the surface to form a hot layer, which progresses downward faster than the regression of the liquid surface. When this hot layer, called a "heat wave", reaches water or water in oil emulsion in the bottom of the tank, the water is first superheated and then boils, almost explosively, overflowing the tank. Oils subjected to boilover consist of components having a wide range of boiling points, including both light ends and viscous residues. These characteristics are present in most crude oils and can be produced in synthetic mixtures.*"

The NFPA-30 boilover definition adopts Hall's hypothesis [4] with regard to the driving force of the heat wave inside the liquid bulk, with one minor difference. The minor change is that Hall did not clearly mention whether, during boilover, the water just boils, or whether it becomes superheated. But the NFPA-30 definition emphasizes that the water is first superheated and then it boils, which requires that the temperature of the water layer at the bottom of the tank must exceed the atmospheric boiling temperature of water (100°C).

Unfortunately, a number of boilovers associated with spectacular storage tank fires have occurred in the last century. Some of these accidents resulted in high loss of life and significant property damages.

In Japan, for example, two boilover fires have occurred since World War II: the first at Yokkaichi in October 1954, and the second after an earthquake in June 1964 at Niigata [5].

In Tacoa, Venezuela in 1982, one of the worst tank fire catastrophes occurred involving a tank with a diameter of 60 m, a height of 17 m, and a volume of 38,000 m^3. This tank fire killed about 150 firefighters [5].

The following year, another boilover fire occurred at the Amco Refinery tank farm in Wales, UK. A fire started in a normal floating-roof crude oil storage tank, which was 78 m in diameter and had a volume capacity of 94,000 m^3. Unfortunately, hours later, the floating roof lost its structural integrity and started to sink into the crude oil bulk. Due to limited foam resources, the fire was allowed to burn freely. After a short period, loud spitting and crackling noises with an increase in flame intensity forced the fire service to evacuate the scene. The rare phenomenon of multiple boilovers occurred in that incident. At each boilover, the steam ejected the tank material almost 914.4 m (3000 ft) into the air [5,6]. Although the incident did not jeopardize life or production, the estimated loss of crude oil was £4 M (at 1983 prices). A number of short video clips, recording this rare multiple-boilover scenario, are available on the internet [6].

Although crude oil tank fires and boilovers are rare events, their destructive power and potential for loss of life and property are so high that there is a need for a better understanding of how, when and why boilovers occur. Increase of knowledge in this area will lead to the development of tools to predict the occurrence of boilovers and to develop methodologies and technologies to mitigate their impact.

The first attempt towards understanding the boilover problem was an experimental research effort in 1925 by the Chief Engineer of the Standard Oil Company of California, Hall [4]. Around 100 tests were carried out in an effort to explain the inconsistencies of the previous tank fire data records. One of the most important findings of his work was to identify three physical conditions which must exist in the contents of a burning tank in order for a boilover event to occur. These conditions are: (1) the presence of water, (2) the occurrence of a heat wave, and (3) significantly viscous content.

The presence of water in the oil tank is the first condition for boilover to occur. Basically, the energy generated from the conversion of water to steam is the source of forces behind ejecting oil out of the tank. The forces developed out of steam should be enough to overcome the crude oil surface tension and head force developed from oil weight.

Naturally, mineral water is present in oil reservoirs in a separate layer at the bottom of the tank. However, water can also be found in the crude oil content in the emulsified form due to process needs [2]. For instance, one step in the downstream process of crude oil, specifically in the Gas Oil Separation Plant, is washing the crude oil with water. This step is to remove salts which may cause corrosion [7]. Industrial fire inspection routines might also contaminate the tank contents with water during the annual live fire performance tests.

The percentage of emulsified water in an oil tank varies with the oil source. For example, Arab light crude contains less than 0.3% water in emulsified form [8]. Usually crude oils are stored in tanks for various processing requirements over long periods of time, and during this interval, water settles down to the bottom of the tank due to its larger specific gravity as

compared with the conventional crude oils [2]. The presence of the water layer at the bottom of the tank increases the likelihood that a boilover event will happen. However as stated by Hall [4], increasing the thickness of the water layer at the bottom of the tank does not guarantee that boilover will in fact occur.

The second condition necessary for boilover is the presence of a heat wave. A heat wave is generally related to the thermal properties of crude oils and specifically to the rate of heat penetration in the oil bulk. Heat must be carried down into the liquid faster than the descending rate of the burning surface. This can happen, only, if the hydrocarbon fuel mixture has a wide range of boiling points and densities [4].

The third condition for the occurrence of boilover identified by Hall relates to the viscosity of the oil. The crude oil must be viscous, or at least the residue at the bottom of the tank should be of a viscous nature. Once the heat reaches the water and converts it into steam, that steam must pass through a viscous medium and generate foam as it rises up though the oil above [4].

Although we have a better knowledge of the necessary conditions for boilover to occur there is still a lack of computer models that can be used to predict whether boilover will occur and the time of occurrence. Such tools would be invaluable to fire services as they could better plan their activities at the fire scene to minimize the possibility of subjecting firefighters to the dangerous conditions caused by boilovers.

The research topic of this thesis is the development of a mathematical model using Computational Fluid Dynamics (CFD) methods to study heat and mass transfer, and fluid flow conditions in a crude oil tank subjected to a fire which eventually will lead to boilover. The model solves the governing equations of mass, momentum, and energy using an implicit time marching scheme and the control-volume formulation with the SIMPLEC algorithm. The studies conducted using the model focus on calculating the transient, coupled heat and mass transfer taking place in the tank as a result of exposure to external radiation due to the fire. The absorbed radiant heat flux at the surface of the oil is calculated using a constant flame temperature of the self-sustaining crude oil combustion.

The objectives of this investigation are the following:

(1) to mathematically study heat penetration in the crude oil bulk due to a fire
(2) to analyse the results of the model to gain understanding of the thermodynamic processes involved during a fire in a crude oil tank, and
(3) to determine the impact of various parameters on heat and mass transfer.

2. LITERATURE REVIEW

The study of oil tank fires has always been of significant interest to fire safety science due to the significant risk they present to life safety and properties. Almost all industrial facilities have a storage tank area. Therefore, in order to increase safety levels at these liquid storage facilities, a number of theoretical and experimental studies have been conducted and published in the open literature. These initiatives have been undertaken in order to promote understanding of the heat transfer mechanisms at play in burning oil. Indeed, some of this work has been very well recognized and has made major contributions toward society's ability to maintain safe workplaces, by improving the regulation of industrial oil tank facilities and contributing to firefighting operational tactics. In this chapter, a scientific, constructive and comprehensive review of burning oils will be undertaken to technically evaluate prior experimental and theoretical boilover scenario studies. The information provided is meant to act as a basic introduction for any further investigation focusing specifically on boilover phenomena, or, more generally, on any other subject related to conventional crude oil, such as natural diffusion pool fires.

Subsection 2.1 covers the fundamentals of physical chemistry for crude oils. It defines different types of crude oil, and presents their thermal and physical properties as a function of temperature. It also discusses the classification process of crude oils, based on different physical factors such as boiling points and densities.

In the second part of section 2.1, the review focuses on crude oil storage tank fires, which could be considered pool fires with two minor differences. These two differences are that (1) the liquid is surrounded by a metal wall, and (2) the natural diffusion flame is at an elevated position relative to the surface of the fuel. Subsection 2.2 justifies the physical arguments using experimental results from small- and large-scale crude oil storage tank fires.

The third subsection reviews the literature dealing with mathematical modeling of crude oil fires. It presents a number of mathematical models which can be utilized to estimate temperature profiles in the bulk of a burning liquid under similar boundary conditions.

2.1 Review of the Physical Chemistry of Crude Oil

Knowledge of the physical properties of crude oil is the first step in the solution process of the heat and mass transport equations. This section covers the following items: (1) crude oil definition, (2) crude oil composition, and (3) crude oil thermal and physical properties. The goals of this review are to determine appropriate values of the physical properties of crude oil, to gain understanding of the distillation dynamics occurring in an oil tank during a fire, and to determine the effect of crude oil composition on its physical and thermal properties.

2.1.1 Crude Oil Definition and Physical Classifications

Crude oil is a brownish-green to black, flammable, viscous, and multi-component mixture of hydrocarbons extracted in liquid form from sedimentary rock underneath the earth's surface [9][10]. Scientists generally agree that crude oils are made from marine animal and plant debris which has been cooked naturally for ages under high temperatures and pressures [9].

From a chemical composition point of view, crude oils consist of an exceedingly complex and structured mixture of hydrocarbon compounds, non-hydrocarbon compounds, and organometallic compounds [9][10]. The hydrocarbon components in crude oil can be arbitrarily grouped into three or sometimes four types based on the relative ratio of these hydrocarbons in crude oil mixture. The following terms describes three types of crudes :(1) Paraffinic, high ratio of paraffinic hydrocarbons, (2) Naphthenic, high ratios of naphthenic and aromatic hydrocarbons, and (3) Asphaltic, large amount of polynuclear aromatics, and asphaltene [10].

The Bureau of Mines Correlation Index (BMCI) is a useful measure for indicating the crude class or type. BMCI relates the mid-boiling temperature in degree Celsius at which 50 vol % of the crude is distilled, and the specific gravity of a crude oil as shown in Equation 2.1 [10].

$$BMCI = 48{,}640 / (T_{mb} + 273.15) + (473.6\, SG - 456.8) \qquad (2.1)$$

Where BMCI = Bureau of Mines Correlation Index, dimensionless
T_{mb} = temperature at the mid-boiling point, °C
SG = specific gravity of crude oil, dimensionless

A low value of BMCI reflects high paraffin content in the crude oil mixture, while, a 100 indicates a high percentage of aromatics.

Each class of the hydrocarbons has its own physical characteristics and an influence on the overall mixture properties. Table 2.1 gives a practical example of how many hydrocarbons can be physically isolated from Ponca Crude oil [10][11].

Table (2.1): Types of Hydrocarbons Isolated from Ponca Crude, Generated from [10, 11]

Hydrocarbon type	Basic Structures	Number Isolated	Fractions where found
Paraffins: • C_nH_{2n+2} where n: number of carbon atoms • Carbons are joined by single bonds • Occur in most crude oils but vary in concentrations • Branched paraffins found throughout the boiling range			
n-Paraffins	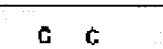	33	All Distillates
Branched Paraffins	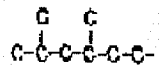	41	Gasoline, Light Gas Oil
Cycloparaffins: • Saturated cyclic hydrocarbons, also known as naphthenes • Specifically in gasoline, have 5-6 carbon atoms arranged in a ring • Lower members of naphthenes are cyclopentane and cyclohexane • Most individual cycloparaffins are isolated in the boiling range of gasoline and kerosene			
Monocycloparaffins		39	Gasoline, Kerosene
Bicycloparaffins	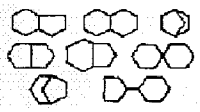	29	Gasoline, Kerosene
Tricycloparaffins		3	Gasoline, Kerosene
Aromatics: • Some carbon atoms arranged in a ring joined by aromatic bonds. • Lower members of aromatic compounds present in a small quantity in crude oils			
Mononuclear Aromatics	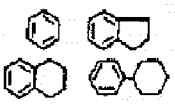	48	Gasoline, Kerosene, Light Gas Oil
Dinuclear Aromatics	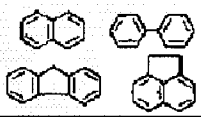	60	Kerosene, Light Gas Oil
Trinuclear Aromatics	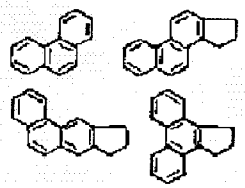	10	Heavy Gas Oil-Light Lubricant
Tetranuclear Aromatics	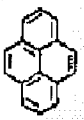	3	Heavy Gas Oil-Light Lubricant

Even though crude oil is a complex mixture in nature, its chemical analysis provides fairly similar results [10]. For comparison purposes, Table 2.2 shows and compares the ultimate analysis by weight percentage for four different crude oils.

Table (2.2): Analyses of Crude Oils, Collected from [10].

	Ultimate Analysis, Weight %				
Product	Carbon	Hydrogen	Sulfur	Nitrogen	Oxygen
California Crude	84.00	12.70	0.75	1.70	1.2
Kansas Crude	84.15	13.00	1.90	0.45	-
Texas Crude	85.05	12.30	1.75	0.70	-
General Crude	84.80	12.60	1.50	0.40	0.5

Based on their density or specific gravity, crude oils can also be physically classified into three classes: conventional (light) crude oil, heavy crude oil and tar sand oil (bitumen). Figure 2.1 and Table 2.3 show the three classifications of crude oils based on density, and provide the viscosity scale over the density range [11]. In this study, the term "crude oil" is restricted to the conventional crude oil which represents any crude oil with a density less than 934 kg/m^3.

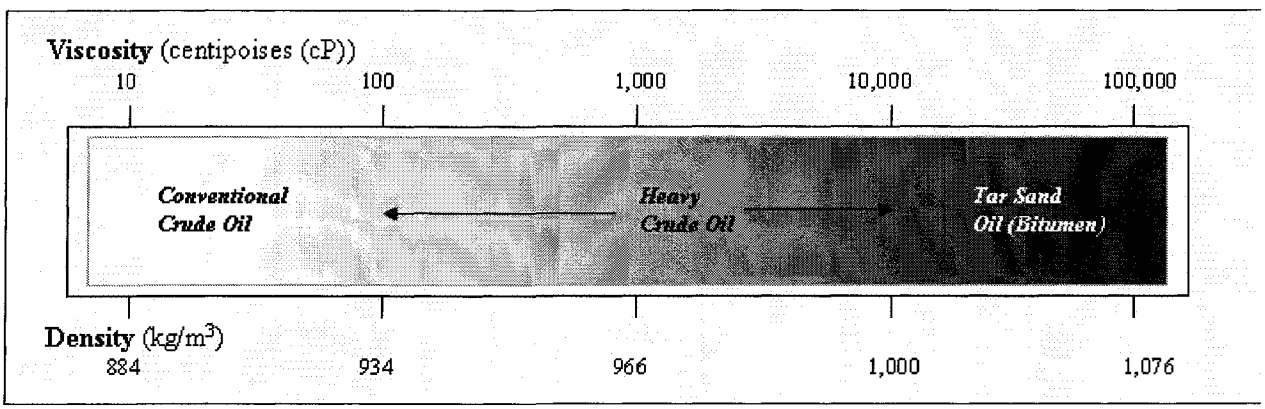

Figure (2.1): Classification of Crude Oils Based on Density, Reproduced from [11].

Table (2.3): Classification of Crude Oils Based on Density, Reproduced from [11]

	Type Of Crude	Characteristics
1	Conventional or "Light" Crude	Density-Gravity range less than 934 kg/m^3 (>20°API)
2	Heavy Crude Oil	Density-Gravity range from 934 kg/m^3 to more than 1,000 kg/m^3 Maximum viscosity of 10,000 mPa.s (cP)
3	Extra Heavy Crude Oil may include atmospheric residuum (T_B > 340°C)	Density-Gravity greater than 1,000 kg/m^3 (<10°API) Maximum viscosity of 10,000 mPa.s (cP)
4	Tar sand bitumen or natural asphalt may include vacuum residuum (T_B > 510°C)	Density-Gravity greater than 1,000 kg/m^3 (<10°API) Viscosity greater than 10,000 mPa.s (cP)

Note: T_B is the temperature at the boiling point.

The crude oil complex mixture can be separated into different fractions with relatively narrow boiling ranges using atmospheric distillation. These fractions are light naphtha, heavy naphtha, kerosene, atmospheric gas oil, vacuum gas oil and vacuum residuum. The boiling point range of these distillated fractions varies from 30°C to 538+°C. Table 2.4 shows the approximate American Society for Testing and Materials (ASTM) boiling point ranges for crude oil fractions, and Figure 2.2 compares four different crude oils based on their distillate chemical composition groups [10].

Table (2.4): Approximate ASTM Boiling Point Ranges for Crude Oil Fractions Generated from [10].

	Boiling Range	
Fractions	**°C**	**°F**
Light Naphtha	30-99	85-210
Heavy Naphtha	88-204	190-400
Kerosene	171-271	340-520
Atmospheric Gas Oil	288-438	540-820
Vacuum Gas Oil	399-566	750-1050
Vacuum Residuum	538+	1000+

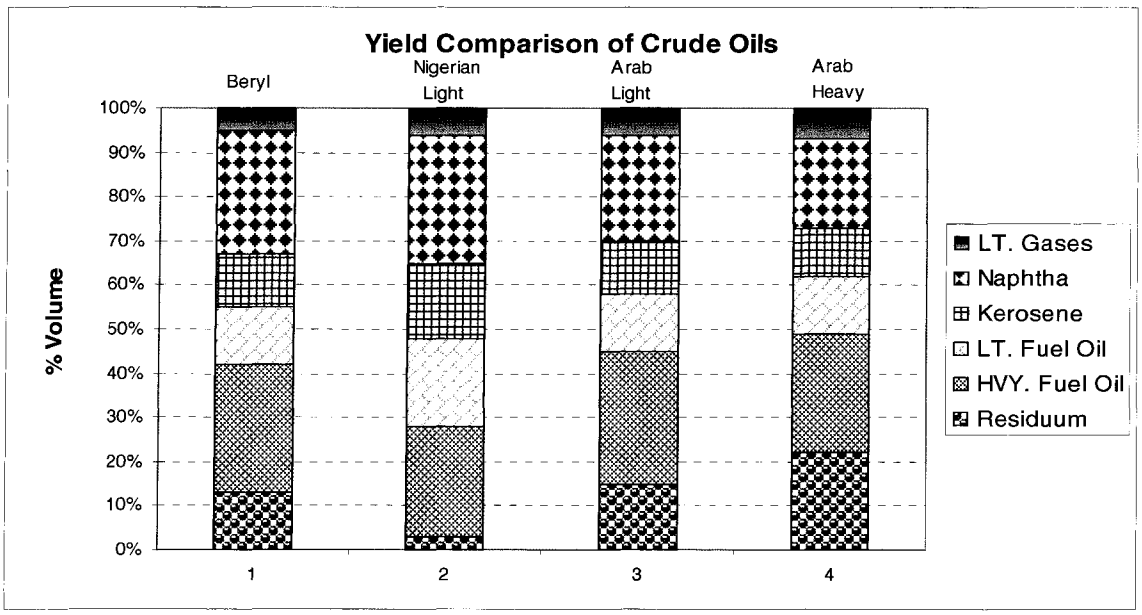

Figure (2.2): Yield Volume Percentage Comparisons of Four Crude Oils, Reproduced from [11].

Figure 2.2 shows the yield volume percentages for Beryl, Nigerian light, Arab light, and Arab heavy crude oils. From this figure it can be seen that the four crude oils have almost the same volume percentages of light gases, kerosene and light fuel oil. However, volume percentage of naphtha and residuum varies between the four crude oils.

2.1.2 Physical Properties of Crude Oils

Thermal and physical properties of crude oil govern the response of the fluid to heat penetration. These thermal and physical properties are the specific gravity, the viscosity, the thermal conductivity, the specific heat, and the latent heat of evaporation. Heat of combustion also plays a role as it governs the heat produced by the combustion of crude oil.

The specific gravity of a liquid is defined as the density of the liquid divided by the density of water at 15.6°C (60°F). The specific gravity of crude oils varies with source locations; however, the extreme limits are 0.65 and 1.07 [9]. A different representation of the density of crude oil is given by the American Petroleum Institute's (API) degree equation. This equation, which is the standard practice in today's petroleum industries, is given by Equation 2.2 [9, 10]:

$$°\text{API} = 141.5/SG - 131.5 \qquad (2.2)$$

where °API = American Petroleum Institute degree, dimensionless
SG = specific gravity of crude oils, dimensionless

Figure 2.3 shows the relation between specific gravity of crude oil and its API degree. As shown in Figure 2.3, high degree API represents a light crude oil, while small degree API represents a heavy crude oil.

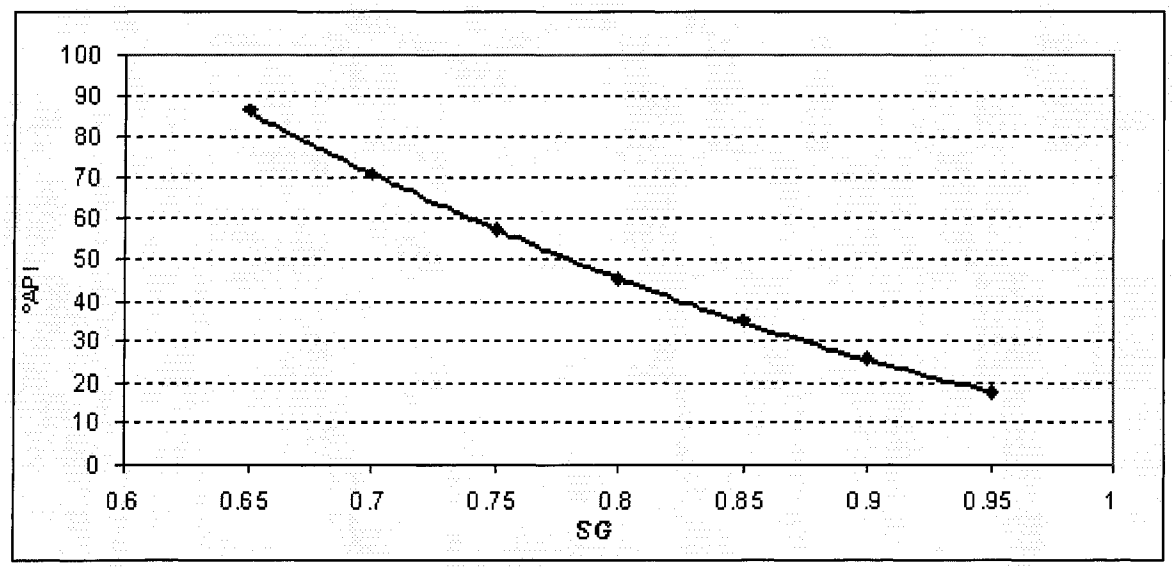

Figure (2.3): Relation between Specific Gravity and °API.

The density of crude oil as a function of temperature can be calculated using Equation 2.3 [12].

$$\rho = \rho_s - \alpha(T - T_s) + \beta(T - T_s)^2 \qquad (2.3)$$

which α and β are functions of specific gravity of crude oils and can be calculated from

$$\alpha = \begin{cases} 66 \pm 5 \times 10^{-5} & \text{for } SG \in (0.65, 0.84) \\ (189.4 - 146.5 \times SG) \pm 3 \times 10^{-5} & \text{for } SG \in (0.84, 1.07) \end{cases}$$

$$\beta = [(-15.4 + 19 \times SG)] \times 10^{-7}$$

Where ρ = density of crude oil as a function of temperature, kg/m^3
ρ_s = reference density at the reference temperature, kg/m^3
SG = specific gravity of crude oil, dimensionless
α = thermal constant, kg/m^3·°C
β = thermal constant, kg/m^3·°C^2
T = specified temperature, °C
T_s = reference temperature, °C

Viscosity is a measure of resistance to flow. In general, viscosities of crude oils decrease as the temperature increases. Figure 2.4 presents the relation between the viscosity and the temperature for crude oil of 35°API, as well as water.

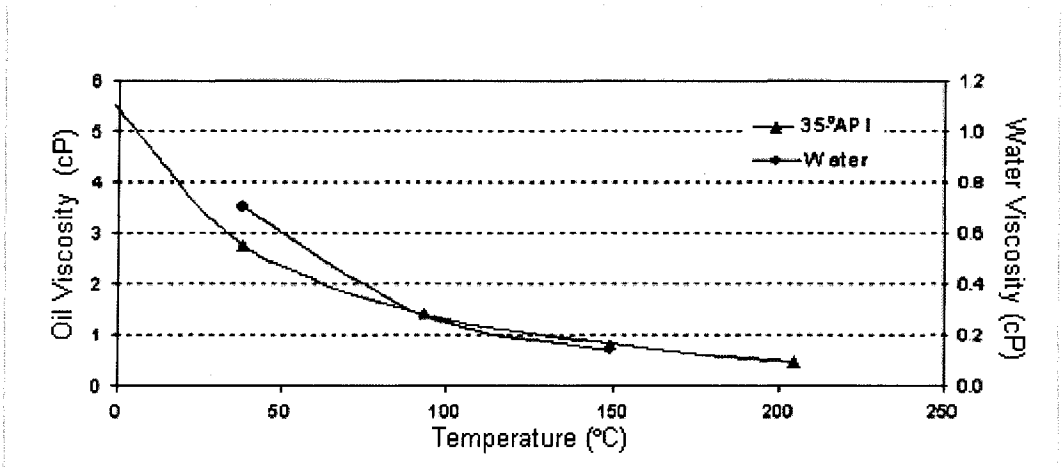

Figure (2.4): Relation between Viscosities of Crude Oil of 35°API and Water with Temperature, Reproduced from [13].

Thermal conductivity is a measure of the ability of a material to conduct heat. The thermal conductivity of crude oils is given by the following equation [14]:

$$k = \frac{0.120 - 8.66 \times 10^{-5} T}{SG} \tag{2.4}$$

where k = thermal conductivity of crude oil, W/m·K
T = temperature, °C
SG = specific gravity of crude oil, dimensionless

The specific heat is defined as the quantity of heat energy required to raise the temperature of a unit of mass of the material by one degree centigrade at constant pressure. The value of specific heat of crude oil as a function of temperature is given by Equation 2.5 [14].

$$C_p = \frac{1.685 + 3.4 \times 10^{-3} T}{SG} \tag{2.5}$$

where C_p = specific heat of crude oil, kJ/kg·K
T = temperature, °C
SG = specific gravity of crude oil, dimensionless

One of the most important parameters in petroleum engineering is perhaps the latent heat of vapourization due to its effect on the distillation process. This is defined as the amount of heat required to vapourize a unit mass of a liquid at its atmospheric boiling point. Latent heat of vapourization decreases as the temperature rises, and it becomes zero at the critical temperature. Generally, the latent heat of vapourization decreases with increasing temperature and pressure. The latent heat of vaporization for conventional

crude oils can be calculated by the relation in Equation 2.6 once the boiling temperature, and specific gravity of crude oil are known [14]:

$$L_H = \frac{251.47 - 377.136 \times 10^{-3} T_B}{SG} \tag{2.6}$$

where L_H = latent heat of vapourization, kJ/kg
T_B = temperature at the boiling point, °C
SG = specific gravity of crude oil, dimensionless

Investigation of the latent heat of vapourization for a series of distillated fractions of Baku Petroleum is summarized in Table 2.5 [12].

Table (2.5): Relation between Specific Gravity, Boiling Temperature, and Latent Heat of Vapourization, Data Collected from [12]

SG	0.640	0.698	0.743	0.762	0.797	0.813
T_B (°C)	40.0	72.8	92.2	100.7	155.7	175.5
L_H (kJ/kg)	337.5	314.0	286.0	279.0	244.4	216.0

Thermal diffusivity of material is the ratio of thermal conductivity to volumetric heat capacity, which can be calculated using Equation 2.7.

$$\alpha = \frac{k}{\rho C_p} \tag{2.7}$$

where α = thermal diffusivity, m^2/s
k = thermal conductivity of crude oil, W/m·K
ρ = density, kg/m^3
C_p = specific heat of crude oil, kJ/kg·K

Figure 2.5 presents the relationship between thermal properties such as thermal conductivity, specific heat, and thermal diffusivity with temperature in the range from 25°C to 225°C for a crude oil with a specific gravity of 0.86. For convenience, the

thermal and physical properties in Figure 2.5 are normalized using their values at 25°C as their reference temperature. The normalized specific heat is lowered by 0.38 to present its values on the same figure. The reference values of the physical parameters used in the normalization calculations are shown in Table 2.6.

Table (2.6): Reference Values Used in Dimensionless Calculations.

Normalized Parameters	Equation	Reference value at $T_o = 25°C$	
Thermal Conductivity	$k' = k / k\,(T_o)$	0.133	W/kg K
Specific Heat	$C_p' = C_p / C_p\,(T_o)$-0.38	1.997	kJ/kg K
Thermal Diffusivity	$\alpha' = \alpha / \alpha\,(T_o)$	7.785×10^{-8}	m^2/s

Note: ' stands for normalized parameters

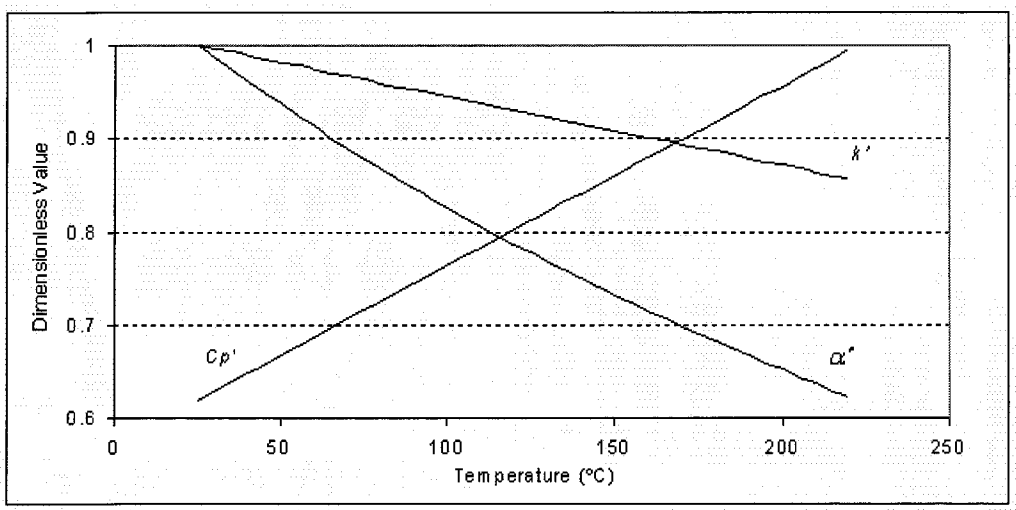

Figure (2.5): Relation between Dimensionless Thermal Properties with Temperature for *SG*=0.86.

2.1.3 Heat of Combustion

The heat of combustion is defined as the total amount of heat released when a unit quantity of a fuel is completely oxidized (at 25°C and at atmospheric pressure)[15].

Chemically, the heat of combustion is the heat energy released when an organic compound is burned to produced water, carbon dioxide, sulfuric acid, and nitric acid [14].

The heat content of crude oils is experimentally found to fall between 41,900 kJ/kg and 46,600 kJ/kg. The heat content of the refined products typically exceeds 46,600 kJ/kg [9].

Experimentally, the high value of heat of combustion for pure crude oils is measured in a oxygen bomb calorimeter. The high value of heat of combustion at a constant volume may also be calculated using the following formula [9]:

$$Q_v = 51{,}961 - 8{,}800\, SG^2 \tag{2.8}$$

The low value of heat of combustion at isobaric conditions (constant pressure) can be calculated using the following equation [9]

$$Q_p = Q_v - 209.52H \tag{2.9}$$

H in Equation 2.10 stands for the mass percentage of hydrogen in crude oils and can be obtained from the following relation [9]

$$H = 26 - 15SG \tag{2.10}$$

Substituting Equations 2.8 and 2.10 into Equation 2.9 gives the isobaric heat of combustion as a function of the specific gravity of crude oil.

$$Q_p = 46{,}513 - 8{,}800\, SG^2 + 3142.8\, SG \tag{2.11}$$

where Q_p = low value of heat of combustion at constant pressure, kJ/kg
Q_v = high value of heat of combustion at constant volume, kJ/kg
H = mass percentage of hydrogen in crude oil, %
SG = specific gravity of crude oil, dimensionless

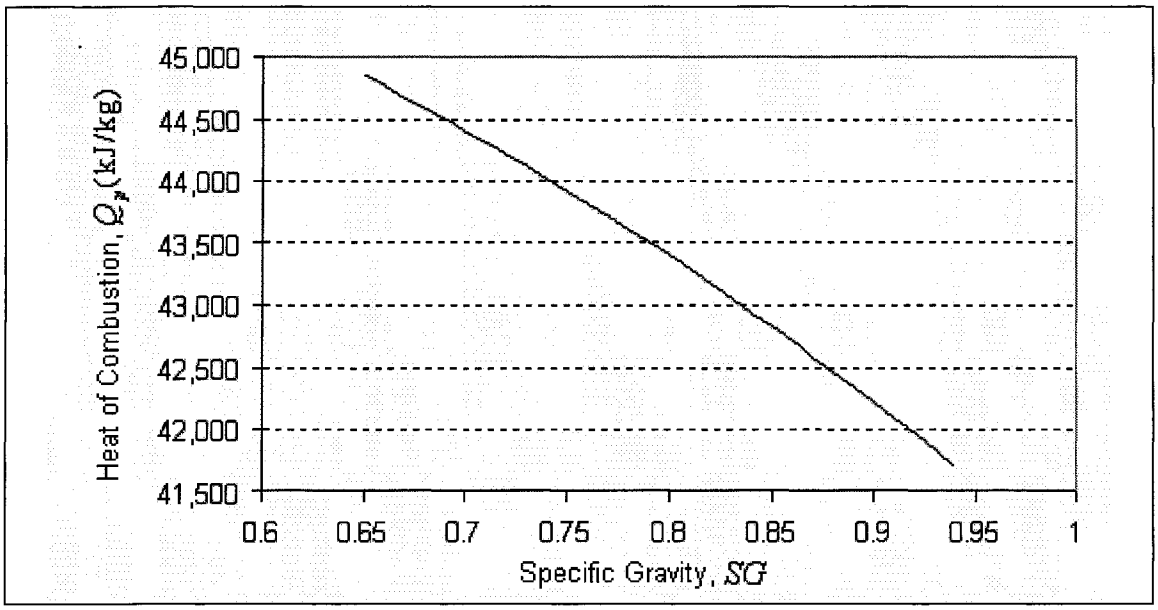

Figure (2.6): Relation between Heat of Combustion at Constant Pressure and Specific Gravity of Crude Oil.

To determine the effective heat of combustion, fourteen different crude oils with densities varying from 780 to 884 kg/m^3 (SG = [0.78, 0.88]) were recently tested using the cone calorimeter at Southwest Research Institute (SwRI) in San Antonio, Texas [16]. The cone calorimeter was designed according to the specifications of ASTM E 1354-97 with some modifications to test a circular pool filled with liquid fuel. The effective heat of combustion $\Delta H_{c,eff}$ for those selected samples was between 37,000 and 38,000 kJ/kg, indicating a combustion efficiency χ_{eff} of about 80% [16].

2.2 Crude Oil Fires

2.2.1 Definition of Pool fires

A fire in a crude oil storage tank is considered a form of pool fire, but with two differences. The first difference is actually that in tank fires, the liquid is surrounded by a metal wall, whereas there is no container present in the case of spilled pool fires. The second difference is that buoyancy-driven flames, resulting from highly exothermic chemical reactions, are at an elevated position in storage tank fires [17]. A naturally burning fire belongs in the "diffusion flames" category, because these are sustained by the meeting of fuel and oxygen in the reaction zone [18].

In general, a pool fire is complicated in nature and therefore its theoretical treatment can be expected to be correspondingly complex [18, 19]. This complexity is associated with the challenge of characterizing the region just above the liquid surface, and within the buoyancy-driven diffusion flames [19]. The subject of pool fires has received considerable research attention both experimental and numerical as evident from the amount of publications on the topic.

2.2.1 Burning Modes and their Rates

Osborne Reynolds explained the three modes of flows in a container (laminar, transition and turbulent) after conducting his famous liquid dye experiments [13]. Similarly, Hottel used the Reynolds fluid flow concepts in 1958 [17, 18] to classify the

burning rates of various flammable liquids into three distinctive flow regions. The Reynolds numbers (Re) were calculated using the relation between parameters of the vapour phase and those of the liquid phase as shown in Equations 2.12 and 2.13 below,

$$\mathrm{Re} = \frac{u_g d \rho_g}{\mu_g} \tag{2.12}$$

$$= \frac{u_l d \rho_l}{\mu_l} \tag{2.13}$$

where Re = Reynolds number, dimensionless
u_l = liquid velocity, m/s
d = pool diameter, m
ρ_l = liquid density, kg/m^3
μ_l = liquid viscosity, kg/m·s
u_g = vapour velocity, m/s
ρ_g = vapour density, kg/m^3
μ_g = vapour viscosity, kg/m·s

Figure 2.7 shows the liquid burning velocity (regression rate) and the flame height as a function of pan diameter of pool fires [17].

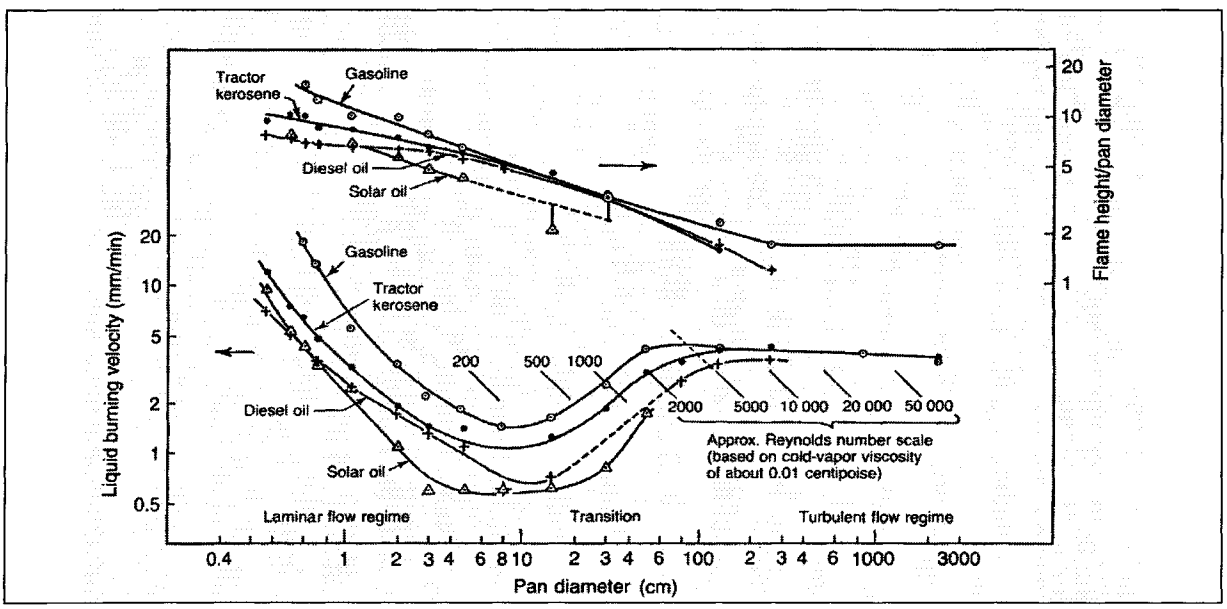

Figure (2.7): Liquid Regression Rate and Flame Height as a Function of Pan Diameter [17].

During the early stage of the burning period (the "transient stage"), the pool fire might tend to act similar to light hydrocarbon fuel fires such as propane and butane, because various amounts of light hydrocarbons in crude oil have flashpoints that are below the ambient temperature. In cases where the vapour burns quickly enough creating significant momentum at the liquid surface, the unsteady flames might take on the characteristics of 'jet fires' [20]. However, this transient jet fire behaviour has not been noticed from the experimental data of burning rate in a 1.9-m pool fire reported by Iwata et al. [8] as shown in Figure 2.8. The figure, however, shows that after a short period of time, the burning rate fluctuates around a value of 0.06 kg/m^{2}s.

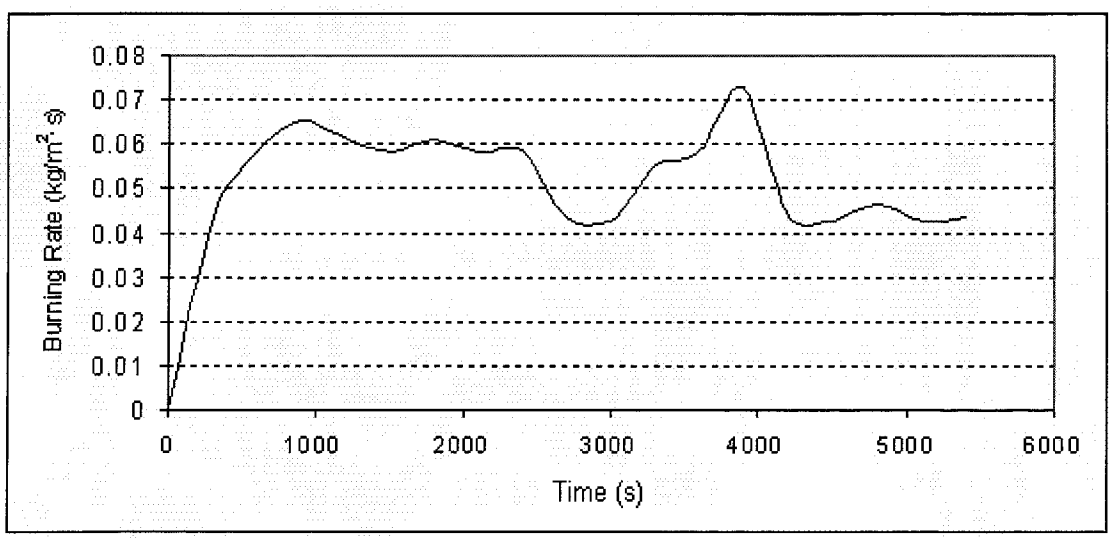

Figure (2.8): Time History of the Burning Rate of Crude Oil with 870 kg/m^3 in a 1.9-m Diameter Pool, Reproduced from [8].

An equation for the burning rate of liquid as a function of the pool diameter under windless conditions, has been developed by Burgess and Zabetakis in 1962 and presented in Lees [17] as follows:

$$\dot{m}'' = \dot{m}''_{\infty}(1-\exp(-\kappa\beta d)) \tag{2.14}$$

where $\dot{m}''_{\infty}$ is the burning rate per unit surface area for a pool of infinite diameter

$$\dot{m}''_{\infty} = 1.27\times10^{-6}\times\rho_l\left(\frac{-\Delta H_c}{\Delta H_L}\right) \tag{2.15}$$

but Babrauskas [17] proposed in 1986 that

$$\dot{m}''_{\infty} = \frac{\sigma T_f^4}{\Delta H_L} \tag{2.16}$$

where $\dot{m}''$ = burning rate per unit surface area, kg/m^2·s
$\dot{m}''_{\infty}$ = burning rate for a pool of infinite diameter, kg/m^2·s
κ = absorption-extinction coefficient, m^{-1}
β = mean beam length corrector, dimensionless
d = diameter of pool fire, m
ρ_l = liquid density, kg/m^3
ΔH_c = heat of combustion, kJ/kg
ΔH_L = total heat of vaporization, kJ/kg
σ = Stefan-Boltzmann constant, 5.6707 x 10^{-8} W/m^2·K^4
T_f = absolute temperature of effective equivalent grey gas, K

For non-circular pools, the effective diameter is equal to the diameter of a circular pool with an area equal to the actual pool area [21].

$$d = \sqrt{\frac{4A}{\pi}} \tag{2.17}$$

where d = effective pool diameter, m
A = actual pool area, m^2
π = pi constant, 3.1459 radians

The intensity of a pool fire is fully characterized by the pool diameter. Babarauskas has discussed some components affecting the liquid burning rate, including pool diameter, lip effects, and wind speed [17]. Generally, from Equation 2.14, the burning rate of the fuel has an exponential relationship with the pool diameter until the burning rate of the fuel reaches a maximum value. However, with a diameter greater than 5-10 m, specifically for crude oils, there is evidence of a slight reduction in the burning rate. The reason for this decrease of burning rate for large-diameter pool fires is presumably due to poor mixing of the flammable vapour with air. Babarauskas has suggested that this influence is unlikely to decrease the burning rate by more than 20% [17].

In small-sized (0.15 m diameter) kerosene pool fires, Joulain [19] experimentally studied the consequences of applying an external thermal radiant heat flux of a similar fuel liquid on the burning rate. The experimental results, presented in Figure 2.9, show that the burning rate increases as the radiant flux increases until the burning rate reaches a maximum value. However, after that stage, the influence of the radiant heat on the burning rate decreases as the applied radiation heat energy increases.

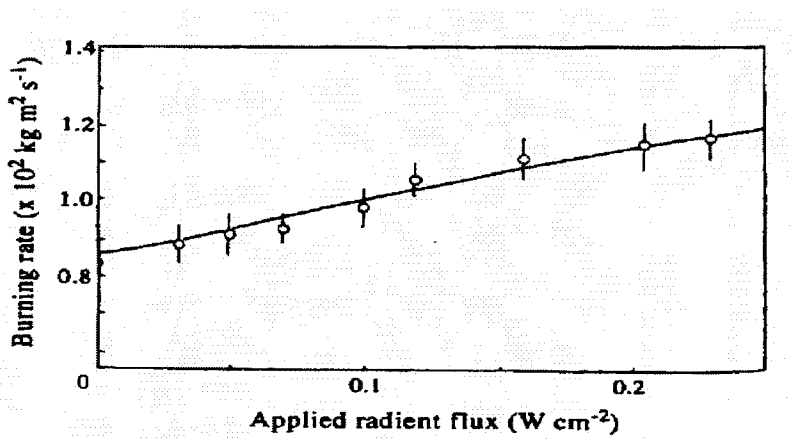

Figure (2.9): Relationship between Burning Rate and Extra Applied Radiant Flux [19]

Babrauskas has also used Reynolds' principle to classify the burning flows of natural diffusion fires based on pool diameter into four distinctive modes. Those four burning modes, caused by self-sustaining combustion, are summarized in Table 2.7 [17].

Table (2.7): Burning Modes as a Function of Pool Fire Diameter [17]

Pool Diameter (m)	Burning Mode
< 0.05	convective, laminar
< 0.20	convective, turbulent
0.2-1.0	radiative, optically thin
> 1.0	radiative, optically thick

For real industrial storage tanks, radiation heat flux is the factor that governs the fuel burning rate as well as fuel temperature. The radiant heat depends on the characteristics of fuel combustion, such as the efficiency of combustion, soot formation, and heat lost by convection to the entrained air [17]. As an example to show the effect of soot formation on the burning rate, Karlsson and Quintiere [22] stated that the diameter dependence is negligible for alcohols which are known for low soot formation.

Hall [18] and Drysdale [15] mathematically presented the effect of pool diameter on liquid burning rates using a simplified, semi-quantitative analysis of heat energy, as shown in Equations 2.18 and 2.19. Equation 2.18 shows that the total heat energy transferred from the flame into the liquid bulk is the sum of heat transfer by conduction between the flame and the tank wall, and the heat by convection and radiation between the flame and liquid surface.

$$\dot{Q}_{total} = \dot{q}_{cond} + \dot{q}_{conv} + \dot{q}_{rad} \tag{2.18}$$

Dividing Equation 2.18 by the surface area of the pool with diameter d and substituting the equation governing conduction, convection and radiation gives Equation 2.19,

$$\dot{Q}''_{total} = \frac{4\sum \dot{q}}{\pi d^2} = \frac{4\psi_1 \pi (T_f - T_l)}{d} + \psi_2 (T_f - T_l) + \psi_3 (T_f^4 - T_l^4)(1 - \exp(-\psi_4 d)) \quad (2.19)$$

where $\dot{Q}_{total}$ = total heat rate from flame into liquid, W
d = pool diameter, m
$\psi_{1,2,3,4}$ = thermal constants
T_f = absolute flame temperature, K
T_l = absolute liquid temperature, K
$\dot{q}_{cond}$ = conduction heat transfer from flame to tank wall, W
$\dot{q}_{conv}$ = convection heat transfer between flame and liquid surface, W
$\dot{q}_{rad}$ = radiant heat transfer between flame and liquid surface, W

Hall [18], using Equation 2.19, had quantitatively pointed out the predominant heat flux as a function of the pool diameter, which consequently controls the burning rate. In the case of large diameters, radiation energy, which is the last term in Equation 2.19, is recognized as the dominant mode [15].

2.2.3 Experimental Values of Burning Rate

The previous subsection discussed the basic scientific concepts dealing with the burning rate of liquid pool fires as a function of the pool diameter. This subsection discusses experimental work on the burning rate of various crude oils.

Equation 2.14, which can be used to calculate the burning rate per unit surface area based on the pool fire diameter, is known by its accuracy in reflecting the experimental data for some hydrocarbon fuels such as gasoline. A survey was conducted to collect available data for gasoline, crude oil and kerosene to be used with Equation 2.14. The collected data are listed in Table 2.8, which also provide the density, heat of combustion, and radiant fraction.

Table (2.8): Thermochemical and Empirical Constants for Gasoline, Kerosene, and Crude Oil.

Material [Reference]	ρ_l (kg/m^3)	$\dot{m}''_\infty$ (kg/m^2·s) x 10^{-3}	$k\beta$ (m^{-1})	ΔH_c (MJ/kg)	Diameter Range(m)	χ_{rad} % Radiation Fraction
Gasoline [17]	740	51	2.1	-	-	18
Gasoline [22]	-	62	-	-	1.5-223	-
Kerosene [17]	820	39	3.5	-	-	-
Kerosene [22]	-	65	-	44.1	20-80	-
Crude Oil *[17]	830-880	22-45	2.8	-	-	18
Crude Oil [22]	-	56	-	-	6.5-31	-
Weathered Crude Oil [19]	800-885	6.6-9.6	-	38.0	-	60-67
Crude Oil [24]	840	33.6-49.1	-	-	-	16-26
Crude Oil [2]	*Arabian light*	44.2	-	-	-	-
Crude Oil [8]	870	60.9	-	-	1.9	-

Note: Data are used for Figure 2.11
Weathered means that crude oil was left at room temperature for a period of time until all light hydrocarbons evaporated

In Table 2.8, the mass burning rate per unit surface area for a pool of infinite diameter for crude oils varies from 22.0 x 10^{-3} kg/m^2·s to 60.9 x 10^{-3} kg/m^2·s. From reference [17], the burning rate $\dot{m}''_\infty$ of crude oils with densities ranging from 830 kg/m^3 to 880 kg/m^3 ranges from 22 x 10^{-3} kg/m^2·s to 45 x 10^{-3} kg/m^2·s. The high values are expected to occur for the low density crude oils. Reference [24], however, shows a large range of the burning rate for crude oil with a density of 840 kg/m^3, while reference [8] shows that a high density crude oil could have a burning rate of 60.9 kg/m^2·s. These data indicate that density alone can not provide an accurate estimation of the burning rate for crude oils.

Koseki and Mulholland [25] reported a relationship between the pre-boilover burning rate and pool diameter based on collected data which are represented in Figure 2.10. The figure shows that the burning rate increases with diameter up to 4.5 mm/min for a diameter of 10 m and then it starts to decrease. This decrease is attributed to poor mixing in large diameter pool fires.

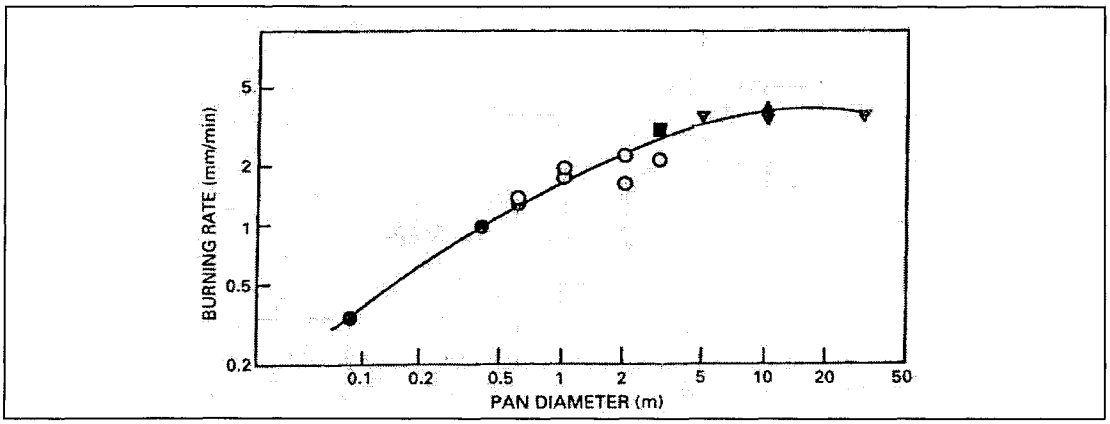

Figure (2.10): Relationship between Burning Rate and Pan (Pool) Diameter Reproduced from [25].

To compare the experimental values of burning rate shown in Figure 2.10 with the values which could be obtained from Equation 2.14, four cases are generated using the data from crude oil from reference [17]. These generated cases are summarized in Table 2.9.

Table (2.9): Four Cases Generated for Crude Oil Using Empirical Values from [17].

Case	ρ_l (kg/ m^3)	$\dot{m}''_\infty$ (kg/m^2·s) x 10^{-3}	$\kappa\beta$ (m^{-1})
1	830	22.0	2.8
2	830	45.0	2.8
3	880	22.0	2.8
4	880	45.0	2.8

Figure 2.11 plots the burning rates for the four cases computed using Equation 2.14 and the experimental data reported by Koseki and Mulholland [25].

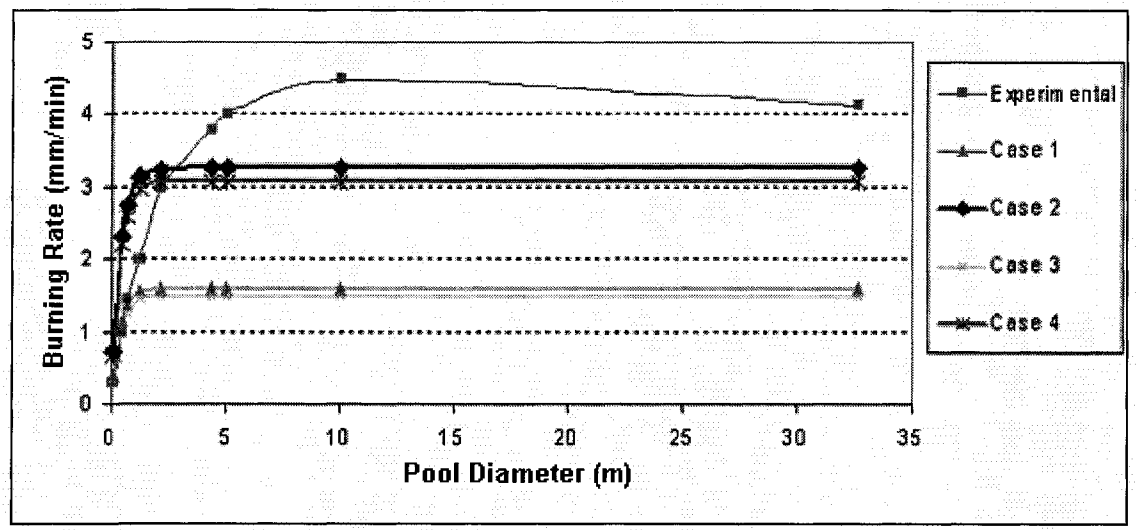

Figure (2.11): Comparison between Burning Rate and Pool Diameter for Experimental and Empirical Values.

This comparison, demonstrated in Figure 2.11, shows that the experimental values of the burning rate are higher than any of the calculated burning rates of the four cases. This variation between experimental and calculated values of burning rates indicates a need for further studies of the burning rate for crude oil pool fires.

2.2.4 The Natural Diffusion Flame of Pool Fires

An important parameter of pool fires is the level of thermal radiation received by objects engulfed in flames as well as by surrounding objects. Generally, studies of pool fires focus on flame geometry, heat release rate, radiant fraction, soot formation, flame temperature, flame emissivity, target absorptivity, view factor, and surface emissive power [17][19].

The flame geometry calculation is generally performed assuming that the flame is a solid, gray emitter with a well-defined shape [26]. The flame shapes of self-sustaining combustion can be treated either as upright/tilted cylinders or as conical [17].

The effect of pool diameter and burning rate on flame height was studied and correlated by many investigators such as Thomas in 1963 and Heskestand in 1983 [17]. Heskestad's correlation, for estimating the height H of a natural diffusion flame in a pool fire, rendered below in Equation 2.20, was recognized for its ability to accurately predict flame height by Shokri and Beyler [21].

$$H = A\,\dot{Q}_{tot}^{2/5} - 1.02\,d \tag{2.20}$$

$$A = 15.6\left[\frac{C_p T_\infty}{g\rho_\infty^2 (\Delta H_c / r)^3}\right]^{1/5} \tag{2.21}$$

where H = flame height, m
A = flame height coefficient, m $kW^{-2/5}$
$\dot{Q}_{tot}$ = total heat release rate, kW
d = pool fire diameter, m
C_p = specific heat of air at constant pressure, kJ/kg·K

g = acceleration of gravity constant, 9.81 m^2/s
T_∞ = ambient air temperature, K
ρ_∞ = ambient air density, kg/m^3
r = mass stoichiometric ratio of air to volatiles, dimensionless
ΔH_c = heat of combustion, kJ/kg

In Equation 2.21, the ratio $\Delta H_c / r$ remains within the range of 2,900 to 3,200 kJ/kg for a large number of liquid fuels under normal atmospheric conditions, which causes A to fall between 0.226 and 0.240 m $kW^{-2/5}$, with a typical value of 0.235 m $kW^{-2/5}$. However, A might still deviate from that range for fairly common flammable hydrocarbon fuels, such as gasoline 0.200 m $kW^{-2/5}$ and acetylene 0.211 m $kW^{-2/5}$ [26].

Iwata and Koeski [24] experimentally showed that Equation 2.20 might not be applicable for large-scale pool fires. Their fire experiment was conducted on a 20-m pool filled with a conventional crude oil. The ratio of flame height-to-diameter was 0.88 using Equation 2.20, while the experimental value of that ratio was found to be 1.9 ± 0.3. The explanation for their finding was that Equation 2.20 was developed using flame height data measured from small-size pool fires.

Blinov and Khudiakov in 1957 [17] found that the relation between the ratio of flame height-to-pool diameter and pool diameter as shown earlier in Figure 2.7. This ratio decreases when the pool diameter increases in the laminar and transition regimes. Then, the ratio remains fairly constant in the turbulent flow regime. Bratz and Schonbunches [27] represented this relation in a small sketch shown in Figure 2.12.

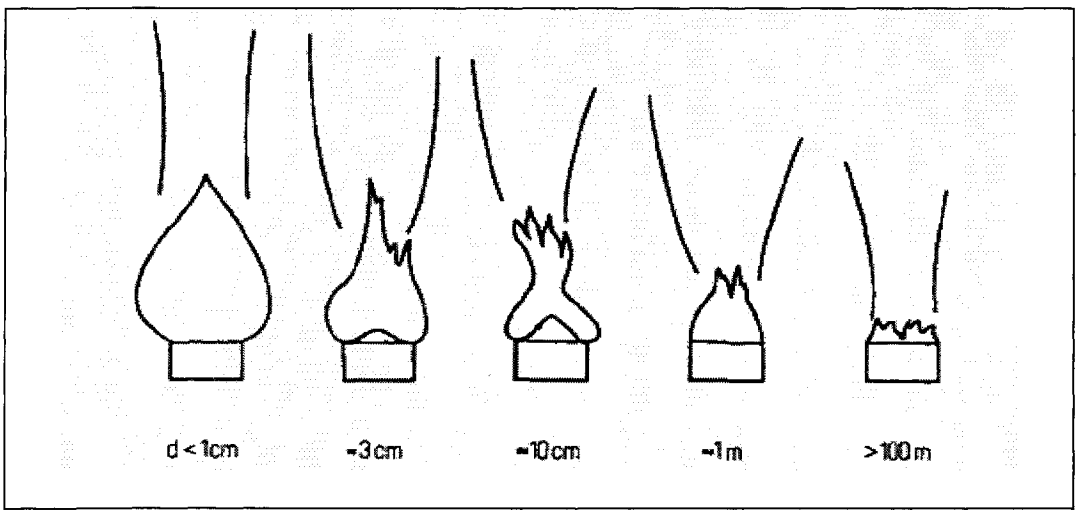

Figure (2.12): Flame Height Representation Scale with Pool Diameter, Taken from [27].

The total heat release rate can be determined knowing the average burning rate as a function of the pool diameter (covered in Section (2.2)). Equation 2.22 calculates the total heat release rate of a crude oil fire as a function of the pool diameter and specific gravity, as below [17]:

$$\dot{Q}_{tot} = \dot{m}'' A \, \Delta H_c \tag{2.22}$$

where $\dot{m}'' = \dot{m}''_{\infty}(1 - \exp(-\kappa\beta d))$

$Q_p = 46{,}513 - 8{,}800\,SG^2 + 3142.8\,SG$

$\dot{Q}_{tot}$ = total heat release rate, kW

$\dot{m}''$ = mass burning rate per unit surface area, kg/m^2·s

ΔH_c = heat of combustion, kJ/kg

A = pool fire surface area, m^2

$\dot{m}''_{\infty}$ = mass burning rate for a pool of infinite diameter, kg/m^2·s

κ = absorption-extinction coefficient, m^{-1}

β = mean beam length corrector, dimensionless

d = diameter of pool fire, m

SG = specific gravity of crude oil, dimensionless

Q_p = low value of heat of combustion at constant pressure, kJ/kg

The radiation heat fraction for hydrocarbons in pool fires usually lies in the range of 0.18-0.40 [9]. For crude oil combustion, Koseki and Mulholland [25] experimentally calculated the radiative energy fraction χ_{rad} from the net calorific potential of the flame $\dot{Q}_{tot}$ using Equation (2.23):

$$\chi_{rad} = \frac{\dot{Q}_{rad}}{\dot{Q}_{tot}} = \frac{4\pi L^2 \dot{q}''}{\dot{Q}_{tot}} \tag{2.23}$$

where χ_{rad} = radiant heat fraction, dimensionless
$\dot{Q}_{tot}$ = total heat release rate, kW
$\dot{Q}_{rad}$ = radiant heat release rate, kW
$\dot{q}''$ = irradiance heat flux, kW/m^2
L = horizontal distance measured from pool centre, m
π = pi constant, 3.1459 radians

In experiments, the irradiance heat flux $\dot{q}''$ was measured at a distance L which was equal to five times the pool diameter as suggested by Iwata and Koseki [24]. The radiative energy fraction χ_{rad} in the steady state burning mode of pool fires was about 0.30-0.40 [25]. In another set of crude oil experiments, Iwata and Koseki [24] showed the relation between the radiation fraction and the pool diameter. The average irradiance heat fluxes used to calculate the radiation fraction were at a distance of three times the pool diameter. The radiative fractions that were calculated are summarized in Table 2.10. The data shows that the radiative fraction decreases as the pool diameter increases. The explanation for this finding was the large-scale high soot formation due to poor ventilation [24].

Table (2.10): Calculated Radiative Fraction as a Function of Pool Diameter for Oils [24]

Pool Diameter (m)	5	10	20
χ_{rad} (Radiative Fraction) %	26 ± 5.5	22.4 ± 3.8	16.1 ± 4.3

After reaching a maximum value, the effective emissive power of flames decreases with increasing the pool diameter [21], as it can be seen in Table 2.11 which is a summary of experimental data generated by Shorki and Beyler [21]. This reduction in the effective power is related to poor ventilation and smoke blockage in large diameter pool fires. However, Koseki and Mulholland [25] said that smoke blockage influences the returned effective emissive power and consequently affects the burning rate.

Table (2.11): Relation between Effective Emissive Power and Pool Diameter [21]

Fuel	Pool Diameter (m)	Data Point	Effective Emissive Power (kW/m^2)
Kerosene	30.0	4	31
	50.0	4	16
Fuel Oil	1.6	4	56
Gasoline	1.0	5	41
	1.12	3	34
	1.5	3	44
	6.0	3	37
JP-4	1.22	4	66
JP-5	2.44	4	44
	3.05	4	57
	5.5	4	69
LNG	14.6	4	61
	16.2	4	52
	18.3	4	54
	24.1	3	46

Flame temperature and flame volume are other physical parameters which can be used to indicate the intensity of a pool fire. Experimentally, flame temperature can be recorded during tank fires. For a general industrial application, a 2-m hydrocarbon fuel pool fire is assumed to have a flame temperature of 900°C with an emissivity of 0.9 [17].

For conventional crude oils, Figure 2.13 shows an example of time history of temperature recoded along the flame axis in a 20-m pool fire reported by Iwata and Koseki [24]. The temperature at the base of the flame was measured to be between 1,000°C and 1,300°C.

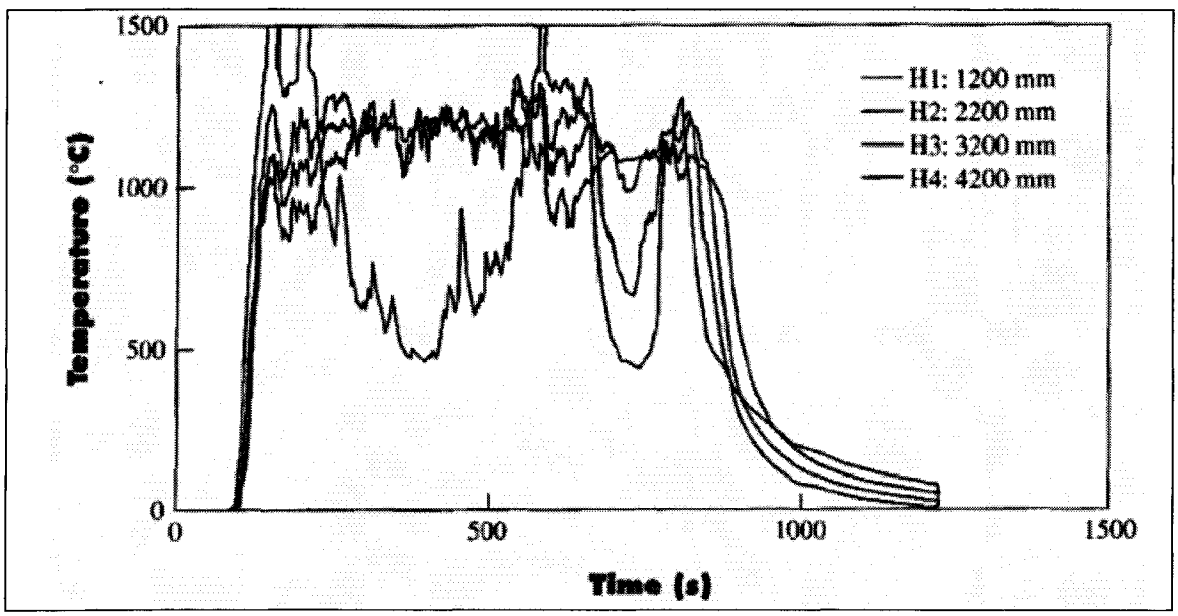

Figure (2.13): Temperature History of Flame Axis at Various Height Locations [24].

Iwata and et al. [8] investigated the Infra Red (IR) images for crude oil pool fires with a diameter of 1.9 m. Figure 2.14 represents the absolute flame temperature. The maximum flame temperature in that fire was 1,152°C (1,420 K).

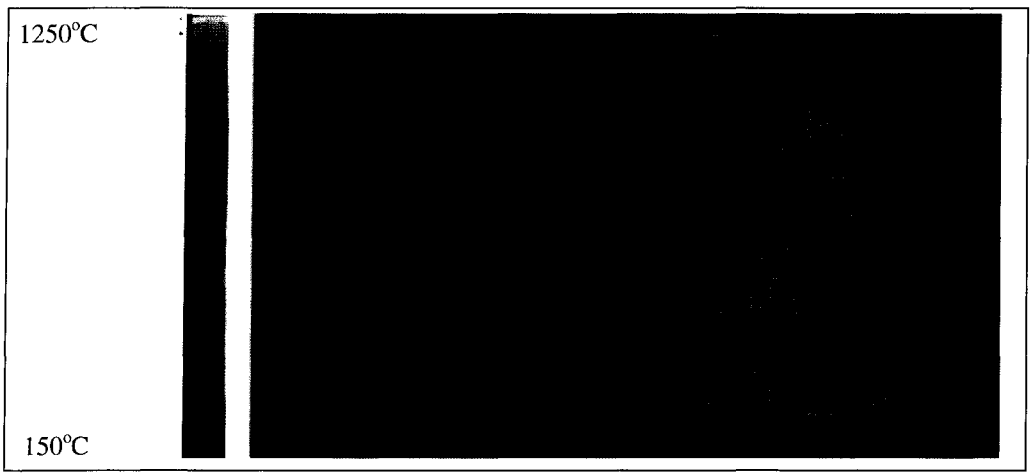

Figure (2.14): IR-Images for Absolute Flame Temperature of Crude Oil Pool Fire at Steady State (Left) and Boilover (Right), Reproduced from [8].

The effective emissive power from the flames can be determined using Equation 2.24 using the flame temperature and emissivity.

$$E = \varepsilon \sigma T_f^4 \tag{2.24}$$

where E = effective emissive power from flame into liquid, W/m^2
ε = emissivity of flame, dimensionless
σ = Stefan-Boltzmann constant, 5.6707 x 10^{-8} W/m^2·K^4
T_f = absolute flame temperature, K

Hall [18] suggested that the liquid fuel temperature does not have any influence on the flame temperature; however, the flame temperature has a major influence on the liquid temperature.

2.2.5 Liquid Fuel Temperature

The liquid fuel temperature increases as a result of radiation heat energy from the flame. This thermal energy is transmitted within the liquid bulk by conduction and convection. This section investigates the liquid fuel temperature profile to understand the physical response and identify any physical processes that might occur.

It is generally accepted that in crude oil fires with no water layer, the temperature of the liquid rises first to a certain temperature at which light hydrocarbons evaporates and then, the temperature rises again to another higher distillation point. These steps of temperature rises are repeated several times until the oil liquid is fully burned. In some cases, the burning fire might leave a dense black liquid (residue) at the bottom of the tank [18]. The properties of the residue are very different from those of the original crude oil. For example, in a particle use, the flashpoint was higher than the original, and the density was about 950-990 kg/m^3 whereas the original crude oil density was 850 kg/m^3 [28].

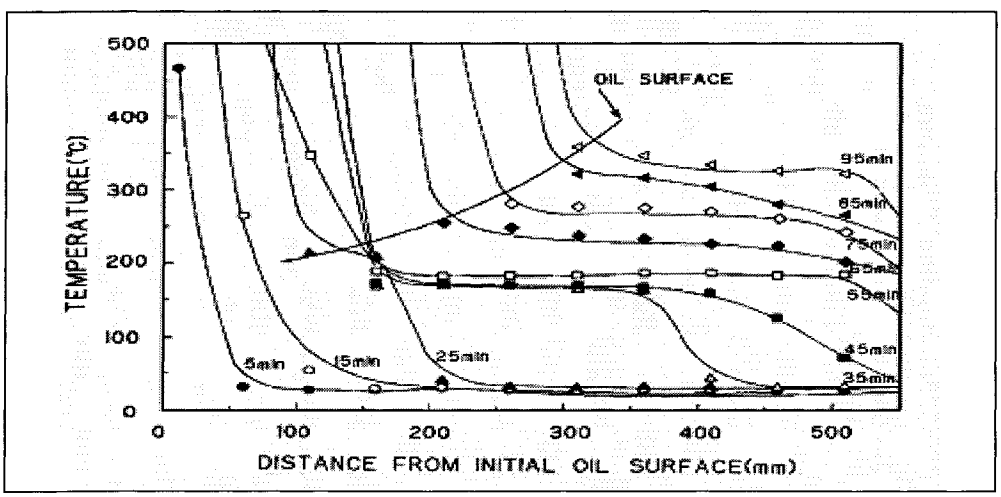

Figure (2.15): Temperature Distributions during Burning of Crude Oil, Reproduced from [8]

To illustrate the expected distillation process from experimental results, Figure 2.15 shows the temperature profiles of a 0.5 m crude oil layer in a 4-m diameter tank obtained from [8]. As shown in Figure 2.15, in 55 minutes, the crude oil temperature is uniform over the hot zone except at a small layer under the fuel surface. The liquid bulk temperature continues to rise with time. Figure 2.16 shows temperature profiles in the oil layer of a test using a tank of 1.9 m diameter with the oil thickness of 0.4 m and water layer thickness of 0.3. Temperatures shown in Figure 2.15 and Figure 2.16 at different depths were taken at the centre of the tank.

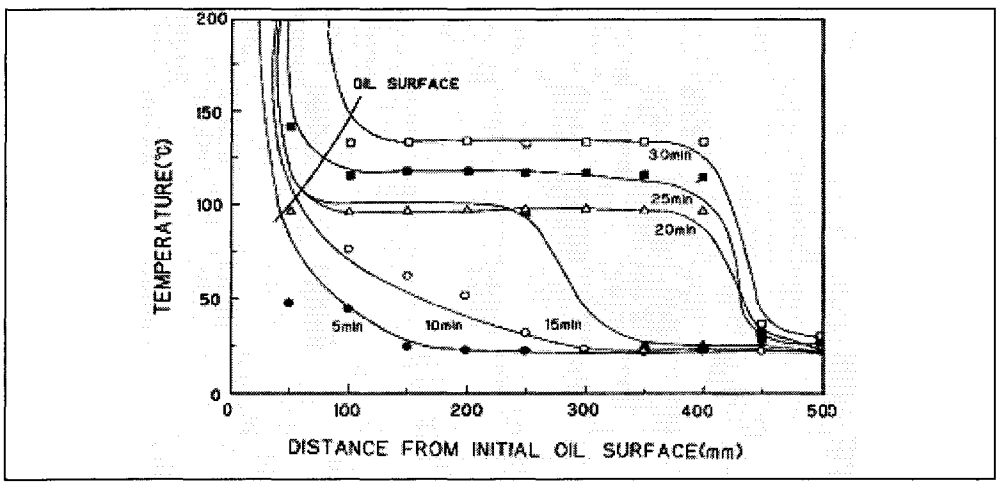

Figure (2.16): Vertical Temperature Distributions during Burning of Crude Oil Reproduced from [8]

The isothermal layer temperature is a function of the thermal and physical fuel properties. The hot zone temperatures during the boilover event vary from one experiment to another. For example, the isothermal oil temperature of Sarukawa light crude oil was about 130°C [8]. In other experiments conducted by Husa et al. [29], the local oil temperature was about 235°C-260°C in the light crude oil hot layer. The temperature profile in the Arabian light crude oil combustion experiment, which was conducted by Broeckmann and Schecker [2] in a 1-m diameter pan, showed that the

isothermal oil layer temperature of the developed hot zone was between 150°C and 170°C. Even thought, all of the above crude oils are classified as conventional type, each one has its own hot zone temperature.

Hall [4] has suggested that the distillation of light hydrocarbon fractions in the hot zone layer causes a formation of denser surface layers. However, Burgoyne and Katan [30] agree with Hall's concept of a flash distillation of light components of crude oil inside the liquid bulk, but disagree with the formation of a denser surface layer. This illustrates the need for further research to understand the thermal and physical processes taking place in the crude oil during a fire.

2.3 Mathematical Models

The NFPA as discussed in Section 2.1 indicates that boilover occurs when the developed hot zone in an oil storage tank reaches the surface of the water layer. This understanding came from analyzing various comprehensive experimental results which show the temperature distribution inside the liquid bulk.

In the last two decades, a number of mathematical studies have been conducted which have resulted in models that calculate the temperature profiles of the oil and water layers. In this section, a review of these mathematical models is presented and the assumptions and approximations used are discussed.

2.3.1 One-Dimensional Semi-Infinite Element Model

A one-dimensional model was developed by Torero et al. [23] to study and analyze a slick of burning crude oil floating on water. The main objective of this model was to determine the burning rate, which might constitute a hazard to off-shore exploration, production and transportation.

The conduction heat energy for a one-dimensional semi-infinite element is governed by Equation 2.25

$$\frac{\partial^2 T}{\partial z^2} = \frac{1}{\alpha_l}\frac{\partial T}{\partial t} \tag{2.25}$$

where α_l is the thermal diffusivity of the fuel. Equation 2.25 can be solved analytically after applying the initial and boundary conditions. The solution gives the temperature profile in the oil layer domain by the following equation:

$$\frac{T - T_\infty}{T_s - T_\infty} = \exp\left(-\frac{r(t)}{\alpha_l}\left(z - z_s(t)\right)\right) \tag{2.26}$$

Here, the regression rate r(t) was assumed constant, where $r(t) = \frac{\partial z_s(t)}{\partial t} = \frac{\dot{q}''_s - \dot{q}''_{cond}}{L_H \rho_l}$, and the net heat flux into the oil layer $\dot{q}''_s$ was,

$$\dot{q}''_s = \chi_{ret}\frac{4\rho_\infty C_p\left(T_{\infty,a} g\left(T_f - T_\infty\right)\right)^{1/2} d^{1/2}}{\pi} \tag{2.27}$$

The conduction heat flux was computed using $\dot{q}''_{cond} = -\lambda_l \left.\frac{\partial T}{\partial z}\right|_{y=y_s(t)}$ (2.28)

where T = fuel absolute temperature, K
T_∞ = fuel absolute ambient temperature, K

T_s = fuel temperature at surface, K
T_f = average flame temperature, K
α_l = thermal diffusivity of fuel, m^2/s
λ_l = thermal conductivity of fuel, W/m K
$z_{s,i}$ = characteristic length for fuel layer, m
C_p = specific heat at constant pressure for air, J/kg·K
$T_{\infty,a}$ = ambient temperature of air
ρ_∞ = density of the air at ambient temperature
g = acceleration of gravity constant, 9.81 m/s^2
d = pool surface diameter, m
χ_{ret} = fraction of total heat absorbed by liquid surface, dimensionless
t = time, s
$\dot{q}''_s$ = heat flux rate absorbed by fuel surface , W/m^2
$\dot{q}''_{cond}$ = heat flux rate conducted though fuel layer, W/m^2
π = pi constant, 3.1459 radians
z = depth distance in fuel layer, m
r = regression rate, m/s
L_H = latent heat of evaporation, J/kg
ρ_l = fuel density, kg/m^3

2.3.2 One-Dimensional Two-Layer Conduction Model

The thermal diffusivity of water is of significant importance once the heat wave reaches the water layer. At this time, the water layer starts acting as if it is a heat sink. To improve the previous concept presented in subsection (2.3.1), Torero et al. [23] included the thermal diffusivity of the water layer using an equivalent thermal diffusivity for both layers as shown in Equation 2.29.

$$\alpha_{EQ} = \frac{r\, z_{s,i}}{\alpha_l}\left(\sqrt{\alpha_w} + \sqrt{\alpha_l}\right)^2 \tag{2.29}$$

Equation 2.29 was substituted into Equation 2.26 and solved for the average regression rate $r(t)$ giving:

$$r(t) = \frac{1}{L_H \rho_l}\left[\chi_{ret}\left(\frac{4\rho_\infty C_p\left(T_{\infty,a} g\left(T_f - T_\infty\right)\right)^{1/2}}{\pi}\right)d^{1/2} - \frac{\alpha_l \lambda_l (T_s - T_\infty)}{z_{s,i}\left(\sqrt{\alpha_w} + \sqrt{\alpha_l}\right)^2}\right] \tag{2.30}$$

where T_∞ = fuel absolute ambient temperature, K
T_s = fuel temperature at surface, K
T_f = average flame temperature, K
α_l = thermal diffusivity of fuel, m^2/s
α_{EQ} = equivalent thermal diffusivity, m^2/s
α_w = thermal diffusivity of water, m^2/s
λ_l = thermal conductivity of fuel, W/m K
$z_{s,i}$ = characteristic length for fuel layer, m
C_p = specific heat at constant pressure for air, J/kg·K
$T_{\infty,a}$ = ambient temperature of air, K
ρ_∞ = density of the air at ambient temperature, kg/m^3
g = acceleration of gravity constant, 9.81 m/s^2
d = pool surface diameter, m
χ_{ret} = fraction of total heat absorbed by liquid surface, dimensionless
t = time, s
$\dot{q}''_s$ = heat flux rate absorbed by fuel surface, W/m^2
$\dot{q}''_{cond}$ = heat flux rate conducted though fuel layer, W/m^2
π = pi constant, 3.1459 radians
z = depth distance in fuel layer, m
r = regression rate, m/s
L_H = latent heat of evaporation, J/kg
ρ_l = fuel density, kg/m^3

This model accurately computed the regression rate of fuel layers thicker than 2 mm [23].

In the two models presented, pure conduction was assumed to be the main medium for heat penetration into the bulk of the liquid. According to Hall [4], the amount of heat able to penetrate below the fuel surface is larger than the amount that can be

transferred by conduction. For this reason, Hall had experimentally investigated the surface layer, looking for further explanations, and found that beside conduction, there is a heat wave traveling through the liquid layer.

2.3.3 One-Dimensional Thermal Energy Model

In 1995, Broeckmann and Schecker [2] developed a one-dimensional energy model to predict the temperature profile in a 2-m diameter crude oil storage tank due to fire. The governing differential Equation 2.31 was numerically solved for a two-zone fuel.

$$\frac{\partial T}{\partial t} = \frac{\partial}{\partial z}\left(a_\varepsilon \frac{\partial T}{\partial z}\right) + v_a \frac{\partial T}{\partial z} + \frac{k}{\rho C_p}\dot{q}_{rad}\exp(-\eta z) \tag{2.31}$$

where, T = fuel temperature, °C
t = time, min
a_ε = modified thermal diffusivity, m^2/min
z = distance to the fuel surface, m
v_a = burning velocity, m/min
k = thermal conductivity, W/m·K
$\dot{q}_{rad}$ = radiant heat flux, W/m^2
ρ = fuel density, kg/m^3
C_p = specific heat, J/kg K
η = absorption coefficient of burning fuel, m^{-1}

The maximum temperature for the upper region of the fuel was restricted to the boiling temperature of the fuel at each time step. The radiation heat was assumed to be absorbed exponentially into the liquid bulk. The radiant heat flux into the liquid bulk was experimentally obtained to be 40 kW/m^2 for a crude oil fire in a 2-m diameter storage tank. The modified thermal diffusivities were assumed to be 30 mm^2/min in the hot zone

and 4.5 mm^2/min in the cold zone. These figures were found by trial and error. A linear reduction of the thermal diffusivities was assumed between the zones. The radiant energy absorption coefficient of the burning fuel was set between 100-150 m^{-1}. Tank wall heat fluxes were claimed to be the main reason behind the accumulated errors in their approach to small-sized diameter storage tank calculations.

Broeckmann and Schecker [2] had said in their conclusion " *is still impossible to predict the hot-zone temperature before experimentation, as it is influenced by too many parameters. Experimental inaccuracies and variations make further validation of the model very difficult.*"

2.3.4 Finite Element Energy Balance Model

A finite element was developed by the Japanese Heat and Flow Research Institute in 1997 [31]. The main objective of this model was to investigate the heat transfer mechanisms between the tank wall and the surrounding (flame, fuel, surrounding air) in a medium-scale test. The focus was to explain the phenomena observed in the hot zone forming pool fires. The model assumed that the physical properties of the tank walls were temperature independent. Flame temperature was assumed to be 1,000°C and thermal conductivity of the hot gas was taken as k = 0.24 kW/m^2K. Moreover, the convective fraction of the total input heat to the fuel surface from the flame and the gas above the fuel surface was taken as 20%, independent of the fuel type.

The model calculations did not show a significant difference in the rate of heat transfer between the wall and the hot-zone in small-size pool fires. The justification was that the model did not consider the large decrease of the growth rate of the hot-zone thickness, and specific heat of liquid with time.

The literature review on mathematical modelling of the conditions in the crude oil bulk during a fire indicates the need to further investigate the problem. This investigation should be done to ensure a better understanding of the processes taking place in the tank during a fire that lead to a boilover.

3. PROBLEM DEFINITION

3.1 Introduction

Since the 1950s, a total of 450 tank fire incidents have occurred [32]. Although the occurrence of storage tank fires is quite low, the consequences of these fires are quite high, both in terms of potential for life loss and property damage. The potential for high levels of damage is also due to the fact that as the tank diameter increases so does the probability that the fire will be left to freely burn until all the fuel has been consumed. This results in heavy smoke filling the environment causing health and environmental problems. As a result of these concerns, a project has been initiated in 2005 and is being carried out by the Resource Protection International on behalf of sixteen oil companies. The project is called LASTFIRE and some of its objectives are to experimentally study boilover, to estimate the boilover time and its intensity [32].

Experimental studies of the behaviour and the resulting consequences of crude oil tank fires can provide solutions and techniques on how to extinguish large crude oil tank fires of 100 m or more in diameter [32]. Once crude oil tank fire behaviour is understood, mathematical models can be developed to accurately estimate boilover time, burning rate, the magnitude of the radiation heat flux from the fire, flame height and fire spread from one tank to another.

Some of the technical questions which have already been raised in the review of previous studies and are considered in this study are:

- What are the heat and mass transfer processes taking place in the tank during a fire?
- What is the effect of crude oil composition on the oil liquid temperature?
- What is the effect of the oil viscosity on the liquid temperature profile?
- What are the effects of the thermodynamic properties of oil?
- What is the effect of the water layer on the temperature profiles in the oil?
- What is the effect of cooling the walls of the tank during the fire period?

3.2 Problem Definition

To provide answers to the questions raised above and to achieve the objectives of this work as described in Chapter 1, this study aims at developing a mathematical model to study heat and mass transfer in crude oil storage tanks subjected to a fire at the liquid top surface. Figure (3.1) shows a schematic of the physical domain of the engineering problem.

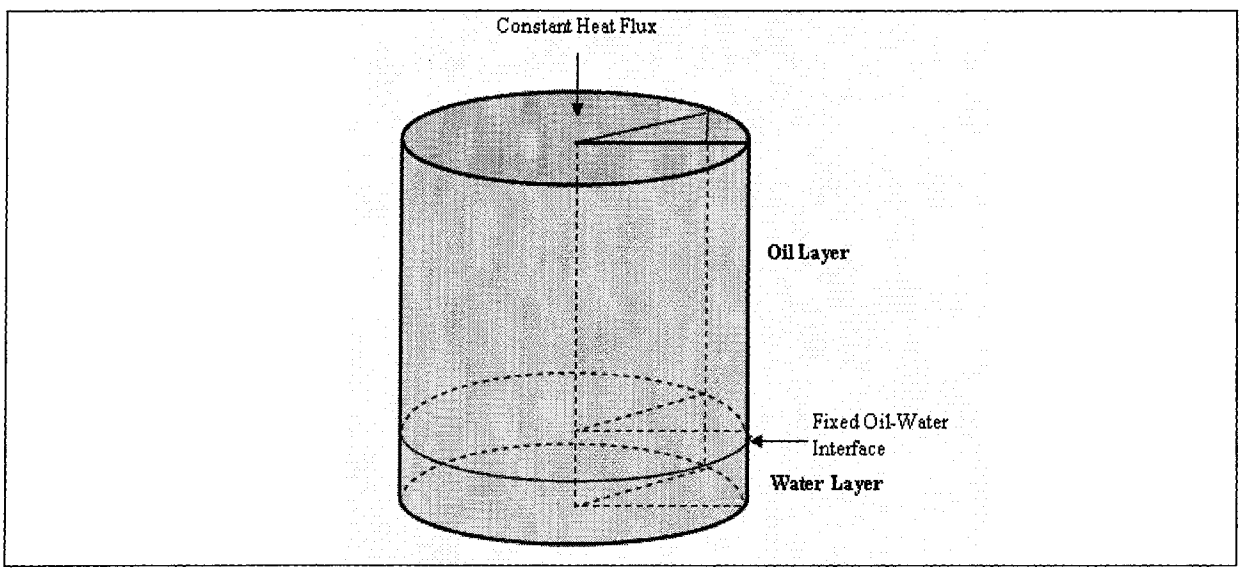

Figure (3.1): Physical Domain of the Engineering Problem.

To simplify the mathematical model, the tank considered for the study is an open tank without a cover or a floating roof. The tank is filled with crude oil that is assumed to be homogenous with uniform properties. This assumption is necessary to avoid considering chemical kinetics, interactions and physical separations in the forms of extraction and absorption which might happen in the multi-component substance under temperature gradients. The physical properties of the crude oil including the density are specified as a function of temperature, an assumption that together with buoyancy causes fluid movements in the tanks.

To realistically simulate crude oil storage tanks, a water layer is added at the bottom of the tank. The thermal and physical properties of water are assumed to be dependent of temperature. A pure conduction mechanism is assumed to transmit all thermal energy at the interface layer between water and oil. For simplicity, the interface between the oil and water layers is assumed to be fixed and free of shear stress.

As a result of the combustion of the vapours above the surface of the crude oil, a constant radiant heat flux is received and totally absorbed at the surface of the crude oil. The radiant heat flux is computed based on experimental data for flame temperatures. Details on the radiant heat flux calculation can be found in Chapter 4.

The incident radiant heat flux increases the temperature at the surface of the oil layer resulting in heat transfer by conduction to the bulk of the liquid and in fuel evaporation. The developed model considers this process by solving the fundamental equations of mass, momentum and energy as described in Chapter 4. The results of the mathematical model include temperature and velocity profiles in the oil and water layers, and fuel evaporation rates with time. The model also predicts the time for the heat wave to reach the water layer.

4. MATHEMATICAL MODELLING

4.1 Governing Equations

The unsteady, turbulent, free convective and non-isothermal motion of the fluid contained in a cylindrical enclosure is modeled using the Boussinesq approximation form of the Navier-Stokes equations for the density variation [34]. Fluid properties such as kinematic viscosity (υ), thermal diffusivity (α), thermal conductivity (k), and coefficient of thermal expansion (β) are assumed constant at each time step. The viscous dissipation term in the kinetic energy is neglected. Chemical kinetics are also neglected in the liquid bulk. A constant heat flux at the oil surface is assumed as a source term of the energy equation. Density variations due to thermal expansion and/or distillation effects are the driving forces in the vertical direction of the coupled momentum equations and thermodynamic equilibrium governs the equations of state. Under these circumstances, the governing equations, for mass, momentum, and thermal energy in the three-dimensional form, are listed below:

The continuity equation, Equation 4.1, expresses the law of mass conservation. Equation 4.1 states that the net rate of mass flux in and out of the control volume is equal to zero.

$$\iint \rho(v \cdot n) dA = 0 \tag{4.1}$$

Where the physical interpretation of $v \cdot n$ is the component of velocity vector v in the direction of the vector n normal to the surface element dA [36].

The Navier-Stokes equation, which represents the vector momentum equations, and the kinetic energy *(convection-diffusion)* equation are mathematically represented in the following general integral form [36]:

$$\int_{\Delta t}\frac{\partial}{\partial t}\left(\int_{CV}(\rho\phi)dV\right)dt+\int_{\Delta t}\int_{A}n\cdot(\rho\phi v)dA\,dt=\int_{\Delta t}\int_{A}n\cdot(\Gamma_{\phi}\,grad\,\phi)dA\,dt+\int_{\Delta t}\int_{CV}S_{\phi}dVdt \qquad (4.2)$$

Where ϕ = general variable representing velocities in momentum equations, and temperature in the energy equation.
ρ = density of fluid, kg/m^3
V = volume, m^3
t = time, s
v = velocity vector, m/s
Γ_{ϕ} = diffusion coefficient
A = surface area of control cell, m^2
S_{ϕ} = volumetric rate of generation

To measure the ratio of the buoyancy forces relative to the viscous forces acting on the fluid, and for faster convergence of the numerical technique, a normalization scheme is introduced. Details on how the governing equations for cylindrical coordinates were normalized are provided in Appendix A in partial differential form.

The governing equations are solved over the computational domain shown in Figure 4.1. As shown in the figure, only a section of the physical domain is used because the solution is assumed to be independent of the angular location.

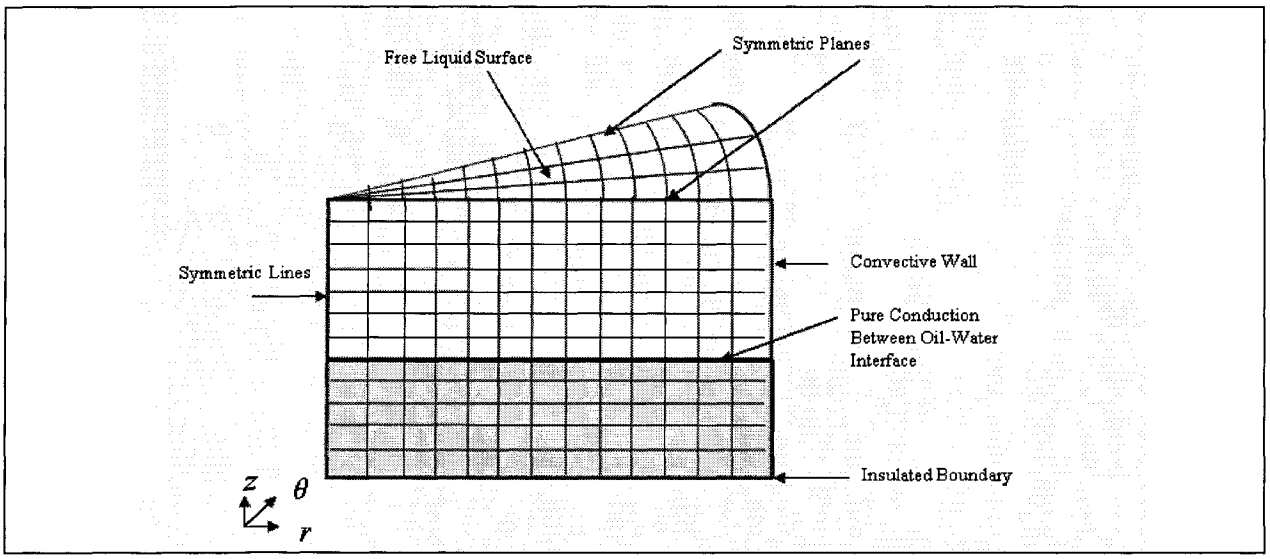

Figure (4.1): Schematic showing Calculation Domain Used in This Research.

4.2 Numerical Solution of Governing Equations

The general transport Equations 4.1 and 4.2 can be solved analytically under a very limited set of initial and boundary conditions and for a limited number of geometric shapes. However, for most cases, numerical solutions become obligatory. The mathematical problem is reduced once the domain is defined and discretized at a number of points (grid points). The governing equations are transformed into a system of algebraic equations that can be solved numerically using a computer. As a consequence of the discretization, the solution is no longer exact, but only an approximation. In general, depending on the nature of the scientific problem, the accuracy of the solution can be improved by decreasing the mesh size, increasing the iteration cycles, changing the iterative method, and/or decreasing the size of the time marching step. Many discretization methods have been used in the past for solving the governing partial differential equations. The most commonly used methods are the finite difference, finite element, and control-volume.

The finite difference method was described in 1768 by Euler, which makes it the oldest discretization method, while the finite element method (FEM) and its mathematical foundations were established early in the 20th century by Ritz and Galerkin [33]. The control-volume formulation of discretization is the third technique that was originally developed as a special finite difference formulation [36]. This method divides the calculation domain into a finite number of non-overlapping cells at which conservation is established. For this work, the control-volume discretization method is used to convert the governing partial equations into a set of algebraic equations. The control-volume formulation of discretization is the method used in commercial CFD packages because its mathematical concepts are easy to understand and have physical meaning [36].

4.2.1 Discretization of the Transient Term

Crank-Nicolson's (Crank and Nicolson, 1947), explicit and fully implicit schemes are the three best-known schemes to approximate the transient term in the multi-dimensional unsteady momentum and convection-diffusion energy equations [36].

The fully implicit scheme is used in this work. In the fully implicit scheme, both sides of the set of algebraic equations contain parameters at the new time step. The system of algebraic equations is solved iteratively within each time step. The fully implicit scheme is unconditionally stable once all coefficients are positive. To increase accuracy of this first order scheme, a small time step should be applied [36].

4.2.2 Discretization of the Remaining Terms of the Governing Equations

Integrating the remaining terms of Equations 4.2 over the control volumes surrounding the grid points gives the general form of the algebraic equation. A typical grid point P,in r-θ plane and its associated control volume are shown in Figure 4.2 [35].

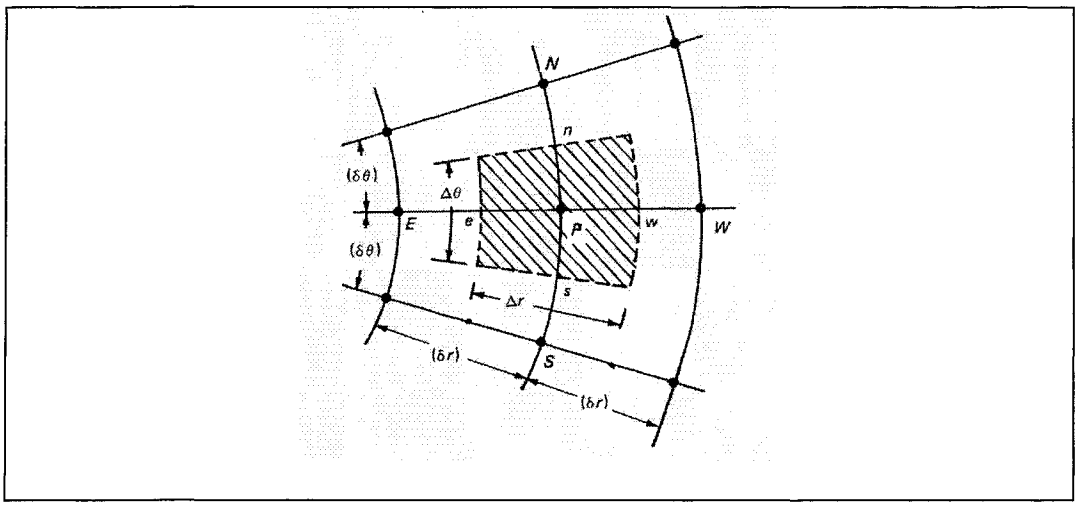

Figure (4.2): Control Volume of r-θ Plane in Cylindrical Coordinates.

The integrations in terms of control face fluxes after applying Fick's law [35] with a diffusion coefficient Γ_ϕ , a convected flow with velocities (u ,v ,w), a volumetric rate of generation S, and density ρ give the following general equation

$$J_r^e + J_\theta^n + J_z^t = J_r^w + J_\theta^s + J_z^b + S\Delta V \tag{4.3}$$

Where: $J_r^e = \rho u\phi - \Gamma\dfrac{\partial\phi}{\partial r}$ (4.4)

$$J_\theta^n = \rho v\phi - \Gamma\frac{\partial\phi}{\partial\theta} \tag{4.5}$$

and $$J_z^t = \rho w\phi - \Gamma\frac{\partial\phi}{\partial z} \qquad (4.6)$$

represent the radial, circumferential and axial components of the total flux ϕ due to convection and diffusion. The value of the normal flux component is assumed uniform over the control volume surface. The subscripts on J indicate direction, while the superscripts on J indicate the face side of the control volume. For example, J_θ^n indicates the circumferential component of flux at the north face of the control volume. In Equation 4.3 , S represents the source term at point P, and its value is uniform over the control volume.

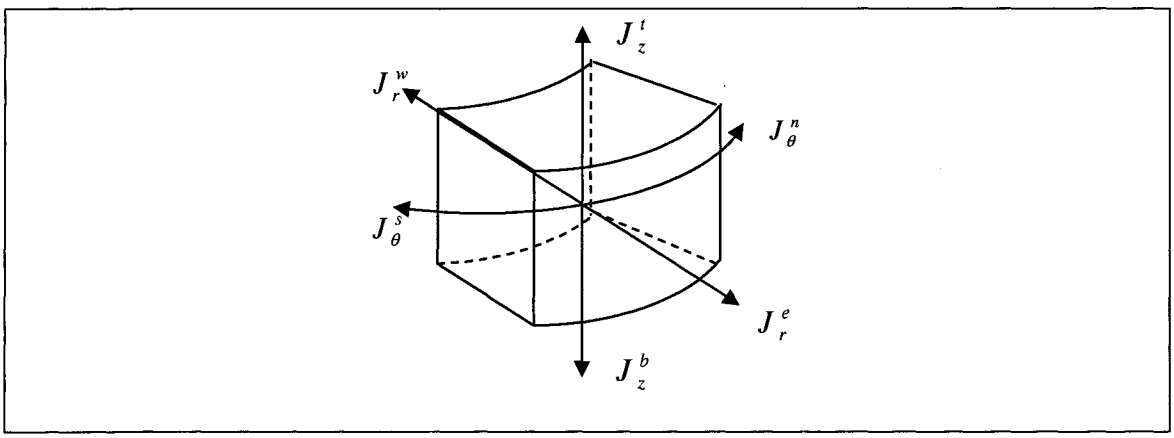

Figure (4.3): Typical Control Volume with Neighbouring Fluxes

The next step is to represent the six different flux components J, in Equation 4.3, in terms of ϕ at point P and its neighbours E, W, N, S, T and B. This step is done using the general form of Patankar [35], to obtain the general algebraic equation in the following form

$$a_p\phi_p = a_E\phi_E + a_W\phi_W + a_N\phi_N + a_S\phi_S + a_T\phi_T + a_B\phi_B + b \qquad (4.7)$$

where $a_E = D_e A(|P_e|) + [|-F_e, 0|]$, $a_W = D_w A(|P_w|) + [|F_w, 0|]$

$a_N = D_n A(|P_n|) + [|-F_n, 0|]$, $a_S = D_s A(|P_s|) + [|F_s, 0|]$

$$a_T = D_t A(|P_t|) + [|-F_t, 0|],\ a_B = D_b A(|P_b|) + [|F_b, 0|]$$

$$a_p = a_E + a_W + a_N + a_S + a_T + a_B + a_p^0 - S_p$$

and F_e: indicates the strength of the convection term at the east face of the control volume.

D_e: shows the diffusion conductances at the east face of the control volume

P_e: represent the ratio between convective and diffusion and is called the local Peclet number $P_e = F_e / D_e$.

[| |]: This operator represents the maximum quantity contained in the brackets. Upwind, central and hybrid schemes are the three different schemes that can be used to solve Equation 4.7.

S: The source term is linearized to give $S = S_c + S_p \phi_p$

b: The source term in Equation 4.7 includes the transient source term and is equal to $S_c + a_p^0 \phi_p^0$, where $a_p^0 = \frac{\rho c_p V}{\Delta t}$ and ϕ_p^0 is the initial value of the field variable.

4.2.3 The Pressure Correction Equation

The continuity Equation 4.1 is integrated over the control volume resulting in a velocity-correction formula. However, after rearrangement, it is converted into a pressure correction under the assumption that the density does not directly depend on field pressure. The general form of the pressure correction is in Equation 4.8 .

$$a_p p_p = a_E p_E + a_W p_W + a_N p_N + a_S p_S + a_T p_T + a_B p_B + b \tag{4.8}$$

Where

$$a_E = \rho_e d_e r \Delta\theta \Delta z$$

$$a_W = \rho_w d_w r \Delta\theta \Delta z$$

$$a_N = \rho_n d_n \Delta z \Delta r$$

$$a_S = \rho_s d_s \Delta z \Delta r$$

$$a_T = \rho_t d_t r \Delta r \Delta\theta$$

$$a_B = \rho_b d_b r \Delta r \Delta\theta$$

$$a_p = a_E + a_W + a_N + a_S + a_T + a_B$$

$$b = \left[(\rho u^*)_w - (\rho u^*)_e\right] r \Delta\theta \Delta z + \left[(\rho v^*)_s - (\rho v^*)_n\right] \Delta r \Delta z + \left[(\rho w^*)_b - (\rho w^*)_t\right] r \Delta\theta \Delta r$$

Where the * represents velocities computed based on guessed pressure.

4.2.4 Differencing Schemes for the Connective Terms

For computing the cell face values for the convective terms in Equations 4.7-4.9, a linear interpolation between the value ϕ_p and ϕ_E can be used to give ϕ_e [1]. However, this scheme gives a reasonable solution only when the grid Peclet number is very small (<2) [36]. *Hadjisophocleous* [37] stated "*The use of the central difference scheme for higher absolute Peclet numbers result in negative coefficients, which violates the stability criterion, and produces unrealistic results. The use of very*

refined meshes may overcome these deficiencies but this results in expensive computations and large computer storage requirements." However, one of the major problems with the central differencing scheme is its inability to identify the flow direction [37].

In order to account for the effect of flow direction on the overall fluid calculation in the central differencing scheme, the upwind scheme is used. A detailed assessment of the upwind scheme can be found in [35].

The third scheme which is a combination of upwind scheme and central difference is the hybrid. The upwind scheme is used at any grid point with a local Peclet number of 2 or more and the central difference scheme elsewhere. The computer model used for this study uses the hybrid scheme for solving the momentum equations and the upwind scheme for solving the energy equation.

4.3 Implementation of Boundary Conditions

Solving the governing equations 4.1 and 4.2 requires defining the initial and boundary conditions. These conditions should be physically and reasonably realistic. In the following subsections, the boundary conditions of the momentum equations, pressure correction equation, and thermal energy equation are discussed.

4.3.1 Momentum Equations

Two types of boundary conditions for the momentum equations were used. The first deals with solid non-slip walls, where the normal and tangential velocity components on the boundary are set equal to zero $u = v = w = 0$. The second boundary condition deals with shear free surfaces, at which the normal velocity component and the normal derivative of the tangential velocity components are zero.

$$u = \frac{\partial v}{\partial r} = \frac{\partial w}{\partial r} = 0$$

4.3.2 Pressure Correction Equation

For a given normal velocity at the sidewall which is equal to zero, the velocity does not require any correction and pressure at that sidewall does not appear in the calculation of the boundary coefficient. Hence, no boundary conditions are needed for the pressure correction equation.

4.3.3 Energy Equation

Three different thermal boundary conditions were used for the energy equation. Those conditions are the insulated boundary for the tank centreline and tank bottom, a convective boundary with a constant heat transfer coefficient for the sidewall surface, and finally conduction heat transfer between the oil and water layers.

a) Insulated Boundary

The normal temperature gradient was taken to be zero at the insulated boundaries. This is conveyed into the finite difference equations by setting the value of temperature at an external point to be equal to the temperature of the control volume near the boundary.

b) Convective Boundary

The convective heat transfer in the sidewalls was approximated using the following energy balance equation

$$Q = -kA\frac{\partial T}{\partial r} = hA(T_w - T_\infty) \tag{4.9}$$

where the heat transfer coefficient at the sidewall was assumed constant. Details on how to discretize Equation 4.9 are provided in Appendix B. After discretizing Equation 4.9, the linearized source terms were as follows:

$$S_c = \frac{2hkAT_\infty}{h\Delta r + 2k} \tag{4.10}$$

$$S_p = \frac{2hkA}{h\Delta r + 2k} \tag{4.11}$$

where S_c = constant source term
S_p = source term function of cell temperature
h = convective heat transfer coefficient, W/m^2 K
k = thermal conductivity of oil, W/m^2 K
A = vertical Area of control cell, m^2
T_∞ = ambient temperature, °C
Δr = width of control cell, m

c) Conduction Boundary

Almost a similar approach to the convective heat transfer boundary condition was used for conduction heat transfer between the oil and water layer using the following equation

$$Q = -kA\frac{\partial T}{\partial z}\bigg|_{oil} = -kA\frac{\partial T}{\partial z}\bigg|_{water} \tag{4.12}$$

Details on how to discretize Equation 4.12 are provided in Appendix B. After discretizing Equation 4.12, the linearized source terms were as follows:

$$S_c = \frac{2k_{oil}k_{water}A}{k_{oil}\Delta z_{water} + k_{water}\Delta z_{oil}} T_{water/oil} \tag{4.13}$$

$$S_p = \frac{2k_{oil}k_{water}A}{k_{oil}\Delta z_{water} + k_{water}\Delta z_{oil}} \tag{4.14}$$

where S_c = constant source term
S_p = source term function of cell temperature
k = thermal conductivity of water or oil, W/m^2 K
A = vertical area of volume control cell, m^2
T_∞ = temperature of water or oil, °C
Δz = height of control volume cell, m
$T_{water/oil}$ = T_{water} if control volume is in water, °C
T_{oil} if control volume is in oil, °C

d) Heat Flux Boundary

At the top surface of the oil, a constant radiant heat flux is assumed. The heat flux is calculated from a constant flame temperature. The heat flux value is incorporated into the discretization of the energy equation with the constant source term S_c as shown in Equation 4.7.

e) Top Layer Temperature

The top layer temperature of the crude oil is assumed to be maintained at the boiling temperature. This was done as follows: at any given time step, once the energy equation is solved, if the control volume has exceeded the specified boiling temperature, the constant source term for the energy equation is recalculated so that the control volume temperature is reduced to the boiling temperature. Equation 4.15 is used to modify the source term for the energy equation to incorporate the energy removed from the system.

$$S_c(new) = \rho C_p V(T - T_B)/\Delta t \tag{4.15}$$

This energy is used to calculated the amount of oil evaporated

$$\rho C_p V(T - T_B)/\Delta t = \dot{m} L_H \tag{4.16}$$

where S_c = constant source term
ρ = crude oil density, kg/m^3
V = volume of control cell, m^3
T = temperature of cell, °C
T_B = temperature at boiling point, °C
$\dot{m}$ = mass evaporation rate, kg/s
L_H = latent heat of evaporation, J/kg

4.4 Solution of the Algebraic Equations

The algebraic equations that resulted from the discretization process of the governing partial differential equations can be solved using either direct or iterative solution methods [35].

4.4.1 Direct Methods

A direct method is a highly economical solution for a linear problem because such a technique requires no iteration. Some methods of the direct method family are the Gaussian elimination and Cramer's rule matrix inversion [36]. However, one of the well-known procedures of the direct method is the Tridiagonal-Matrix algorithm (TDMA) [35]. TDMA is also called Thomas Algorithm which is a combination of forward elimination and backward substitution [36].

4.4.2 Iterative and Mixed Methods

Iterative methods solve the system of equations through an iterative process using a simple algorithm. Simple examples of non-direct iterative methods are the Jacobi and Gauss-Seidel point-by-point methods. A general form of the iterative method is represented in Equation 4.17.

$$\phi_p = \omega\phi_{p\,new} + (1-\omega)\phi_{p\,old} \tag{4.17}$$

An under-relaxation iterative method requires ω, which stand for the relaxation factor, to be positive real number less than 1. An over-relaxation iterative method requires ω to be positive real number over 1.

A convenient combination of the TDMA and Gauss-Seidel method is called a line-by-line method [36]. To overcome and handle nonlinearity issues of the algebraic equations, over-relaxation is often used in conjunction with the Gauss-Seidel method ending in a method recognized as the Successive Over-Relaxation Scheme (SOR) [35].

4.4.3 The Adopted Methods

The computer model used for this study adopts an iterative method using the TDMA line-by-line with alternating directions is used to solve the algebraic equations derived from the momentum and energy equations. Under-relaxation is essential to prevent mathematical divergence. The under-relaxation coefficient used in the program is 0.8 which was found by trial and error. For the solution of the pressure correction equation, the model uses a multi-grid approach.

4.4.4 Numerical Parameters

a) Convergence Criteria

Test runs for a number of simulated cases showed that an under-relaxation factor of approximately 0.8 is sufficient to achieve convergence for solving the momentum equation with a residual of 1.0×10^{-4}. The over-relaxation factor for the pressure correction equation is 1.3 which also gives a yield of a residual value of 1.0×10^{-4}. To satisfy the energy equation, an under-relaxation factor 0.8 is sufficient to achieve residual values of 1.0×10^{-4}. For the SIMPLEC routine which is defined in section 4.4.5, 20 cycles were enough to yield a solution with a residual norm of the continuity equation down to 1.0×10^{-4}. These values have been found by many trials and have been used in all simulated cases.

b) Grid Size

A grid size of 32,3,32 for r, θ, and z directions respectively was found to provide grid independent solutions. This grid was used for all simulated cases.

c) Time Step

As discussed early in subsection (4.4.1) , the fully implicit time marching scheme is unconditional stable once all coefficients are positive. However, a small step is needed to increase the accuracy of the first order numerical approximation, based on a number of trials, a time step of one second was found sufficient. This time step had been used for all simulated cases.

4.4.5 The SIMPLEC Algorithm

The solution procedure adopted to calculate the flow field was the semi-implicit method for pressure linked equations-consistent algorithm (SIMPLEC) of Van Doormal and Raithby (1984) [35][36]. The sequence of the operations of the SIMPLEC algorithm is summarized into the following points:

- Guess the pressure, velocities and temperature fields,
- Calculate pseudo-velocities
- Solve pressure equation
- Set pressure as calculated pressure
- Solve the discretized momentum equations
- Solve pressure correction equations
- Correct velocities

- Solve for temperature profile
- Check for convergence; set the calculated values as the guessed values
- If the convergence is achieved, move into the next time step, otherwise, repeat the steps

4.4.6 Computer Model

An existing computational fluid dynamics program written in FORTRAN 77 code was adopted for this study [37]. The program was originally developed to study the steady state temperature profile in a small size storage tank exposed to an external heat source at the bottom of the storage tank.

To simulate the current problem, the following modifications were made.

(1) Modified the model to comply with the compiler used and performed required tests to ensure that model functions properly.

(2) Converted the model from a steady state model to a transient model.

(3) Modified the model to incorporate the water layer.

(4) Tested energy balance equations to check accuracy of evaporation calculations and boundary conditions.

(5) Developed evaporation subroutine, water layer loop, density variations, physical properties as a function of control volume temperature, and finally subroutine for boundary conditions.

(6) Modified output data and displace solutions using the MATLAB program.

4.5 Physical Properties of the Fluids

The physical properties of crude oils are directly related to specific gravity, while, the crude oil specific gravity is a function of chemical compositions. For simplicity, and due to limited technical information in the open literature, crude oil has been assumed to be a homogenous fluid with a density of less than 934 kg/m^3. This assumption neglects all chemical kinetics, interactions and physical separations in the forms of extraction and absorption which might happen in the multi-component substance under temperature gradients. The physical properties of crude oil including the density are specified as a function of control volume temperature. This assumption allows for a density gradient which the a driving force for non-isothermal flow calculations approximated by the Boussinesq method.

To simulate the boilover event, a water layer has been added at the bottom of the tank which acts as a heat sink. The thermal and physical properties of water and the thermal expansion due to temperature rise was taken into consideration in calculating the buoyancy forces. A pure conduction mechanism was assumed to transmit all thermal energy at the interface between water and oil. For simplicity, the boundary between oil and water layers is assumed to be fixed. The governing equations for the water layer are exactly the same for the crude oil layer. Table 4.1 summarizes the thermodynamic properties used in the model.

Table (4.1): Summary of Thermodynamic Properties of Crude Oil and Water as a Function of Domain Temperature [12][38]

Parameter		Unit	Governing Equations
Crude Oil			
ρ	Density	kg/m^3	$\rho_s - \alpha(T-T_s)+\beta(T-T_s)^2$
α	Thermal Constant	$kg/m^3\,^oC$	$\alpha = \begin{cases} 66\pm5\times10^{-5} & for\ SG\in(0.65,0.84) \\ (189.4-146.5\times SG)\pm3\times10^{-5} & for\ SG\in(0.84,1.07) \end{cases}$
β	Thermal Constant	$kg/m^3\,^oC^2$	$\beta=[(-15.4+19\times SG)\pm2]*10^{-7}$
k	Thermal Conductivity	W/m·K	$(0.120-8.66\times10^{-5}T(^oC))/SG$
C_p	Specific Heat	kJ/kg K	$(1.685+3.4\times10^{-3}T(^oC))/SG$
L_H	Latent Heat of Vaporization	kJ/kg	$(251.47-377.136\times10^{-3}T(^oC))/SG$
Q_p	Low Heat of Combustion	kJ/kg	$46{,}513-8{,}800SG^2+3142.8SG$
Water			
k	Thermal Conductivity	W/m·K	$-0.2758+4.6120\times10^{-3}\times T(K)+5.53910\times10^{-6}\times T^2(K)$
μ	Thermal Viscosity	kg/m·s	$\log\mu=10.2158+1.7925\times10^{-3}/T(K)+1.77\times10^{-2}\times T(K)-1.26\times10^{-5}\times T^2(K)$
C_p	Specific Heat	kJ/kg K	$(72.0-3.9\times10^{-2}\times T(K)-2.11\times10^{-4}\times T^2(K)+5.34\times10^{-7}T^3(K))/16\times10^{-3}$
β	Thermal Expansion Coefficient	$1/^oC$	$5.7160\times10^{-4}(1-T(K)/647.13)^{0.7143}$

Table 4.2 also shows a summary of all physical and thermodynamic properties which were obtained from published articles. The right column of Table 4.2 is a comparison between calculated parameters and referenced data. The table clearly demonstrates the lack of data for crude oils as well the variation between the values provided.

Table (4.2): A Summary of Thermal Properties of Crude Oils in the Literature.

Parameter / Reference	[28]	[5]	[5]	[23]	[24]	[8]	Table (4.2) (20 °C)
Density kg/m^3	850	840	845	845	840	870	860
Flash Point °C	< -15	< -15	< 0	-	< 0	< -23.0	-
Kinematic Viscosity m^2/s $\times 10^{-6}$	0.69	6.9	5.5	983	5.14	8.7	-
Pour Temperature °C	-15	-15	-	-	-	< -38	-
Carbon Fraction	0.838	0.838	0.862	-	-	-	-
Surface Temperature °C	-	-	-	205	-	-	-
Latent Heat of Vaporization kJ/kg	-	-	-	250	-	-	212 *
Thermal Conductivity W/m K	-	-	-	0.132	-	-	0.133
Specific Heat kJ/kg K	-	-	-	2.3	-	-	1.9
Thermal Diffusivity m^2/s$\times 10^{-8}$	-	-	-	6.79	-	-	7.25
Sulfur wt%	-	-	-	-	2.29	0.34	-
Carbon wt%	-	-	-	-	84.3	-	-
Hydrogen wt%	-	-	-	-	12.5	-	-
Nitrogen wt%	-	-	-	-	<1.0	-	-
Water Content wt%	-	-	-	-	-	< 0.3	-

*Value calculated at 205.0°C

One of the important physical properties is the density of the crude oil. Density gradient is the driving force causing natural movements in the liquid bulk. During the fire exposure period, the liquid bulk might encounter a distillation process of light hydrocarbons which feeds the flame. This physical process is taken into account during the density calculation using similar behaviour to the True Boiling Point (TBP) distillation curve for crude oil with an initial specific gravity equal to 0.7 [39].

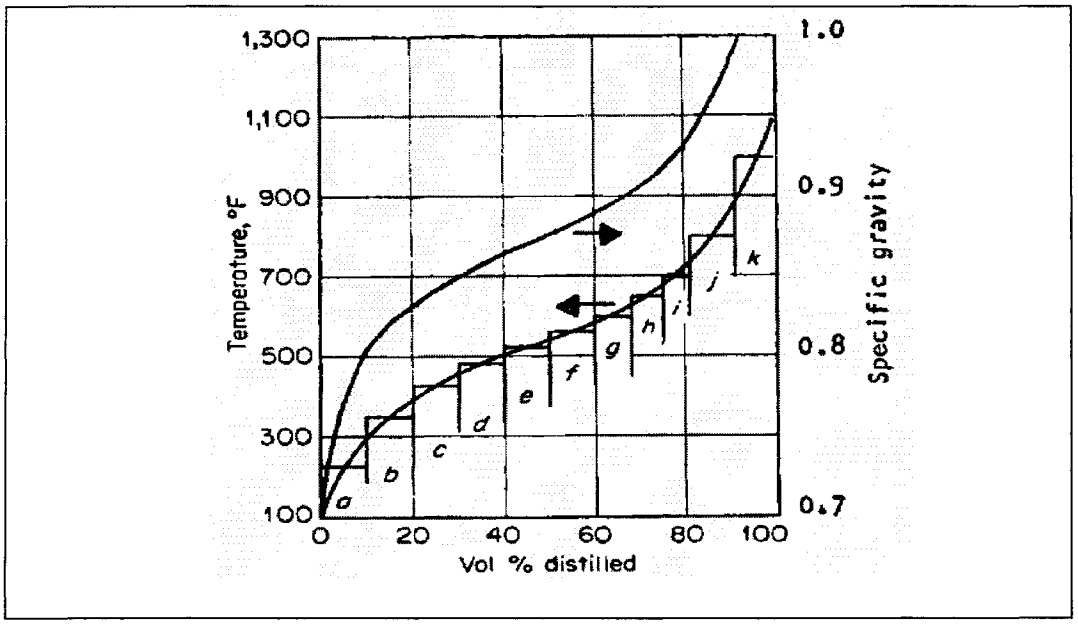

Figure (4.4): TBP Distillation Curve for Light Crude Oil [39]

Reproducing data in Figure 4.4 and plotting specific gravity versus the temperature in Figure 4.5 shows a linear relation between the density of crude oil and the distillation temperature.

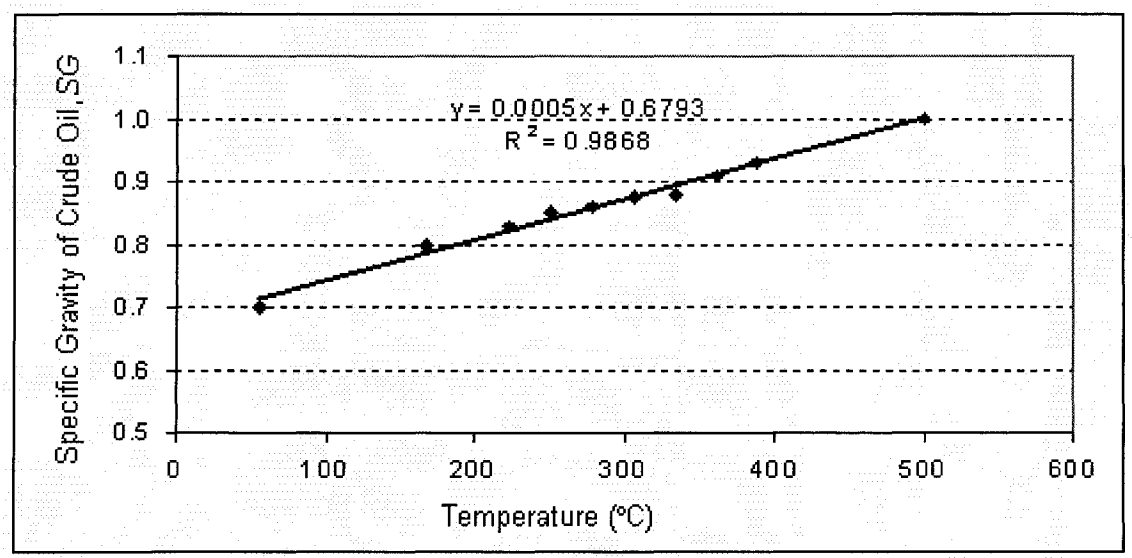

Figure (4.5): Relation between *SG* of Crude Oil and Temperature.

Assuming a linear relation between density and temperature, Equation 4.18 is derived to approximately calculate the crude oil density due to physical distillation as a function of domain temperature. The slope of this equation is the same as the slope in Figure 4.5, and the density at room temperature is the density of crude oil considered.

$$\rho = 0.5 \times T + 859.3 \tag{4.18}$$

where ρ = density of crude oil, kg/m^3
T = temperature of crude oil, °C

4.5.1 Flame Temperature

Iwata and Koseki [24], as shown in Figure 2.13, plotted the experimental data of the flame temperature for 840 kg/m^3 crude oil burned in a 20-m diameter pan versus the time. This result shows that the average flame temperature is 1,180°C (1,453 K) which is used to calculate the radiant heat flux into the crude oil tank bulk.

Data on flame temperature, pool diameter and applied heat flux has been collected to determine the emissivity. This data is presented in Table 4.3.

Table (4.3): Emissivity Calculation using Flame Temperature and Heat Flux

Ref.	Pool Diameter (m)	Heat flux (kW/m^2)	Flame Temperature (°C)	Calculated Average Emissivity
[2]	1.00	16.0	1,000	0.08
[2]	2.00	40.0 (exp) 45.0 (cal.)	800.0 (steady) 1,100-1,300 (boilover)	1.6 0.70-0.45
[24]	20.0	-	1,000-1,300	-
[31]	0.60	-	1,000 (assumption)	-
[8]	1.90	-	900-1,100 (boilover)	-

The data shows the need to look for another method to approximate the applied heat flux into the liquid bulk, because the data in Table 4.3 show a great variation in the flame emissivity.

4.5.2 Radiant Heat Flux into Crude Oil Liquid Bulk

The radiant heat transfer can also be approximately calculated using the Stefan-Boltzmann law of thermal radiation assuming a gray body surface. An emissivity value of 0.25 was computed assuming a complete combustion [17]. Absorption from vaporization fuel has been neglected. Therefore, a radiant heat flux of 60 kW/ m^2 can be calculated based on a 1,450 K flame temperature and a unity view factor. To double check the accuracy of the assumption, backward calculations using previous experimental results were performed using Equation 4.19 and summarized in the Table 4.4. The calculations were performed assuming an adiabatic storage tank, a 0.06 kg/m^2.s constant mass lost rate, 2300 J/kg.K as specific heat, 200 kJ/kg as a latent heat of vapourization.

$$\dot{Q}_r'' = \frac{\rho\, A\, l\, C_p (T_f - T_o) + \dot{m}_\infty'' t_{BO}\, A\, L_H}{(t_{BO} A)} \tag{4.19}$$

where, $\dot{Q}_r''$ = radiant heat flux, W/m^2
ρ = density of crude oil, kg/m^3
A = tank surface area, m^2
l = fuel height, m
C_p = specific heat, J/kg K
T_f = hot zone temperature, °C
T_o = initial fuel temperature, °C
$\dot{m}_\infty''$ = burning rate flux, kg/m^2 s
t_{BO} = boilover time, s
L_H = latent heat of vapourization, J/kg.

Table (4.4): Summary of Backward Calculation of Average Surface Radiant Heat Flux [8]

Fuel Thickness(mm)	Pool Diameter (m)	Fuel Temperature (°C)	Boilover Time (min)	Average Burning Rate (mm/min)	Calculated Average Heat Flux (kW/ m^2)
100	1.9	135	12.0	3.8	45.0
200	1.9	135	15.0	(3.5-4.2)	61.0-63.0
400	1.9	135	30.0	3.2	61.0
400	4.0	330	95.0	3.3	54.0

Those backward calculations provide a justification of using a radiant heat flux of 60 kW/m^2 for a 1.9-m diameter pool fires filled with conventional crude oil.

5. RESULTS AND DISCUSSIONS

A mathematical investigation has been conducted to study heat and mass transfer in a crude oil storage tank subjected to a heat flux from a fire burning at the top of the oil surface. Due to the complexity of the problem considered and the lack of knowledge on the governing physical phenomena taking place in the crude oil during the fire, the investigation is divided into two stages. The first stage of numerical investigation is carried out to study the effect of various physical parameters on the conditions in the tank bulk. Comparisons of the numerical results obtained from these exploratory simulations with available experimental data would provide some guidance in determining the relative importance of the various processes. After selecting the most appropriate model to represent the heat and mass transfer in the crude oil bulk, a parametric study is conducted to show the effects of selected physical parameters on the natural convective heat flows.

5.1 Exploratory Simulations

The computer program was developed with the flexibility to vary the governing equations so that solutions can be obtained for four different conditions:

- conduction only,
- conduction and diffusion governed by buoyancy driven flows due to thermal expansion.
- conduction and diffusion governed by buoyancy driven flows due to distillation process.
- conduction and diffusion governed by buoyancy driven flows due to combined effects of thermal expansion and distillation process.

For most simulated cases, a storage tank with a diameter of 1.9 m and oil thickness of 0.1 m was considered. The top of the oil surface was subjected to a radiation heat flux of 60 kW/m^2, and the side walls of the tank were assumed to be adiabatic. A water layer of thickness 0.7 m was considered at the bottom of the tank. These parameters were selected to match the dimensions of the experimental set-up used in [8] so that comparisons can be made between the model predictions and the experimental data. The kinematic viscosity for all simulations was assumed constant at $6.0x10^{-6}$ m^2/s. The results of these simulations are discussed in the following sections.

5.1.1 Conduction Effects

For this simulation, the convective terms in the governing equations have been set to zero assuming that only conduction heat transfer takes place in the liquid bulk during the fire. It is recognised that Hall [4] has reported that a calculation based on the known conductivity of crude oil does not reflect the rapid penetration of heat in advance of the burning surface. Nonetheless, a number of researchers have studied heat transfer through a thin layer of oil over water considering conduction to be the dominant heat transfer mechanism. This assumption is supported by the fact that in cases where a liquid is subjected to heating from above the effect of natural convection flow is reduced. Therefore, conduction effect in the crude oil layer temperature was numerically investigated.

The numerical simulation results of the model for the conduction case are shown in Figure 5.1. The figure shows temperature profiles in the oil at the centre of the tank as a function of depth from the oil surface for different times. The top surface of the oil is maintained at 150°C which is the temperature at which it was assumed that boiling takes place. The figure demonstrates that as time advances the temperature of the bulk liquid increases, however, the heat wave has not reached the bottom of the tank by 300 seconds. A similar temperature profile in the oil at 5 minutes (300 seconds) has been reported by [8] and shown in Figure 5.2. Although tank dimensions and liquid levels are not the same as the ones used for the numerical results, the figure indicates that during the initial stages of the fire, conduction is the main mechanism of heat transfer in the oil. As time progresses, however, Figure 5.1 shows that the temperature of the oil becomes linear with height. This profile does not represent experimental findings that show a uniform bulk liquid temperature.

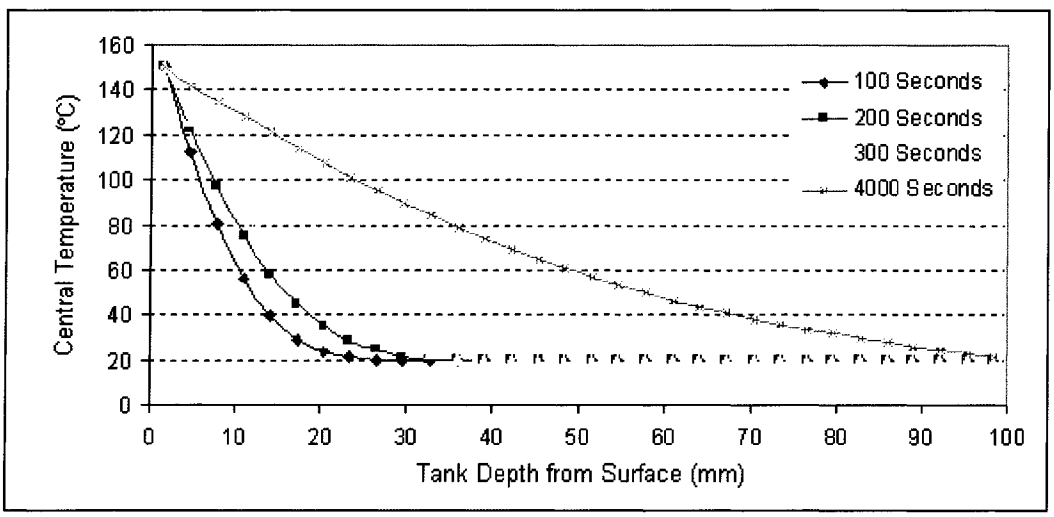

Figure (5.1):. Predicted Temperature Profile at the Centre of the Tank at Different Times.

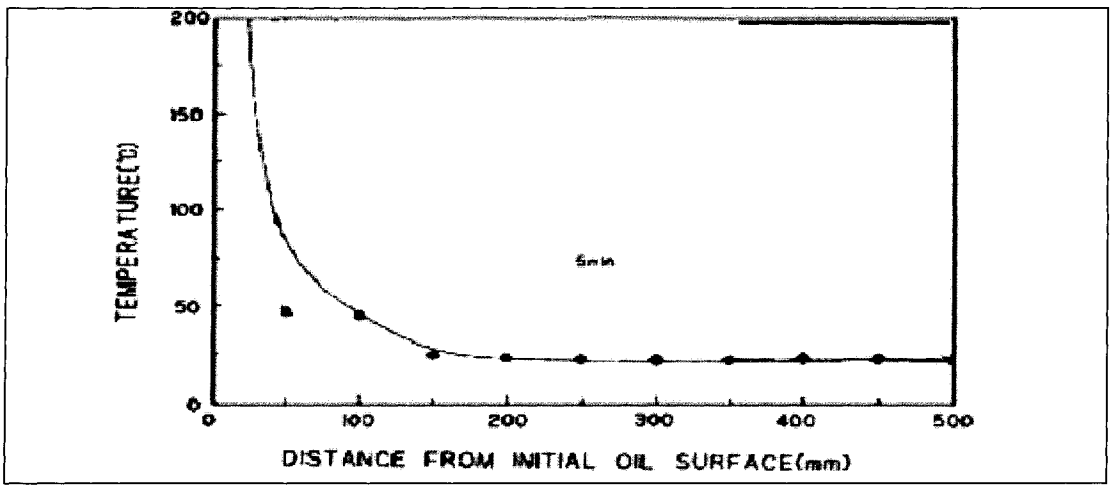

Figure (5.2):. Measured Liquid Temperature at Various Heights for a 1.9 m of Crude Oil Pool Fire, Reproduced from [8]

Iwata and et al. [8] reported that a variation of $\pm 10°C$, in temperature measurements existed between points at the same height but at different radial distances. The numerical predictions of temperature differences in the liquid between centre, middle and wall locations, using pure conduction as the governing heat transfer mechanism as shown in Figure 5.3 have no significant horizontal temperature variations. This result is expected because an insulated boundary condition was imposed at the tank wall. At 300 seconds, the predicted temperature of crude oil has reached 40°C at 25 mm from the oil surface.

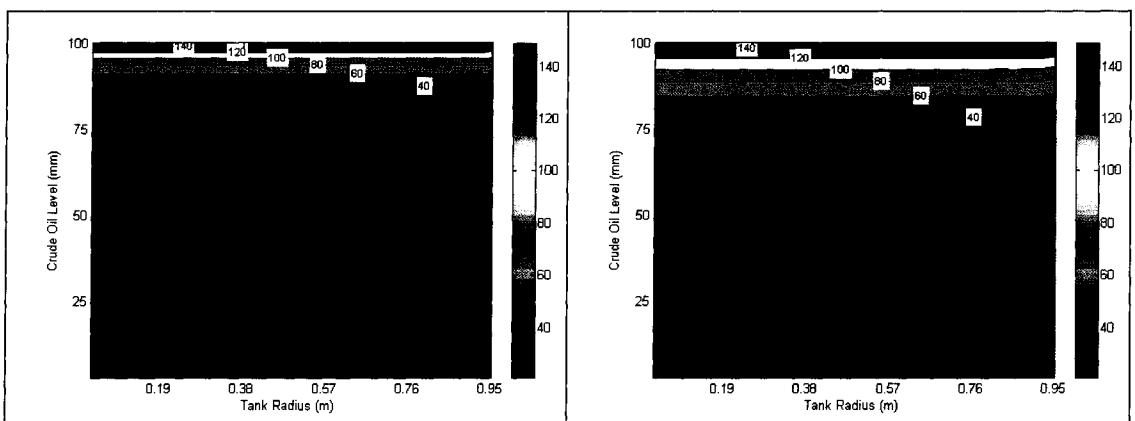

(a) Simulation Time = 100 seconds | (b) Simulation Time = 300 seconds

Figure (5.3): Predicted Temperature Distribution in the Oil at Different Times.

In summary, studying this numerically simulated scenario shows that conduction heat transfer is responsible for carrying the heat energy during the early stage of the fire, however, conduction heat transfer alone is not a sufficient mechanism to develop the hot zone noticed in the experimental data. Therefore, heat penetration governed by conduction and diffusion heat transfer has to be considered. This consideration will allow having convective flows due to density gradients which definitely will have an effect on overall heat penetration rate in the crude oil bulk.

5.1.2 Buoyancy Effects Due To Thermal Expansion

The predictions of the simulation for temperature profiles with buoyancy effects on the natural convection flows due to the thermal expansion of the oil at high temperatures are shown in Figure 5.4. The thermal expansion coefficient in all the numerical cases was 5.02×10^{-4} $^{o}C^{-1}$. In this study, the density gradient, which is the source in the momentum equation for the natural convective flows developed within the liquid bulk, is approximated by the temperature gradient with the help of the thermal expansion coefficient. This approach is basically the basis of Boussinesq approximation.

Figure 5.4 presents isothermal lines in degrees Celsius for a vertical section in the crude oil at 200 seconds and 300 seconds. Even though, the tank is insulated, the results still show a significant variation in the temperature along the radial direction and indicate that the heat wave reaches deep into the oil at the centre of the tank. At 200 seconds, at the middle of the fuel, the temperature near the centre of the tank was around 100°C,

while the temperature near the tank wall was 80°C. This result shows a variation of 20°C, which agrees with Iwata and et al. [8] experimental findings. Figure 5.4 b shows a variation of about 50°C between the central oil temperature and the oil temperature at the wall at 300 seconds.

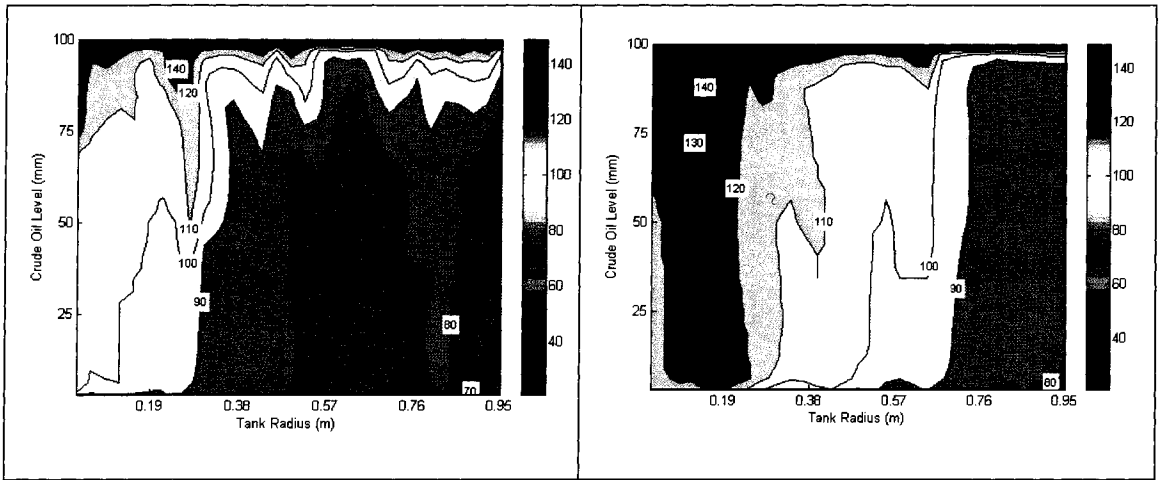

(a) Temperature (°C) distribution in the crude oil at 200 seconds

(b) Temperature (°C) distribution in the crude oil at 300 seconds

Figure (5.4):. Temperature Distribution in the Crude Oil Layer.

Figure 5.5 shows the predicated centerline temperature profiles in the oil along the tank height at different times. At 100 seconds, the figure shows a steep gradient at the top of the oil surface with temperature decreasing from 150°C to 60°C within 20 mm of the crude oil layer depth. Following this, the temperature of the liquid is uniform, with a slight decrease of 5°C near the bottom of the oil layer due to the effect of the water-oil interface.

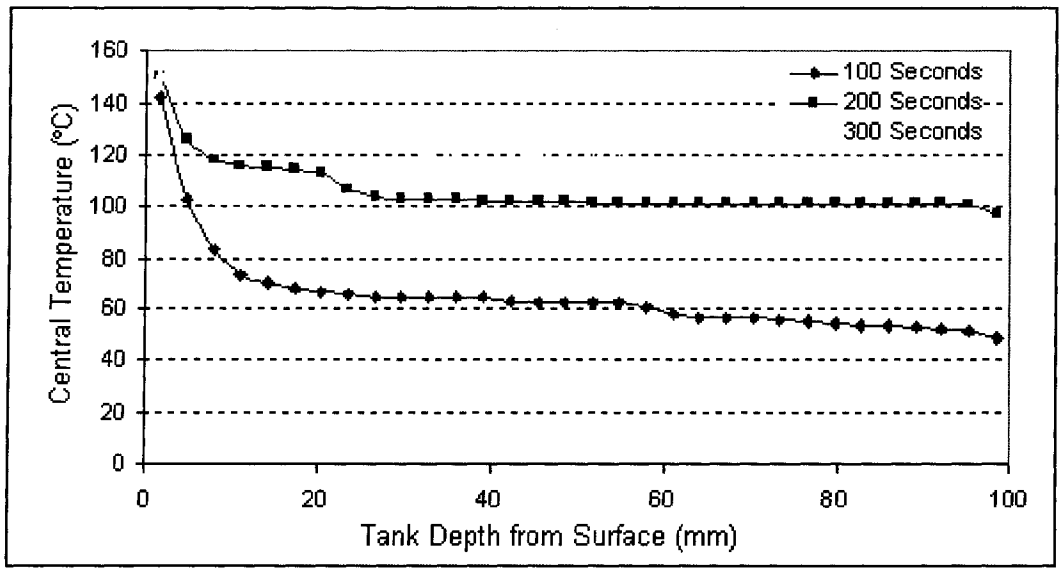

Figure (5.5):.Predicted Central Temperature Profiles in the Oil at Different Times Using the Thermal Expansion.

The temperature profiles predicted from this simulation have a similar trend as the experimental data obtained from tests by [8] shown in Figure 5.6. These experimental tests have been conducted using emulsified crude oil. This numerical comparison demonstrates that convective flows play a significant role in the heat penetration rate in crude oil tanks.

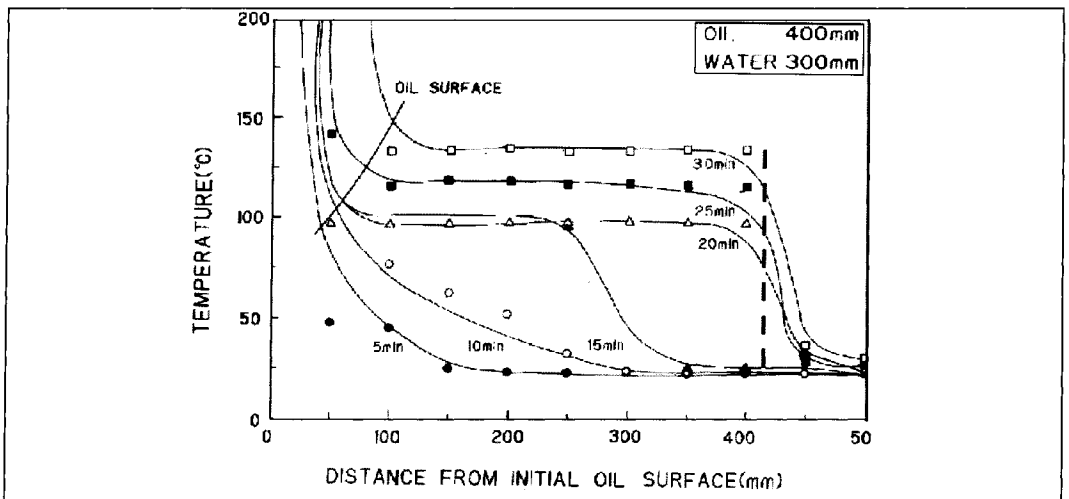

(Note): The dashed line represets the oil-water interface temperature

Figure (5.6). Experimental Vertical Temperature Distributions during Burning Of Crude Oil [8]

Figure 5.7 presents the predicted average temperature of the oil with time. As the figure shows the average temperature of the oil reaches 100°C within the first 300 seconds of the simulation time. The average temperature is a weighted average that considers the different control volume sizes from the centre to the wall of the tank.

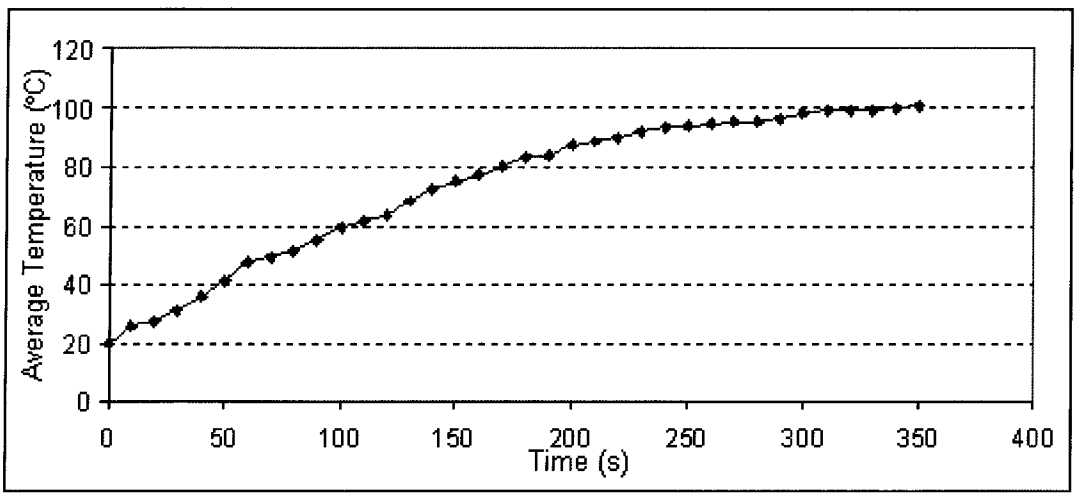

Figure (5.7): Average Temperature of the Oil Layer with Time.

A comparison between Figures 5.5 and 5.6 indicates that buoyancy effects due to thermal expansion could be the governing mechanism of heat transfer in a thick layer of crude oil exposed to a fire at the surface.

5.1.3 Buoyancy Effects Due to Distillation Process

The effect of natural convection flows caused by density changes due to evaporation has been numerically studied. The increase of the density of crude oil is due to the distillation process occurring inside the liquid in which light hydrocarbons evaporate causing a density gradient within the crude oil hot layer. The density variation with temperature due to distillation process was adopted from a True Boiling Point curve. The density and temperature were assumed to have a linear relation which was

approximated using Equation 4.18. Density gradients were numerically considered as a source term in the vertical momentum equation resulting in fluid motion.

Figure 5.8 shows the predicted temperature distribution in the oil at 50 seconds and 100 seconds. As shown in the figure, density effects have a significant impact on heat transfer in the oil due to the sinking of the heavier oil resulting from the evaporation process. At 100 seconds the bulk of the oil has an almost uniform temperature of 130°C.

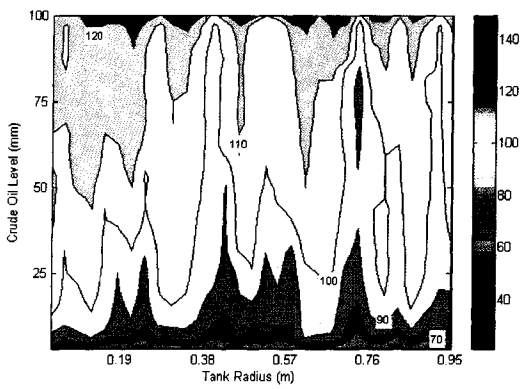

(a) Cross section temperature profile of crude oil from tank centre to wall (left to right), at time 50 seconds.

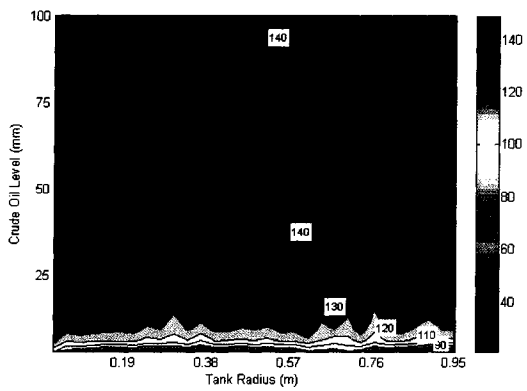

(b) Cross section temperature profile of crude oil from tank centre to wall (left to right), at time 100 seconds.

Figure (5.8): Comparison between Vertical Isothermal Lines Affected By Density at Different Times.

The impact of the density gradients approximated by distillation effect only on heat transfer in the oil can also be seen in Figure 5.9 which depicts temperature profiles in the oil at the centre of the tank. Temperature profiles in Figure 5.9 are representing the temperature of the simulated crude oil at different simulated times. For example, at 140 seconds, the figure shows a slight drop at the top of the oil surface with temperature decreasing from 150°C to 140°C within 10 mm of oil layer. Following this, the

temperature of the liquid is uniform except at the bottom where it drops by 50°C due to the effect of the water-oil interface.

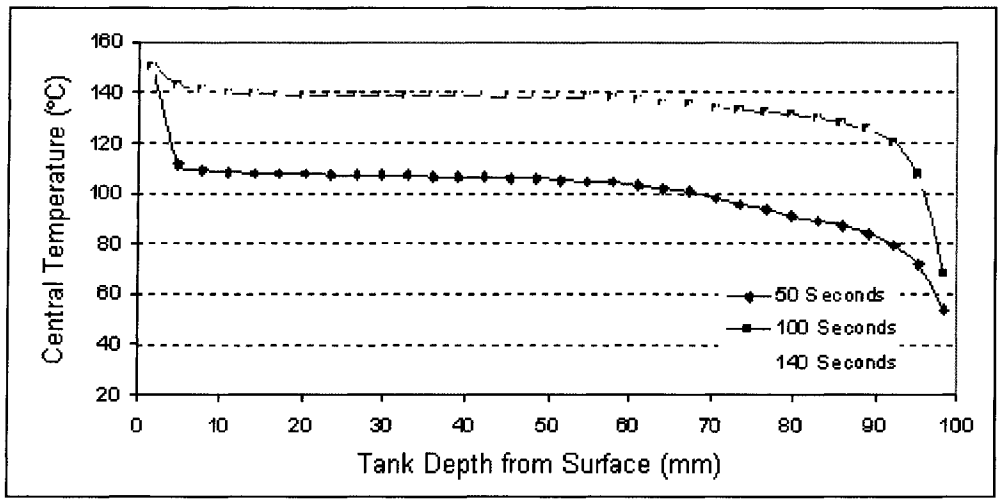

Figure (5.9): Central Temperature Profiles along Tank Height at Different Times for Density Gradient Approximated by Distillation Effect Only.

Figure 5.10 shows the average oil temperature with time for this simulation. This figure shows that within 80 seconds the average oil layer reaches a temperature of 135°C. Although the temperature profiles have a similar trend to the experimental profiles, this result is not physically realistic because of the fast mixing of the oil. Boilovers in tanks with similar dimensions occurs at 730 seconds which is much longer than the 80 seconds predicted by this simulation.

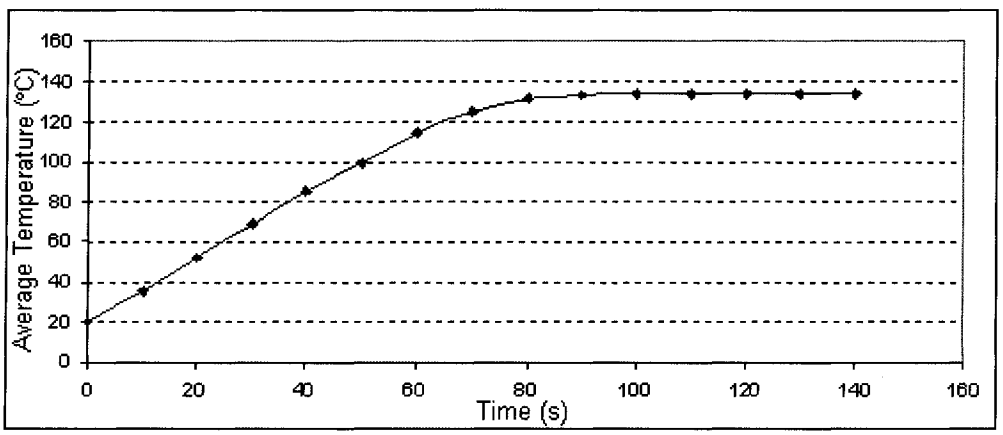

Figure (5.10) Average Oil Temperature with Time for Density Gradient Case Approximated by Distillation Effect Only.

5.1.4 Combined Density Effects

The fourth exploratory simulation in this study combines the competing influences of thermal expansion and distillation effects on calculating the density gradient within the liquid bulk. The objective of this case is to simulate the combined effect of distillation and thermal expansion occurring in the liquid. Figure 5.11 shows the predicted vertical temperature distribution in the tank at 200 seconds and 300 seconds. As it can be seen from the figure, a thin hot layer develops at the top surface of the tank whose depth increases slightly with time. The figure also shows that there is a small variation of temperatures along the radial direction.

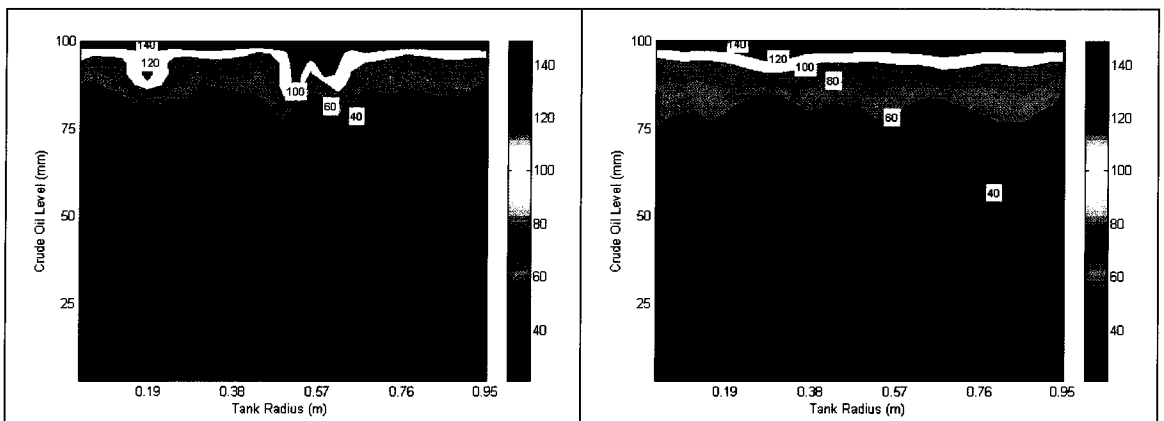

(a) Simulation Time = 200 seconds. **(b)** Simulation Time = 300 seconds.

Figure (5.11) Vertical Temperature Distribution in the Oil at Different Times.

Figure 5.12 shows the development of the average crude oil temperature with time. The average crude temperature increases slowly and reaches a value of 55°C in about 300 seconds. Then, the average crude oil temperature remains at a steady state value of 55°C.

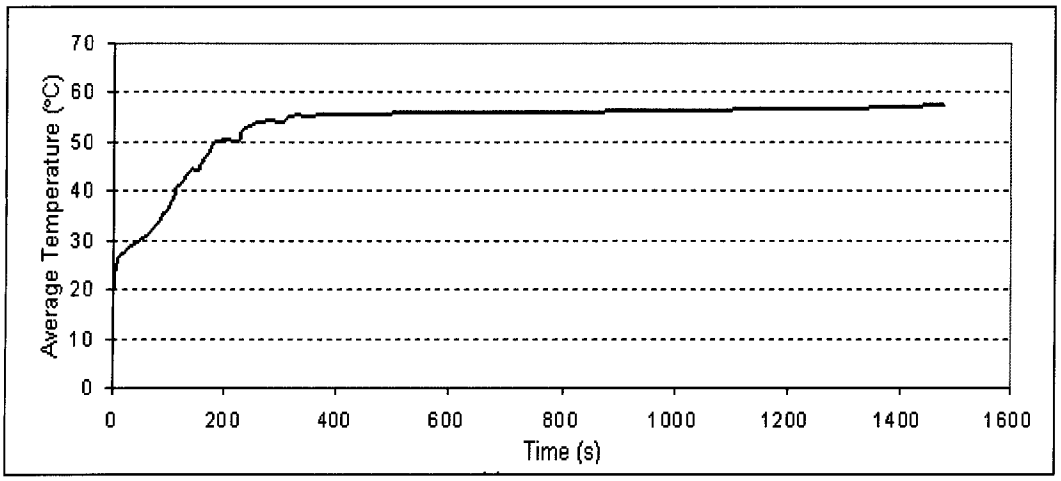

Figure (5.12): Average Oil Temperature with Time for Combined Effects Case.

The results of this simulation indicate that considering density gradient due to the combined effects of thermal expansion and distillation do not lead to realistic temperature development in the crude oil.

Figure 5.13 shows temperature profiles in the oil along the height at different times. At 730 seconds, the figure shows a steep gradient at the top of the oil surface with temperature decreasing from 150°C to 80°C within 20 mm of crude oil layer. Following this, the temperature of the liquid is uniform, with a small decrease of 20°C near the bottom of the oil layer.

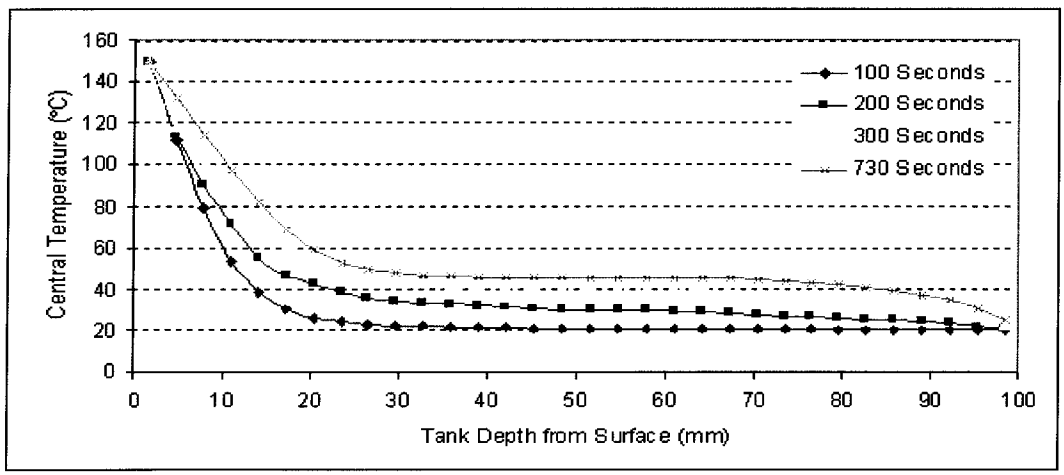

Figure (5.13): Temperature Profiles along Tank Height at Different Times.

5.1.5 Comparison of Result of Exploratory Simulations

This section compares the predictions using the three approaches in modelling heat transfer in the crude oil as a result of fire exposure at the top of the oil, in an effort to select the most appropriate methodology.

Figure 5.14 shows a comparison between the average oil temperatures predicted by the model for the three cases: (1) density gradient affected by thermal expansion, (2) density gradient affected by distillation process, and (3) density gradient affected by thermal expansion and distillation effects.

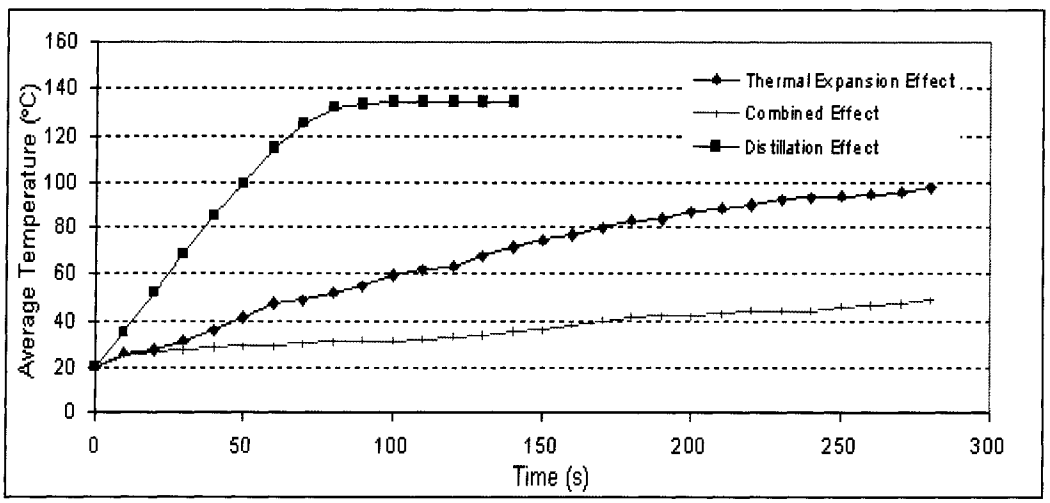

Figure (5.14): Average Oil Temperature History for the Three Simulated Cases.

Figure 5.14 shows that the average temperature of crude oil using thermal expansion only is equal to 100°C at 300 seconds, while the average temperature is 55°C using the coupled effect of thermal expansion and density at around 300 seconds. Using density effect only, the average temperature of the crude oil reaches 132°C in 55 seconds. If the physical parameters of the crude oils can be assumed constant, the time required for the experiment to reach the simulated average temperature can be computed using

Equation 5.1. Calculations were performed assuming an adiabatic storage tank, a 0.06 kg/m^2.s constant mass evaporation rate obtained from experimental data, 2300 J/kg·K as specific heat, 200 kJ/kg as a latent heat. All performed calculations are summarized in Table 5.1.

$$t = \frac{\rho l C_p \Delta T}{\dot{Q}''_{rad} - \dot{m}'' L_H} \tag{5.1}$$

where t = time for experimental to reach simulated temperature, s
ρ = crude oil density, kg/m^3
l = fuel thickness, m
C_p = specific heat, J/kg K
ΔT = temperature rise, °C
$\dot{Q}''_{rad}$ = radiant heat flux, W/m^2
$\dot{m}''$ = evaporation rate flux, kg/m^2.s
L_H = latent heat of evaporazation, J/kg

Table (5.1): Summary of Thermodynamic Calculation to Approximate Experimental Time to Reach the Same Average Oil Temperature

Case	Fuel Thickness (mm)	Average Fuel Temperature (°C)	Applied Heat Flux (kW/m^2)	Simulation Time (seconds)	Eq. (5.1) Time (seconds)
Thermal Expansion Effect	100	100	60.0	300	332
Distillation Effect	100	132	60.0	75	465
Combined Effect	100	55	60.0	300	147

The results from Equation 5.1 show that 147 seconds experimentally are required to heat the oil layer to 55°C, and 465 seconds to heat the oil to 132°C. Therefore, from results in Table 5.1, supported by the discussion in the previous sections demonstrate that buoyancy forces affected by thermal expansion provide the best results in modeling the heat propagation profile inside the crude oil bulk.

5.2 Parametric study of heat transfer in crude oil

The developed computer model with buoyancy effects based on thermal expansion only is used to perform a parametric study to determine the impact of a number of parameters on the conditions in the tank exposed to a fire at the top oil surface. Parameters investigated include wall heat transfer, kinematic viscosity, constant thermodynamic properties and water layer. Simulations performed and values of the parameters considered are shown in Table 5.2. The results of these simulations are discussed in the following sections.

Table (5.2): Cases Used For Parametric Study

Case	Heat Flux (kW/m^2)	Tank Diameter(m)	Oil Thickness(m)	Kinematic Viscosity $\times 10^{-6}$ (m^2/s) *	Water Thickness (m)	HTC ($W/m^2 \cdot °C$)**
A	60.0	1.9	0.100	6.0	0.700	5.5
B	60.0	1.9	0.100	160.0	0.700	Insulated
C*	60.0	1.9	0.100	6.0	0.700	Insulated
D	60.0	1.9	0.100	6.0	0.0	Insulated

* Thermodynamic properties independent of temperature
** HTC stands for Heat Transfer Coefficient

5.2.1 Wall Heat Transfer Effects

A general firefighting practice is to cool the tank walls during tank fires to protect the tank integrity. In most experimental research work details of heat transfer at the tank walls is not provided, so it was assumed that adiabatic conditions existed.

A heat transfer coefficient of 5.5 $W/m^{2o}C$ was applied as a boundary condition at the wall to simulate cooling the storage tank. Figure 5.15 shows a comparison between the case using the heat transfer coefficient and the insulated case discussed in section 5.2.1. For both cases, the heat penetration was from the centre of the tank, while the sidewall in both cases is cooler.

Figure 5.15 compares the isothermal lines at 300 seconds between the insulated and convective tank wall.

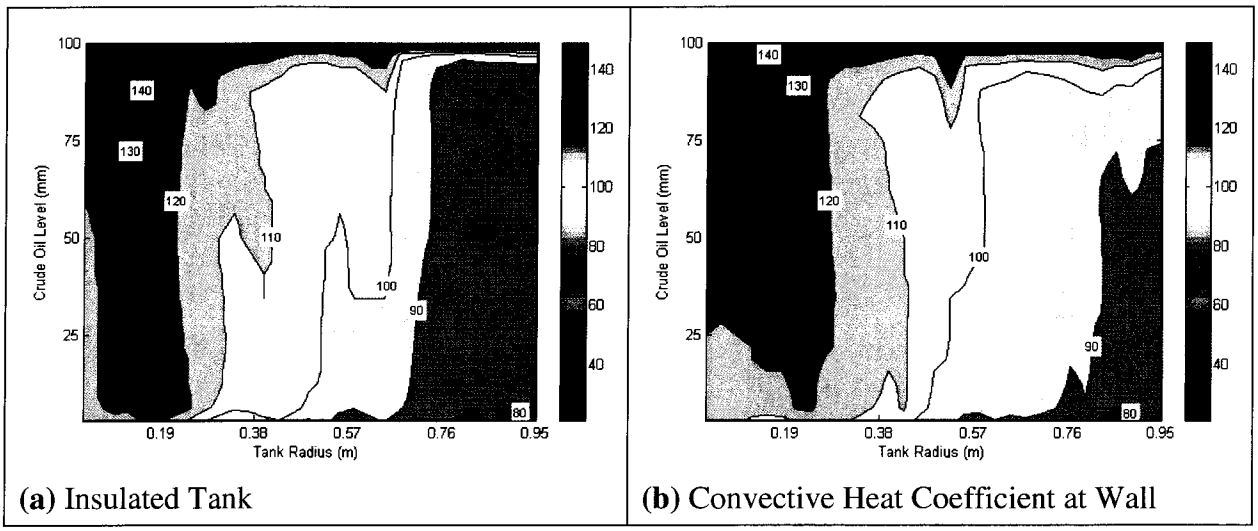

(a) Insulated Tank **(b)** Convective Heat Coefficient at Wall

Figure (5.15): Comparison of Temperature Distribution at 300 Seconds between Insulated and Convective Tank Wall.

A variation of $5^{o}C$ can be seen in the vertical distribution of temperature of the cold area near the wall for both cases as shown in Figure 5.16.

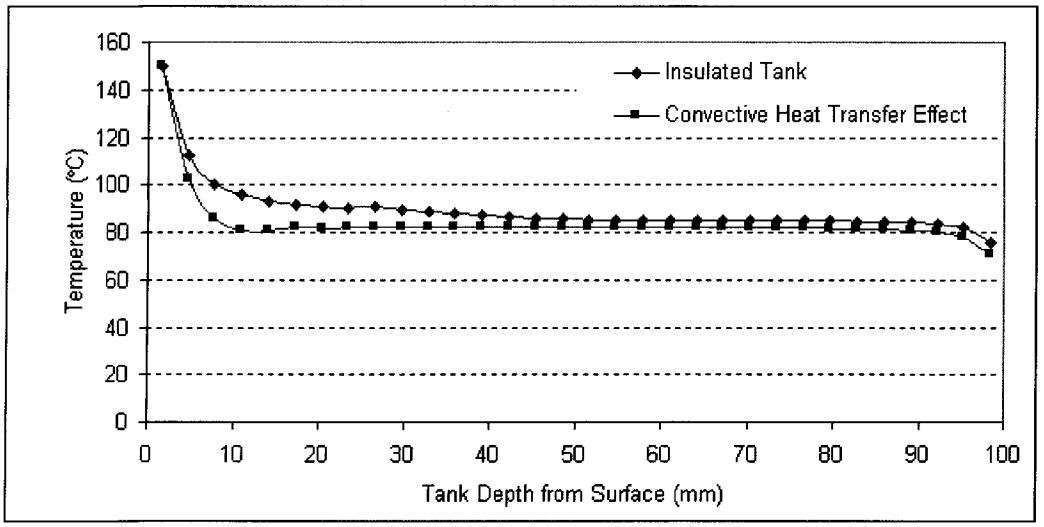

Figure (5.16): Comparison of Temperature Distribution near The Wall at 300 Seconds between Insulated and Convective Tank Wall.

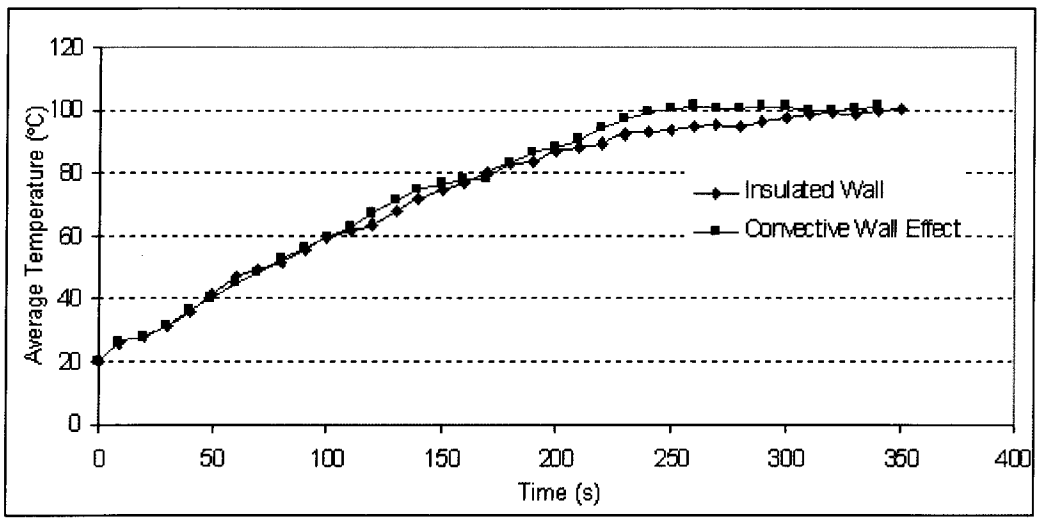

Figure (5.17): Comparison of Average Oil Temperature Between Insulated and Convection Cases.

Figure 5.17 shows that the convective heat transfer at the tank walls has no significant effect for the first 100 seconds. The effect of heat lost through the wall can be seen after 200 seconds, causing an increase of the average tank temperature. This increase in the average temperature is due to the increased circulation inside the oil that causes more mixing of the hot and bulk oil, reducing liquid evaporation.

5.2.2 Kinematic Viscosity Effects

As shown in Figure 2.1 page 12, conventional crude oil viscosities vary from 10 cP to 100 cP. This presents a need to simulate and investigate the kinematic viscosity effects on the overall numerical calculation and particularly on heat penetration in the liquid. A simulation with kinematic viscosity of 160 x 10^{-6} m^2/s was conducted; the results are compared with the results with kinematic viscosity of 6 x 10^{-6} m^2/s in Figure 5.18.

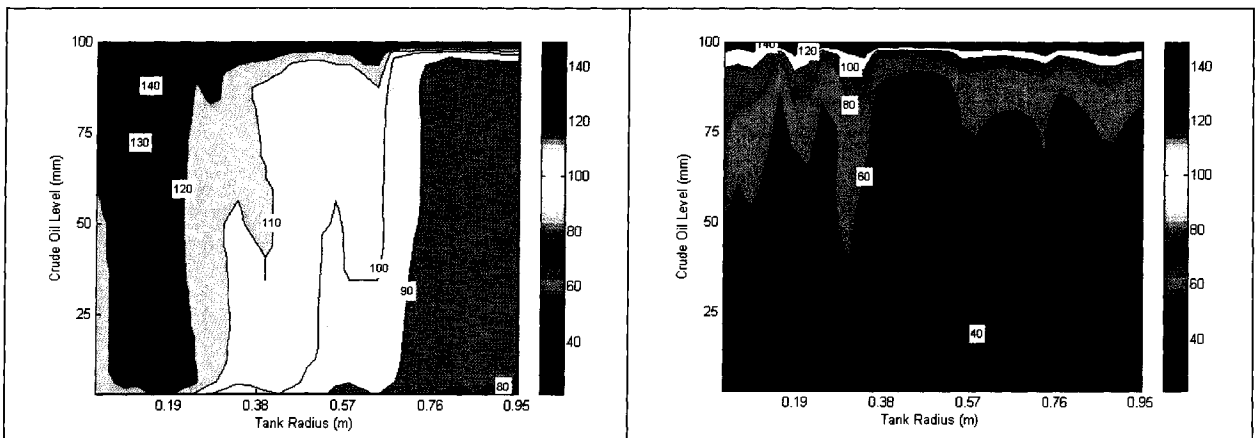

(a) $\upsilon = 6.0 \times 10^{-6}$ m^2/s (b) $\upsilon = 160.0 \times 10^{-6}$ m^2/s

Figure (5.18): Temperature Distribution in Tank for Kinematic Viscosity Effect Study at 300 seconds.

Figure 5.18 shows that the kinematic viscosity plays an important role in the heat transfer in the tank. A kinematic viscosity of 160.0 × 10^{-6} m^2/s shows a smaller variation of the radial temperature and a reduction of heat propagation. Figure 5.19 compares the vertical velocity profiles for the low and high values of kinematic viscosity. In Figure 5.19, the predicted velocity of convective flow at 300 seconds is between -6.0 × 10^{-3} m/s and 5.0 × 10^{-3} m/s.

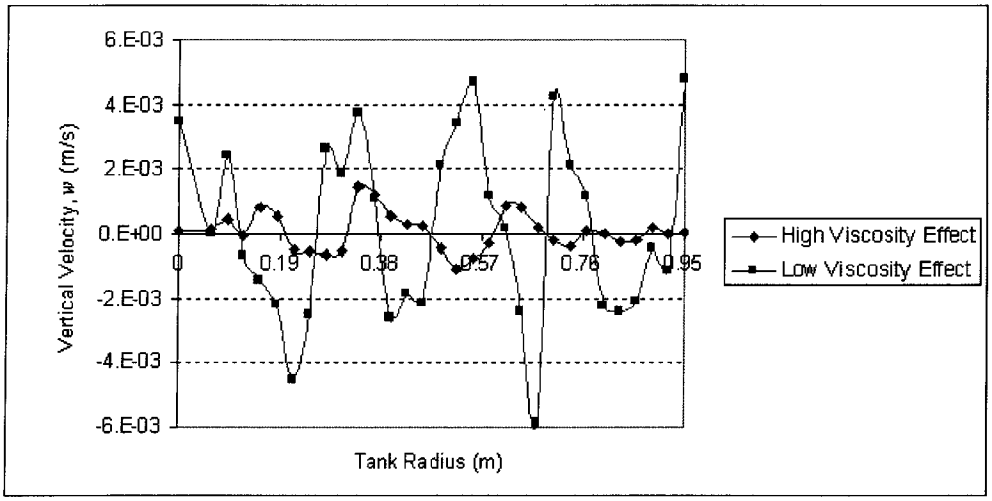

Figure (5.19): Vertical Velocity Profiles with The Radial Distance at 300 Seconds for High and Low Viscosity Effect Study.

Figure 5.20 shows temperature profiles along tank height at different times. At 730 seconds, the figure shows a steep gradient at the top of the oil surface with temperature decreasing from 150°C to 60°C within 20 mm of crude oil layer. The results with the high kinematic viscosity shown in Figure 5.20 are quite interesting as they match the trend of the experimental data, where conduction is dominant at the beginning of simulation, and then convection. A comparison between Figure 5.5 and Figure 5.20 shows that increasing the kinematic viscosity decreases heat penetration rate.

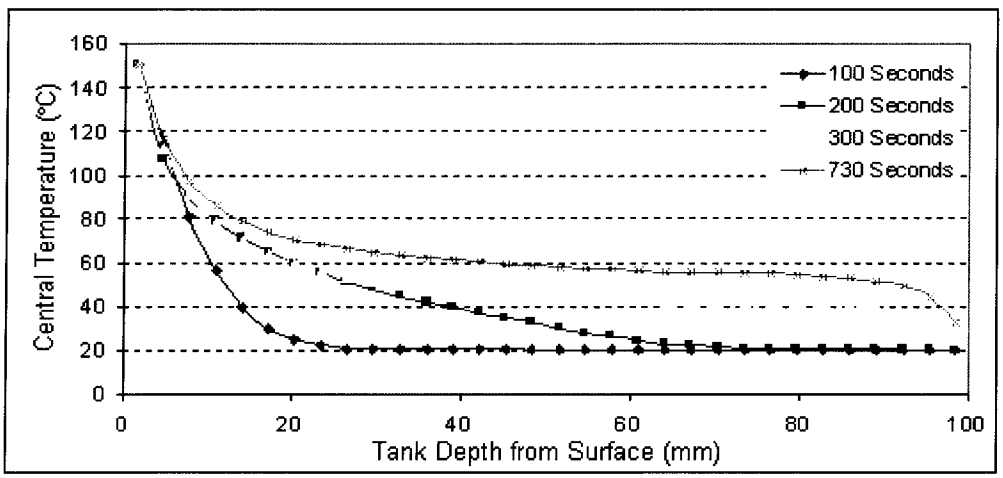

Figure (5.20): Temperature Profiles along Tank Height at Different Times for High Kinematic Viscosity Scenario.

5.2.3 Thermodynamic Property Effects

A numerical case with thermodynamic properties independent of the control volume temperature is performed to determine the effect of the thermodynamic properties on the results. Figure 5.21 shows that when the thermodynamic properties are independent of temperature, the average oil temperature increases at faster rate, however, by 250 seconds the average temperatures of both simulations are the same.

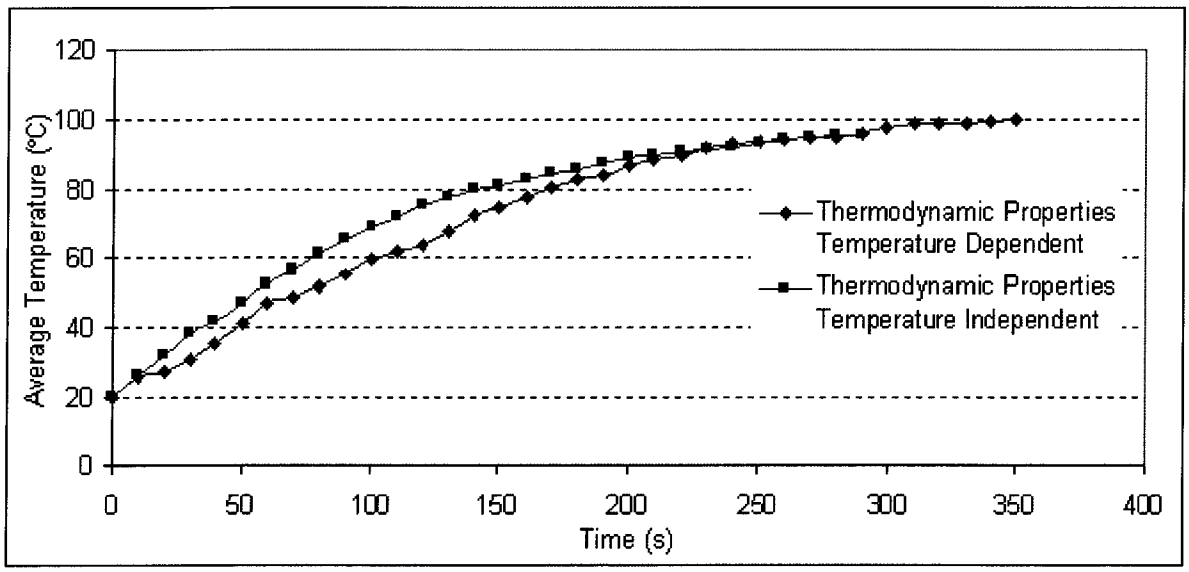

Figure (5.21): Studying the Effect Thermodynamic Properties of Crude Oils on the Numerical Calculations.

At 300 seconds, the average temperature of both cases is around 100°C. The isothermal lines for both cases have a different behaviour as shown in Figure 5.22. As the figure shows the simulation with temperature independent properties results in more mixing of the oil and a lower temperature closer to the wall.

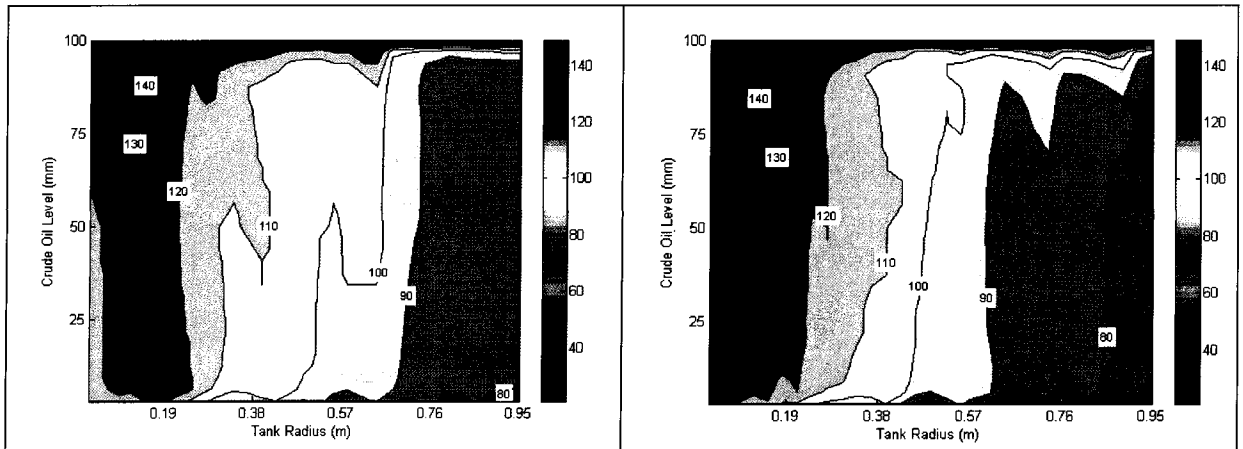

a) Thermodynamic Properties Temperature Dependent

b) Thermodynamic Properties Temperature Independent

Figure (5.22): Comparison between Isothermal Lines at 300 Seconds.

Figure 5.23 compares temperature profiles near the wall for the two cases at 300 seconds. This figure shows that the temperatures of the temperature independent properties are lower than the temperature dependent case.

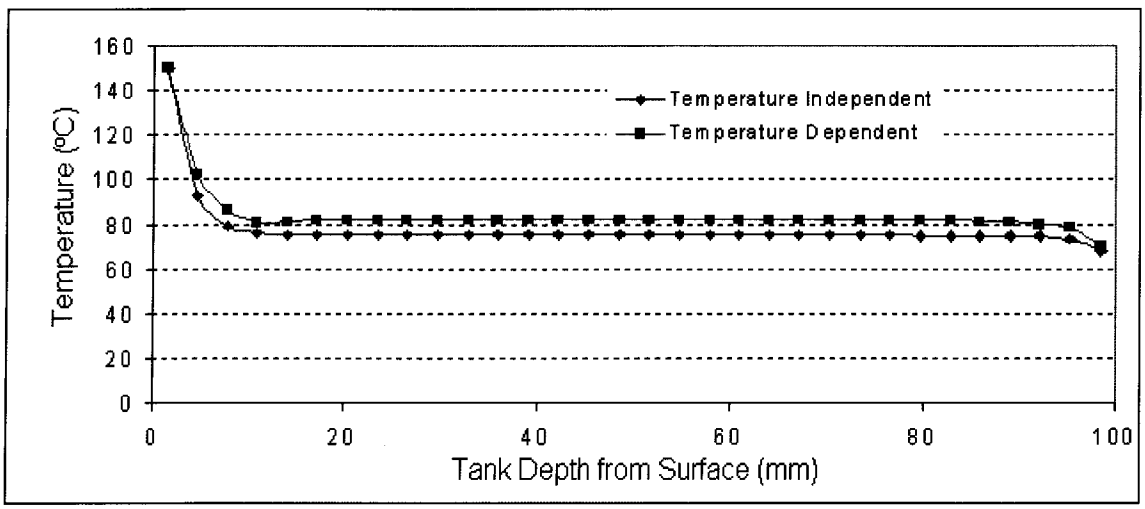

Figure (5.23): Comparison between Vertical Distributions of Temperature at 300 Seconds.

5.2.4 Water Layer Effects

To investigate the effect of the water layer at the bottom of the tank, a simulation was done without a water layer. Figure 5.24 demonstrates that the water layer results in a lower average crude oil temperature, because the water layer acts as a heat sink.

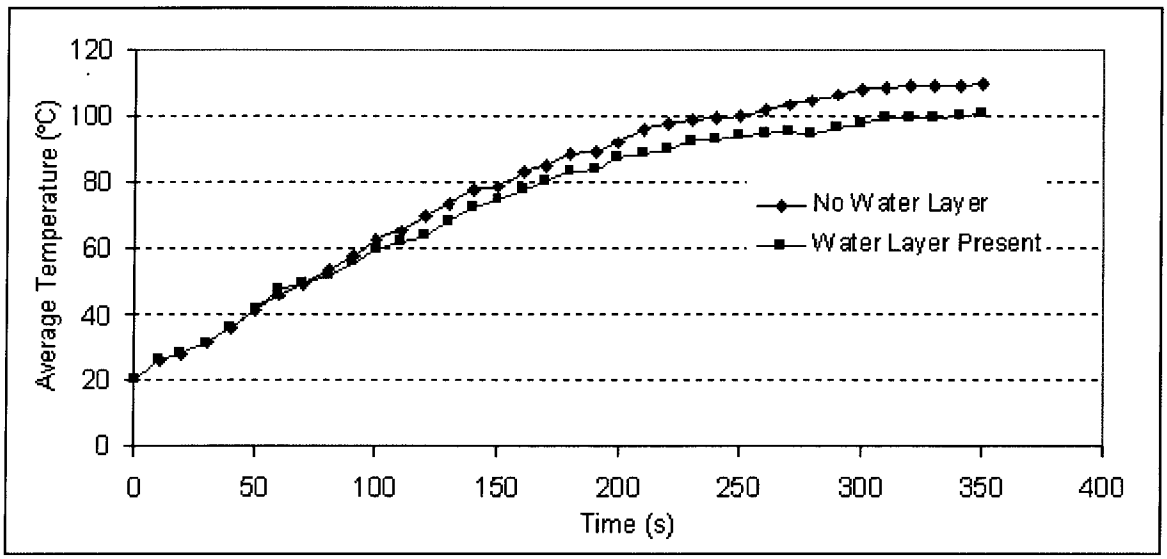

Figure (5.24): Comparison of Average Crude Oil Temperature for Water Effect Study.

Figure 5.24 shows that water layer reduces the average oil temperature. The difference of the average oil temperature at 350 seconds is 10°C .

Figure 5.25 shows a comparison of the temperature distribution in the oil with and without a water layer, demonstrating the higher temperatures with no water layer.

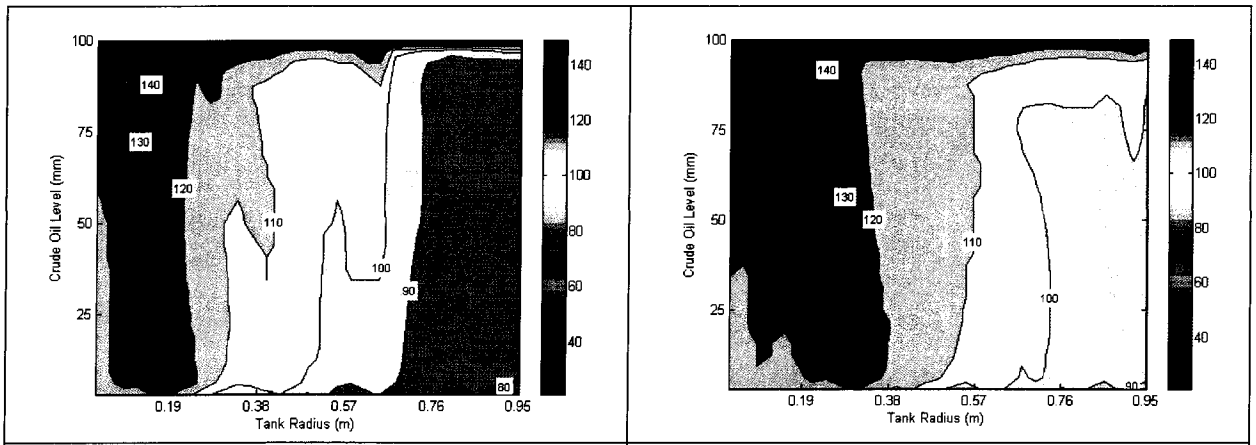

a) Water Layer Present | **d)** No Water Layer

Figure (5.25): Comparison between Isothermal Lines at 300 Seconds.

Figure 5.26 compares vertical temperature profiles at 300 seconds for both cases, no water layer and water layer. As seen in the figure, a difference of 20°C exists between the two cases near the wall from the top to the bottom.

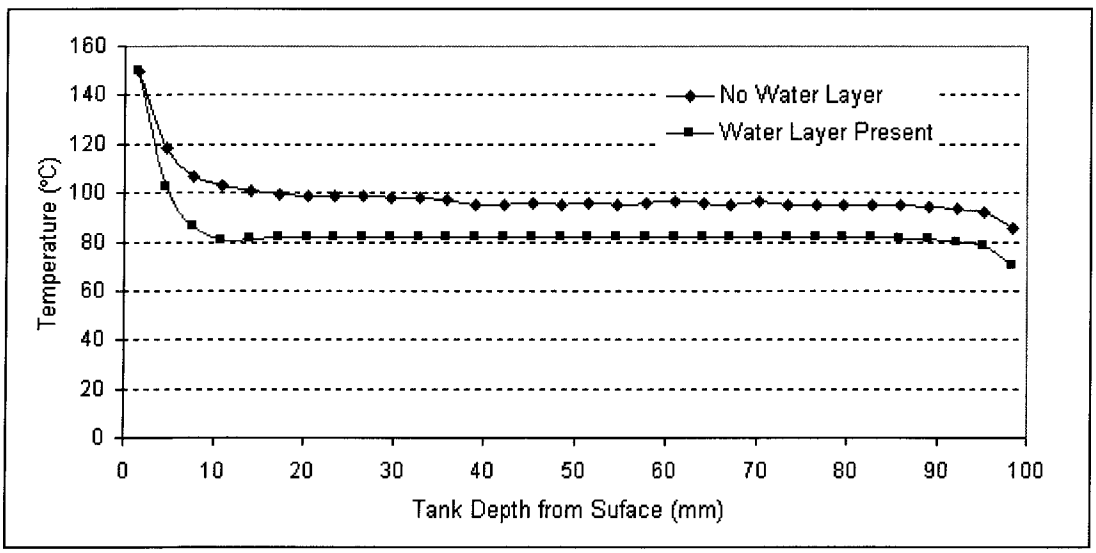

Figure (5.26): Comparison between Vertical Distributions of Temperature at 300 Seconds.

6.0 CONCLUSIONS AND RECOMMENDATIONS

In this thesis, a mathematical study of heat transfer in an industrial crude oil tank during a fire leading to boilover has been conducted. To solve the governing partial differential equations for heat transfer and fluid flow in the crude oil and the water layer, a computational fluid dynamics (CFD) model has been developed. The model solves the governing equations of mass, momentum, and energy using an implicit control-volume formulation with the SIMPLEC algorithm. The studies conducted using the model focused on calculating the transient, coupled heat and mass transfer taking place in the tank as a result of exposure to external radiation due to the fire.

For the study, an existing CFD model was modified to simulate the current problem as follows:

- Modified the model to comply with the compiler used and performed required tests to ensure that the model functions properly.
- Converted the model from a steady state model to a transient model.
- Modified the model to incorporate the water layer.
- Tested energy balance equations to check accuracy of evaporation calculations and boundary conditions.
- Developed subroutines for evaporation, water layer, density variation, physical properties as a function of control volume temperature and finally boundary conditions.
- Modified output data and displayed solutions using the MATLAB program.

A number of conclusions can be drawn from the results obtained from this mathematical investigation:

- Preliminary runs show that simulation which account for buoyancy effects due to thermal expansion provides the best results when compared with experimental data. The predicted temperature profiles in the tank are similar to the profiles obtained by experiments. Direct comparison between the predicted results and experimental data could not be done due to the lack of details of the experimental setup and properties of oil used in the experiments.
- The results show that conduction heat transfer dominates during the early stages of the fire, however, conduction alone could not produce temperature profiles obtained in experiments at later times.
- The predicted outputs show that the water layer at the bottom of the tank acts as a heat sink decreasing the temperature in the tank.
- The convective heat transfer at the walls does not affect significantly the temperature distribution in the tank.
- The results of the study indicate that using temperature dependent properties does not affect the results significantly.
- Oil viscosity was found to influence the results with a high viscosity reducing flow velocities and heat penetration in the oil.

The following items are recommended for future work.

- Modify the model to consider the effect of tank size, thickness of oil and thickness of water layer.
- Consider the effect of different radiation fluxes both at the top surface and the walls of the tank.
- Perform experiments to obtain data for model validation and model development.
- Modify the model to include the effect of void fractions in the oil due to the distillation process.
- Improve the model's solution algorithm to ensure stability. The model was unstable for a number of tests failing to provide converged solutions.
- Modify the model to consider non-homogenous crude oil.

REFERENCES

1. API-2021, "Management of Atmospheric Storage Tank Fires" American Petroleum Institute, 2000 edition.

2. Broeckmann, B. and Schecker, H."*Heat Transfer Mechanisms and Boilover in Burning oil-water systems*" J. Loss Prev. Process Ind. [8][3] pp.137-147 (1995).

3. NFPA-30, "Flammable and Combustible Liquids Code" National Fire Protection Association, 2000 edition.

4. Hall, H. H. "*Oil Tank Fire Boilovers*" Mechanical Engineering, 47 (7), pp. 540-544 (1925).

5. Koseki, H. "*Boilovers and Crude Oil Fires*", Journal of Applied Fire Science, 3 (3), pp.243-271 (1993).

6. www.chemeng.ed.ac.uk/~jskillin/teaching/safety4/jrberts/milford.htm [5/24/2005].

7. Cheremisinoff, N.P. "*Pressure Safety Design Practices for Refinery and Chemical Operations*", William Andrew Publishing/Noyes, pp. 75 (1988).

8. Iwata, Y. Natsume, Y. Koseki, H. and Hirano, T. "*A study on large-scale boilover using crude oil containing emulsified water*", Fire Safety Journal [38] pp.143-155 (2004).

9. Avallone, E., Theodore."*Marks' Standard Handbook for Mechanical Engineers*" McGRAW-Hill, 9th Ed. pp. 7-10:12 (1996).

10. Matar, S. and Hatch, L. "*Chemistry of Petrochemical Processes*" Gulf Publishing, pp.60 (1994).

11. The American Petroleum Institute, Petroleum HPV Testing Group, "*Test Plan-Crude oil Category-Consortium Registration # 1100997* ", (2003) http://www.petroleumhpv.org/Product_Categories/Crude_Oil/Final_TestPlan_Crude%20Oil_11-21-03.pdf

12. Washburn, E. "*International Critical Tables of Numerical Data, Physics, Chemistry and Technology*" Norwich pp.136-161 (2003).

13. Nevers, N. "*Fluid Mechanics for Chemical Engineers*" McGraw-Hill, Singapore, pp. 507 (1991).

14. Speight, J. "*Handbook of Petroleum Analysis*" Wiley-Interscience, New York, Ch.5 pp 127:163.

15. Drysdale, D. "*An Introduction to Fire Dynamics*", 2nd Ed. Wiley, UK (2003).

16. Iwata, Y and Koseki, H. Janssens, M. and Takahashi, T."*Combustion Characteristic of Crude Oils*", Fire Mater. 25, pp.1-7 (2001).

17. Lees, F. "*Loss Prevention in the Process Industries*", 2nd Ed., Butterworth-Heinemann, London, England (1992).

18. Hall, A. R. "*Pool Burning*" Oxidation & Combustion Reviews, 6, pp.169-225 (1973).

19. Joulain, P. "*Convective and Radiative Transport in Pool and Wall Fires: 20 Years of Research in Poitiers*" Fire Safety Journal [25] pp.99-149 (1996).

20. Cowley, L. and Johnson, A. "*OTI-92-596-Oil and Gas Fires: Characteristics & Impact*" , Steel Construction Institute, HMSO, London, 5.3 pp.26 (1992).

21. Shokri, M. and Beyler, C. "*Radiation from Large Pool Fires*" J. of Fire Prot. Engr. 1(4), pp-141:151 (1989).

22. Karlsson, B. and Quintiere, J. "*Enclosure Fire Dynamics*" CRC Press Ch.3.4.2 (2000).

23. Torero, J., Olenick, S. and Vantelon, J.. "*Determination of the Burning Characteristics of a Slick of Oil on Water*" Spill Sci. & Techn. Bulletin [8][4] pp. 379-390 (2003).

24. Iwata, Y and Koseki, H. "*Tomakomai Large Scale Crude Oil Fire Experiments*" Fire Techn. [35][1] pp25-38 (2000).

25. Koseki, H. and Mulholland G. "*The Effect of Diameter on the Burning of Crude Oil Pool Fires*", Fire Technology, pp.54-65 (1991).

26. "SFPE Handbook of Fire Protection Engineering", NFPA, Third Ed. Massachusetts (2002).

27. Bratz, W. and Schonbuches, A. "Warme-und Storfftansport. In Tankflammen" Chem-Ing. Tech. 50 Nr. 8. 5. 573-583. (1978).

28. Koseki, H. Kokkala, M. and Mulholland, George. "*Experimental Study of Boilover in Crude Oil Fires*" Fire Safety Science, pp.865-874 (1991).

29. Husa, J., Fan, W. C. and Liao G. X. "*Study and Prediction of Boilover in Liquid Pool Fires with a Water Sublayer using Micro-explosion Noise Phenomena*" Fire Safety J. 30 pp. 269-291 (1998).

30. Burgoyne, J. and Katan, L. "*Fires in Open Tanks of Petroleum Products: Some Fundamental Aspects*" Journal of the Institute of Petroleum 33(1), pp.158-191 (1947).

31. Nakakuki, A. "*Heat Transfer in Hot Zone Forming Pool Fires*" Combustion and Flame [109] pp.353-369 (1997).

32. Persson, H. and Lonnermark, A. "*Tank Fires-Review of Fire Incidents 1951-2003*" SP Fire Technology Report 2004:14.

33. Tijskens, L.; Hertog, M. and Nicolaï, B. "*Food Process Modelling*" Woodhead Publishing pp.4:61-86 (2001).

34. Gray, D. and Giorigini, A. "*The Validity of the Boussinesq Approximation for Liquids and Gases*", Int. J. Heat Mass Transfer, Vol. 19, pp. 545-551 (1976).

35. Patankar, S. "*Numerical Heat Transfer and Fluid Flow*" Taylor & Francis (1980).

36. Versteeg, H. and Malalasekera, W. "*An Introduction to Computational Fluid Dynamics-The Finite Volume Method*" Pearson Prentice Hall (1995).

37. Hadjisophocleous, G. "*Numerical Studies of Convective Flows Driven by Discrete Sources" U. of New Brunswick Master Thesis* (1985).

38. Yaws, C. " Chemical Properties Handbook" McGraw-Hill, New York, (1999).

39. Perry, R. and Green, D. "Perry's Chemical Engineers' Handbok",7th Ed., McGraw Hill (1997).

Appendix A Normalization of the Governing Equations

Nomenclature

ρ	=	Density, kg/m^3
C_p	=	Specific heat, J/kg K
T	=	Temperature, °C
t	=	Time, s
u, w, v	=	Velocity, m/s
r	=	Radius, m
θ	=	Angle, radian
z	=	Vertical distance, m
k	=	Thermal conductivity, W/kg.K
$\dot{q}$	=	Volumetric heat rate, W/m^3
L	=	Fuel thickness, m
α	=	Thermal diffusivity, m^2/s
P	=	Pressure, N/m^2
μ	=	Dynamic viscosity, Pa·s
g_z	=	Gravitational acceleration constant, 9.81 m/s^2
υ	=	Kinematic viscosity, m^2/s

Subscript

$_{ref}$	=	Reference value
$_o$	=	Initial value

Superscript

$\hat{}$	=	Normalized parameter

Table A-1: Reference Values

Temperature	Pressure	Velocity	Time	Height
$T_{ref} = T_o$	$P_{ref} = \frac{\alpha \upsilon \rho_o}{L_{ref}^2}$	$v_{ref} = \frac{\alpha}{L_{ref}}$	$t_{ref} = \frac{L^2_{ref}}{\alpha}$	$L_{ref} = L$

Steps Used for the Normalization of the Energy Equation in Cylindrical Coordinate

$$\rho_o C_p\left(\frac{\partial T}{\partial t}+u\frac{\partial T}{\partial r}+\frac{v}{r}\frac{\partial T}{\partial \theta}+w\frac{\partial T}{\partial z}\right)=k\left(\frac{\partial^2 T}{\partial r^2}+\frac{1}{r}\frac{\partial T}{\partial r}+\frac{1}{r^2}\frac{\partial^2 T}{\partial \theta^2}+\frac{\partial^2 T}{\partial z^2}\right)+\dot{q}$$

$$\rho_o C_p T_{ref}\frac{\alpha}{L^2{}_{ref}}\left(\frac{\partial \hat{T}}{\partial \hat{t}}+\hat{u}\frac{\partial \hat{T}}{\partial \hat{r}}+\frac{\hat{v}}{\hat{r}}\frac{\partial \hat{T}}{\partial \theta}+\hat{w}\frac{\partial \hat{T}}{\partial \hat{z}}\right)=k_{ref}T_{ref}\frac{1}{L^2{}_{ref}}\left(\frac{\partial^2 \hat{T}}{\partial r^2}+\frac{1}{\hat{r}}\frac{\partial \hat{T}}{\partial \hat{r}}+\frac{1}{\hat{r}^2}\frac{\partial^2 \hat{T}}{\partial \theta^2}+\frac{\partial^2 \hat{T}}{\partial \hat{z}^2}\right)+k_{ref}T_{ref}L_{ref}\hat{\dot{q}}$$

$$\frac{\rho_o C_p}{k_{ref}}T_{ref}\frac{\alpha}{L^2{}_{ref}}\left(\frac{\partial \hat{T}}{\partial \hat{t}}+\hat{u}\frac{\partial \hat{T}}{\partial \hat{r}}+\frac{\hat{v}}{\hat{r}}\frac{\partial \hat{T}}{\partial \theta}+\hat{w}\frac{\partial \hat{T}}{\partial \hat{z}}\right)=\frac{T_{ref}}{L^2{}_{ref}}\left(\frac{\partial^2 \hat{T}}{\partial r^2}+\frac{1}{\hat{r}}\frac{\partial \hat{T}}{\partial \hat{r}}+\frac{1}{\hat{r}^2}\frac{\partial^2 \hat{T}}{\partial \theta^2}+\frac{\partial^2 \hat{T}}{\partial \hat{z}^2}\right)+T_{ref}L_{ref}\hat{\dot{q}}$$

$$\frac{1}{L^2{}_{ref}}\left(\frac{\partial \hat{T}}{\partial \hat{t}}+\hat{u}\frac{\partial \hat{T}}{\partial \hat{r}}+\frac{\hat{v}}{\hat{r}}\frac{\partial \hat{T}}{\partial \theta}+\hat{w}\frac{\partial \hat{T}}{\partial \hat{z}}\right)=\frac{1}{L^2{}_{ref}}\left(\frac{\partial^2 \hat{T}}{\partial r^2}+\frac{1}{\hat{r}}\frac{\partial \hat{T}}{\partial \hat{r}}+\frac{1}{\hat{r}^2}\frac{\partial^2 \hat{T}}{\partial \theta^2}+\frac{\partial^2 \hat{T}}{\partial \hat{z}^2}\right)+L_{ref}\hat{\dot{q}}$$

$$\left(\frac{\partial \hat{T}}{\partial \hat{t}}+\hat{u}\frac{\partial \hat{T}}{\partial \hat{r}}+\frac{\hat{v}}{\hat{r}}\frac{\partial \hat{T}}{\partial \theta}+\hat{w}\frac{\partial \hat{T}}{\partial \hat{z}}\right)=\left(\frac{\partial^2 \hat{T}}{\partial \hat{r}^2}+\frac{1}{\hat{r}}\frac{\partial \hat{T}}{\partial \hat{r}}+\frac{1}{\hat{r}^2}\frac{\partial^2 \hat{T}}{\partial \theta^2}+\frac{\partial^2 \hat{T}}{\partial \hat{z}^2}\right)+L^3{}_{ref}\hat{\dot{q}}$$

Steps Used for the Normalization of the Momentum Equation in the Cylindrical Coordinate

$$\rho_o\left(\frac{\partial u}{\partial t}+u\frac{\partial u}{\partial r}+\frac{v}{r}\frac{\partial u}{\partial \theta}+w\frac{\partial u}{\partial z}-\frac{v^2}{r}\right)=-\frac{\partial P}{\partial r}+\mu\left(\frac{\partial^2 u}{\partial r^2}+\frac{1}{r}\frac{\partial u}{\partial r}+\frac{1}{r^2}\frac{\partial^2 u}{\partial \theta^2}+\frac{\partial^2 u}{\partial z^2}-\frac{u}{r^2}-\frac{2}{r^2}\frac{\partial v}{\partial \theta}\right)+g_z\Delta\rho$$

$$\rho_o\frac{\alpha}{L_{ref}}\frac{1}{\frac{L^2_{ref}}{\alpha}}\left(\frac{\partial \hat{u}}{\partial \hat{t}}+\hat{u}\frac{\partial \hat{u}}{\partial \hat{r}}+\frac{\hat{v}}{\hat{r}}\frac{\partial \hat{u}}{\partial \theta}+\hat{w}\frac{\partial \hat{u}}{\partial \hat{z}}-\frac{\hat{v}^2}{\hat{r}}\right)=-\frac{\alpha\upsilon\rho}{L^2_{ref}}\frac{1}{L_{ref}}\frac{\partial \hat{P}}{\partial \hat{r}}+\mu\frac{\alpha}{L_{ref}}\frac{1}{L^2_{ref}}\left(\frac{\partial^2 \hat{u}}{\partial \hat{r}^2}+\frac{1}{\hat{r}}\frac{\partial \hat{u}}{\partial \hat{r}}+\frac{1}{\hat{r}^2}\frac{\partial^2 \hat{u}}{\partial \theta^2}+\frac{\partial^2 \hat{u}}{\partial \hat{z}^2}-\frac{\hat{u}}{\hat{r}^2}-\frac{2}{\hat{r}^2}\frac{\partial \hat{v}}{\partial \theta}\right)+g_z\Delta\rho$$

$$\frac{\rho_o\alpha^2}{L^3{}_{ref}}\left(\frac{\partial \hat{u}}{\partial \hat{t}}+\hat{u}\frac{\partial \hat{u}}{\partial \hat{r}}+\frac{\hat{v}}{\hat{r}}\frac{\partial \hat{u}}{\partial \theta}+\hat{w}\frac{\partial \hat{u}}{\partial \hat{z}}-\frac{\hat{v}^2}{\hat{r}}\right)=-\frac{\alpha\mu}{L^3_{ref}}\frac{\partial \hat{P}}{\partial \hat{r}}+\frac{\alpha\mu}{L^3_{ref}}\left(\frac{\partial^2 \hat{u}}{\partial \hat{r}^2}+\frac{1}{\hat{r}}\frac{\partial \hat{u}}{\partial \hat{r}}+\frac{1}{\hat{r}^2}\frac{\partial^2 \hat{u}}{\partial \theta^2}+\frac{\partial^2 \hat{u}}{\partial \hat{z}^2}-\frac{\hat{u}}{\hat{r}^2}-\frac{2}{\hat{r}^2}\frac{\partial \hat{v}}{\partial \theta}\right)+g_z\Delta\rho$$

$$\frac{1}{\mathrm{Pr}}\left(\frac{\partial \hat{u}}{\partial \hat{t}}+\hat{u}\frac{\partial \hat{u}}{\partial \hat{r}}+\frac{\hat{v}}{\hat{r}}\frac{\partial \hat{u}}{\partial \theta}+\hat{w}\frac{\partial \hat{u}}{\partial \hat{z}}-\frac{\hat{v}^2}{\hat{r}}\right)=-\frac{\partial \hat{P}}{\partial \hat{r}}+\left(\frac{\partial^2 \hat{u}}{\partial \hat{r}^2}+\frac{1}{\hat{r}}\frac{\partial \hat{u}}{\partial \hat{r}}+\frac{1}{\hat{r}^2}\frac{\partial^2 \hat{u}}{\partial \theta^2}+\frac{\partial^2 \hat{u}}{\partial \hat{z}^2}-\frac{\hat{u}}{\hat{r}^2}-\frac{2}{\hat{r}^2}\frac{\partial \hat{v}}{\partial \theta}\right)+\frac{L^3_{ref}}{\alpha\mu}g_z\Delta\rho$$

Appendix B – Derivation of Algebraic Equations for Boundary Conditions

1) $$Q = kA\frac{\partial T}{\partial r} = hA(T_w - T_\infty)$$

$$Q = \frac{T_{oil} - T_w}{\frac{\Delta r}{2kA}} = \frac{T_w - T_\infty}{\frac{1}{hA}}$$

$$Q = \frac{T_{oil} - T_\infty}{\frac{1}{hA} + \frac{\Delta r}{2kA}}$$

$$Q = \frac{(T_{oil} - T_\infty)}{\frac{2kA + hA\Delta r}{2hkA^2}},$$

$$Q = \frac{(T_{oil} - T_\infty)}{\frac{2k + h\Delta r}{2hkA}}$$

$$Q = \frac{2hkA}{2k + h\Delta r}(T_{oil} - T_\infty)$$

2) $$Q = kA\left.\frac{\partial T}{\partial z}\right|_{oil} = kA\left.\frac{\partial T}{\partial z}\right|_{water}$$

$$Q = \frac{T_{oil} - T_{owi}}{\left.\frac{\Delta z}{2kA}\right|_{oil}} = \frac{T_{owi} - T_{water}}{\left.\frac{\Delta z}{2kA}\right|_{water}}$$

$$Q = \frac{T_{oil} - T_{water}}{\left.\frac{\Delta z}{2kA}\right|_{oil} + \left.\frac{\Delta z}{2kA}\right|_{water}}$$

$$Q = \frac{T_{oil} - T_{water}}{\frac{2k_{water} A\, z_{oil} + 2k_{oil} A\Delta z_{water}}{4k_{oil}k_{water}A^2}}$$

$$Q = \frac{T_{oil} - T_{water}}{\frac{k_{water}\Delta z_{oil} + k_{oil}\Delta z_{water}}{2k_{oil}k_{water}A}}$$

$$Q = \frac{2k_{oil}k_{water}A}{k_{oil}\Delta z_{water} + k_{water}\Delta z_{oil}}(T_{oil} - T_{water})$$